University of Missouri, St. Louis

IRL @ UMSL

12-10-2013

OPTICAL SPECTROSCOPIC STUDIES OF TWO STAR FORMING REGIONS

Kristen Leilani Erickson
University of Missouri-St. Louis, greensilverfish@gmail.com

Follow this and additional works at: https://irl.umsl.edu/dissertation

Part of the Physics Commons

Recommended Citation

OPTICAL SPECTROSCOPIC STUDIES OF TWO STAR FORMING REGIONS

by

KRISTEN LEILANI ERICKSON

A DISSERTATION

Presented to the Faculty of the Graduate Schools of the

MISSOURI UNIVERSITY OF SCIENCE AND TECHNOLOGY

and

UNIVERSITY OF MISSOURI – ST. LOUIS

In Partial Fulfillment of the Requirements for the Degree

DOCTOR OF PHILOSOPHY

in

PHYSICS

2013

Approved by

Dr. Bruce Wilking, Advisor
Dr. John Schmitt, Co-Advisor
Dr. Erika Gibb
Dr. Michael Meyer
Dr. Alexey Yamilov

PUBLICATION DISSERTATION OPTION

This dissertation has been prepared in the style utilized by the <u>Astronomical Journal</u>. Pages 21-71 have been published in that journal. Reproduced by permission of the AAS. Pages 72-126 will be submitted for publication in that journal. An Appendix has been added for purposes normal to dissertation writing.

ABSTRACT

The ϱ Ophiuchi and Serpens molecular clouds are sites of low mass star formation. The goals of this study were to identify young stellar objects (YSOs) and estimate ages and masses in order to infer an initial mass function (IMF), investigate disk evolution, and determine the star-forming history. Optical spectroscopic surveys of an unbiased sample of candidate young stars have been completed. Optical images taken in different photometric bands were used to create color-magnitude diagrams from which sources were selected for spectroscopic observation. In combination with published data, 135 association members in ϱ Ophiuchi and 63 association members plus 16 possible members in Serpens have been identified based on the presence of Hα in emission, lithium absorption, X-ray emission, a mid-infrared excess, and/or reflection nebulosity. Effective temperatures and bolometric luminosities were compared with theoretical tracks and isochrones for pre-main-sequence stars to estimate ages and masses.

Both regions have similar median ages, supporting the idea that star formation is a relatively fast process. In ϱ Ophiuchi, no age spread was found. In Serpens, an age spread of 1-5 Myrs was found; it could not be determined if this age spread was intrinsic or a result of contamination from foreground young stars. Consistent with these ages similar circumstellar disk frequencies were found. In ϱ Ophiuchi, an IMF consistent with the field star IMF for YSOs with masses >0.2 $M_\odot$ was inferred. In Serpens, the IMF was in agreement with the field star IMF for $M>1$ $M_\odot$. Previous studies of these regions have been biased towards particular stages in the star formation process. This study has provided an unbiased sample of pre-main sequence objects, necessary to obtain a complete picture of star formation.

ACKNOWLEDGMENTS

There are many people who have made this dissertation and the research contained within it possible. First and foremost I want to thank my advisor Bruce Wilking. He has been a voice of wisdom throughout the long, difficult and often frustrating process of researching and publishing two papers and turning them into a dissertation. He has shared his data, expertise and ideas with me and kept a sense of humor about the process. I appreciate all his contributions of time, ideas, energy and funding to make my Ph.D. experience productive and interesting.

I would additionally like to thank Michael Meyer for his support in the research and especially in the revision process for my work to date. He has made sure that my data is fully explored, my research is properly conducted and my papers are well written truly representing the research, which was done.

I would like to thank all my collaborators (Bruce and Michael included); they have shared their data, telescope time, funding and expertise with me. They have also stayed up late with me getting proposals done, worked through the night with me at the telescopes, and guided me when I was stuck in the research process.

Thank you also to my dissertation committee for the time and effort you have put into my dissertation, my defense, and me.

I would like to thank all the organizations that funded me making my research possible; Sigma Xi Grants in Aid of Research, NASA/ Missouri Space Grant Consortium Fellowship, Chancellor's Graduate Scholars Dissertation Fellowship, NOAO Thesis-student travel fund, and the Missouri Research Board Grant.

I would like to thank my entire family for all the help, and guidance through the years. Particularly I would like to thank my father, Richard Kartchner and my grandfather, Frank Nelson for setting up telescopes for me every summer that I was growing up. Thank you to my mother Jean Kartchner for all her imaginative ideas and for always believing in me. Also special thanks to my husband, Todd Erickson for being extremely patient as well as for transforming my computer from a magical black box to a useful tool. Thank you also to my mother in law Susan Erickson for all the many hours of babysitting, with out which I would have never completed this dissertation.

TABLE OF CONTENTS

SECTION

LIST OF ILLUSTRATIONS

LIST OF TABLES

1   INTRODUCTION

1.1   STAR FORMATION

Stars, being the main source of light in the universe, determine what can be observed. As a result they are used to establish the nature, structure and evolution of the universe (Larson 2003). Stars also determine the amount of and evolution of elements heavier than hydrogen in the universe. This makes understanding how stars form and evolve very important to understanding the observable universe. It is believed that planets form out of the circumstellar disks around young stars (Ruden 2009). The environment around young stars sets the conditions for planet formation, making star formation the main factor in determining how planets form. Star formation may set limits on the number of planets in the habitable zone, and hence the likelihood of life. This makes star formation a starting point to understanding life in the universe. The most massive stars burn their fuel on a timescale of 10^6 yrs, less than the age of the Galaxy, which demonstrates that star formation is an ongoing process (Lada 1999). Star formation can in theory be observed as it is happening. This makes the study of star formation viable as well as fundamental to our understanding of the universe.

1.2   STAR FORMATION MECHANISMS

Stars form in molecular clouds. There are several proposed mechanisms for star formation. One of the main means to differentiate between these mechanisms is the timescale for star formation (Ward-Thompson *et al.* 2007). A molecular cloud (MC) will remain in hydrostatic equilibrium as long as other forces, for example the thermal kinetic energy, balance the self-gravity of the cloud. Using the virial theorem, the minimum mass required to collapse a cloud, called the Jeans mass,

can be determined. Jeans (1928) was the first to formulate this mass including only thermal kinetic energy and gravitational potential:

$$M_{Jeans} = (\frac{5kT}{G\mu m_H})^{3/2}(\frac{3}{4\pi\rho})^{1/2} \tag{1.1}$$

where k is the Boltzmann constant, T is the temperature, G is the gravitational constant, μ is the mean molecular weight, m_H is the mass of hydrogen and ρ is the density of the cloud. This form of the Jeans mass assumes a constant density. As long as the cloud remains optically-thin, the collapse is isothermal. The free fall time (τ_{ff}) is the characteristic time for a cloud to collapse under its own self-gravity if no other forces exist to oppose the collapse:

$$\tau_{ff} = (\frac{3\pi}{32G\rho})^{1/2} \tag{1.2}$$

where ρ is the density of the cloud. Using a density of 10^8 cm^{-3} gives approximately 10^5 yrs, setting a lower limit on how fast stars can form. At some point the density increases to a point that the star is no longer optically thin and collapse proceeds adiabatically. At this stage, the gas and dust begin to heat up and radiate. The Kelvin-Helmholtz time is the time it takes for a star to radiate away all its thermal energy; this sets a limit on the timescale for the pre-main sequence lifetime of a star:

$$\tau_{K-H} = \frac{GM^2}{RL} \tag{1.3}$$

where M is the mass of the star, R is the radius of the star and L is the luminosity of the star. The Kelvin-Helmholtz time determines how quickly a star contracts before nuclear fusion starts. If thermal kinetic energy were the only force opposing gravity, MCs would be expected to collapse rapidly and efficiently into stars. However, observations show that MCs are very inefficient in creating stars. Only 3 - 6% of their

mass goes into stars (Evans *et al.* 2009). Therefore other forces must be present opposing gravity. The two main forces proposed are magnetic fields and turbulence. One method for MC collapse proposed is that MCs form via matter accumulation along flux lines. As magnetic fields can only affect the ionized part of the gas, neutral matter will slip past ions as they are pulled through the field by gravity. This is called ambipolar diffusion (Shu *et al.* 1987; Mouschovias 1991; Nakano 1998). This is a slow process, taking about 10^8 years, hence most MCs observed should be starless (Briceño *et al.* 2007) and, in areas of star formation, a spread of ages on order of 10 Myrs (Hartmann 2001) should be observed. Current observations show that most MCs are active sites of star formation (Elmegreen 2000; Hartmann *et al.* 2001) and that most young clusters do not show evidence for large age spreads (Briceño *et al.* 1997) making ambipolar diffusion an unlikely mechanism for star formation. However there is evidence that magnetic fields are important in dissipating angular momentum (Larson 2003). Another suggested method for star formation is turbulent fragmentation due to gravity. In this theory, turbulence creates density fluctuations within the MC. These regions become unstable against gravity and collapse. In this case, star formation is a quick process, taking approximately 10^7 years and MCs are short-lived (Ballesteros-Paredes *et al.* 2003; Vazquez-Semadeni *et al.* 2005). This picture seems to be in better agreement with observations (Elmegreen 2000; Hartmann *et al.* 2001). There are many other factors that may influence the formation of stars in MCs. These include effects of local density, pressure, rotation, accretion, and the presence of massive stars and YSOs (Ward-Thompson *et al.* 2007; Bonnell *et al.* 2007).

OB associations are associated with giant molecular clouds. A commonly observed property of OB associations is that they are made up of sub-groups that differ in age (Loren 1989; Nutter *et al.* 2006). This suggests that star formation may occur by external triggering (Elmegreen & Lada 1977; Lada 1987).

1.3   STAR FORMATION AND THE INITIAL MASS FUNCTION

The initial mass with which a star forms determines the star's evolution and ultimate death. Therefore a key element in explaining both the evolution and formation of stars lies in understanding what determines the mass with which stars will form. The distribution of masses with which stars form is called the initial mass function (IMF). Stellar mass is not generally a directly observable quantity, ergo it must be derived from other observable quantities such as the luminosity and/or effective temperatures of a star or groups of stars. The first observationally-based field star IMF was derived by Salpeter (1955), who began by counting the number of visible stars within the solar neighborhood (known as a luminosity function). In order to represent the number of stars at birth, a correction must be made to account for massive stars that have moved off the main sequence since the formation of the Galaxy. This correction requires the assumption that the both the birthrate and form of the IMF are constant in time and space. There is no intrinsic reason to assume that either of these quantities are constant in time and or space, however most estimates of the field star IMF made to date include these assumptions (Salpeter 1955; Miller & Scalo 1979; Kroupa 2001; Chabrier 2003). With the additional assumption that all stars counted in the sample are on the main sequence, the main sequence mass-luminosity relation can be used to relate the luminosity function to the mass of the stars in the sample. Salpeter defined the mass function ζ (log m$_{star}$) as the stellar number density n per logarithmic mass interval δ log m:

$$\zeta(\log m_{star}) = \frac{\delta n}{\delta \log m} = \frac{\delta(\frac{N}{V})}{\delta \log m} \qquad (1.4)$$

where N is the number of stars in a volume of space V. Salpeter derived an IMF of the form

$$\zeta(\log m_{star}) \sim m_{star}^{-1.35} \qquad (1.5)$$

for $0.4 < M/M_\odot < 10$. It is noteworthy that this form has survived as the best description of the IMF for stars above 1 $M_\odot$, without much revision (Bonnell, Larson, & Zinnecker 2007). However, there has been some debate on the form of the low mass (below 1 $M_\odot$) IMF. Miller and Scalo (1979) suggested that below 1 $M_\odot$ the IMF flattens out, and can be described by a lognormal function in this range (See Fig. 1.1). Many studies have been done in the low mass range, and observations seem to support both this functional form, with a peak at around 0.2 $M_\odot$ (Scalo 1986; Chabrier 2003), and a series of power laws (Kroupa 2001). However, it is currently unclear if these forms hold below the hydrogen-burning limit (0.08 $M_\odot$) and/or if a low mass cutoff exists (Bastian, Covey, & Meyer 2010). This uncertainty is largely due to a lack of observations sensitive enough to sample completely at and below the hydrogen-burning limit.

The IMF is best observed in young clusters, where large numbers of stellar objects have formed out of the same molecular cloud, and have likely formed at around the same time and under the same conditions. Also there will be little or no loss of objects due to stellar evolution or dynamical effects (Lada 1999, Meyer *et al.* 2000). Another benefit to using young clusters to study the IMF is that young stellar objects (YSOs) are more luminous at this stage in their evolution than once they are on the main sequence, making observation of low mass YSOs easier. However, observing in young clusters also has some disadvantages. Evolutionary models required to derive ages and masses do not necessarily reflect true masses and ages. Different evolutionary models can predict different masses for a star in the same position on an Hertzsprung-Russell (H-R) diagram (a plot of temperature and luminosity which can be used as an evolutionary diagnostic tool)(Hillenbrand *et al.* 2007). Comparison of masses determined via dynamical mass measurements (such as eclipsing binaries) to masses determined by evolutionary models suggests that mass errors may be as much as 30-50% (Hillenbrand & White 2004). Another difficulty
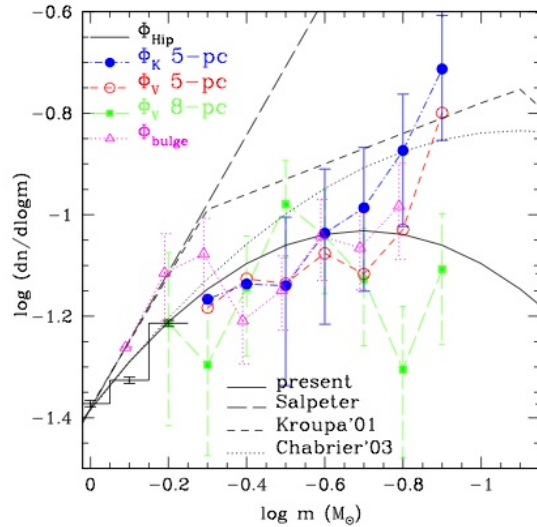
Figure 1.1 The IMF is a plot of the log of the number of stars in the solar neighborhood per unit log mass, vs. log mass of a star. Examples of derived field star IMFs including Salpeter (1955); Kroupa (2001); Chabrier (2003) and Chabrier (2005, labeled present). Color data points are various measurements of the luminosity function (in either V or K band), which is the number of stars N per absolute magnitude interval in a volume of space within 5 or 8 pc as labeled. Φ_{bulge} is a J band luminosity function for stars in the Galactic bulge. Φ_{Hip} was derived using Hipparcos parallax data. Figure taken from Chabrier (2005).

is that regions heavily extincted by dust cannot be observed at optical wavelengths. However this is also an advantage, in that the light from background stars is blocked out, so there is little contamination from these stars. There are two main methods used to derive the IMF in young clusters. The first method determines a luminosity function for stars in a particular star-forming region (Lada & Lada 1995; Lada, Lada, & Muench 1998). As these regions are young, little or no correction needs to be made to account for evolution of higher mass stars (as is done for field stars). As there is no unique mass-luminosity function for pre-main sequence (PMS) stars, this quantity must be modeled using evolutionary models and knowledge of the star-forming history of the region. This has the advantage of providing large samples of stars from which to derive an IMF, but requires making assumptions about the age of the cluster (Lada 1999). The second method is to obtain spectra for a representative sample of stars in the region in order to derive effective temperatures. Then YSOs are placed on an H-R diagram and compared to PMS evolutionary models to obtain both an age and a mass for each YSO. While this method provides fewer stars to work with, it does provide a more direct measurement of the masses and hence the IMF (Lada 1999). YSOs in young clusters are obscured by dust in the cloud, allowing brighter objects to be observed at a greater depth than fainter objects. These bright objects will be over-represented in magnitude-limited samples. This observational bias can be overcome by using an extinction-limited sample to determine the IMF (Meyer *et al.* 2000; Bastian, Covey, & Meyer 2010).

It is currently unclear if the IMF is universal, or it if varies from region to region, particularly near the hydrogen-burning limit. Thorough investigations of the IMF in several star-forming regions ought to give insight on the universality of the IMF. Should the IMF not be universal these studies should also provide insight to what physical properties determine the IMF. Most studies of the IMF in different environments (field stars, young clusters, and old globular clusters) suggest that the

IMF is universal (Meyer *et al.* 2000; Bastian, Covey, & Meyer 2010). However within in our Galaxy, there are two young nearby regions that seem to have IMFs not in agreement with the field star IMF. The Taurus-Auriga Cloud appears to have a deficit of brown dwarfs and a higher characteristic mass compared to the field star IMF (Briceño *et al.* 2002; Luhman 2004). The Upper Scorpius subgroup seems to have an excess of brown dwarfs in comparison to the field star IMF (Slesnick, Hillenbrand, & Carpenter 2008). It is unclear if these brown dwarf excesses and deficits are significant or the result of bias and incompleteness effects.

1.4   EVOLUTION OF YOUNG STELLAR OBJECTS

The evolution of young stellar objects can be classified into four main stages; (1) objects in the main phase of accretion radiate mainly in the far-infrared and submillimeter and display Class 0 spectral energy distributions (SEDs), (2) objects with a warmer central protostar embedded in gas and dust envelope and disk and are accreting material at a lower rate and display Class I SEDs, (3) Classical T-Tauri stars in the final stages of accreting display Class II SEDs and have begun to emerge from the envelope of gas and dust while retaining their disks, and (4) weak emission T-Tauri stars have dissipated most of their gas and dust but are still contracting towards the main sequence when they will begin hydrogen-burning and display Class III SEDs (Lada 1999; Ward-Thompson *et al.* 2007) (See Fig. 1.2). The earliest phases, those displaying Class 0 and I SEDs, are best observed at submillimeter and infrared wavelengths. YSOs displaying Class II and III SEDs are best examined at infrared and optical wavelengths. X-ray emission can be seen during several stages from strong magnetic surface activity and disk interactions, such as when YSOs start to dissipate their disks via winds and planet formation. These stages make it necessary to observe star-forming regions in a variety of wavelengths.
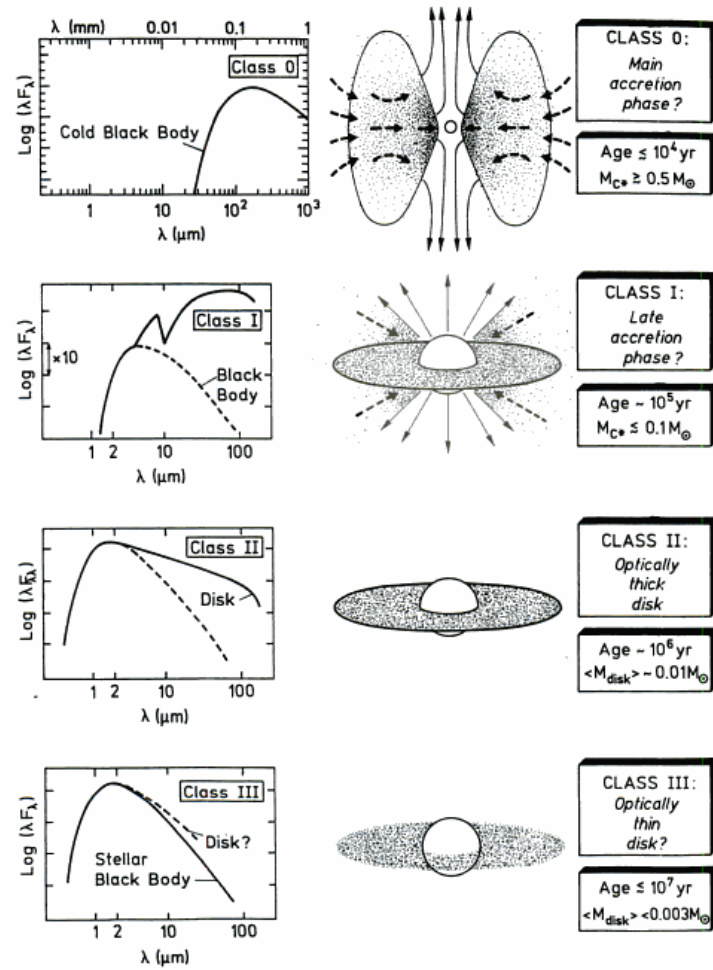
Figure 1.2 A cartoon showing the 4 main evolutionary stages and the SED of each phase (André 1994).

1.5 THE ρ OPHIUCHI AND SERPENS MOLECULAR CLOUDS

The ρ Ophiuchi and Serpens molecular clouds have been identified by previous studies as regions of active star formation. The two regions are located near to the Sun, giving the highest sensitivity to the widest range of luminosities and masses. They are in a ring of OB associations called Gould's Belt. Gould's Belt is tilted approximately 20 degrees to the plane of the Galaxy, and has a diameter of about 1000 pc (See Fig. 1.3). ρ Ophiuchi is located 130 pc from the Sun (Wilking, Gagné, & Allen 2008) (See Fig. 1.4). The distance to Serpens is less clear; some studies report 260 pc (Eiroa, Djupvik, & Casali 2008) while others derive 429 pc (Dzib *et al.* 2011, 2010). This study may shed some light on the actual distance (See Fig 1.5).
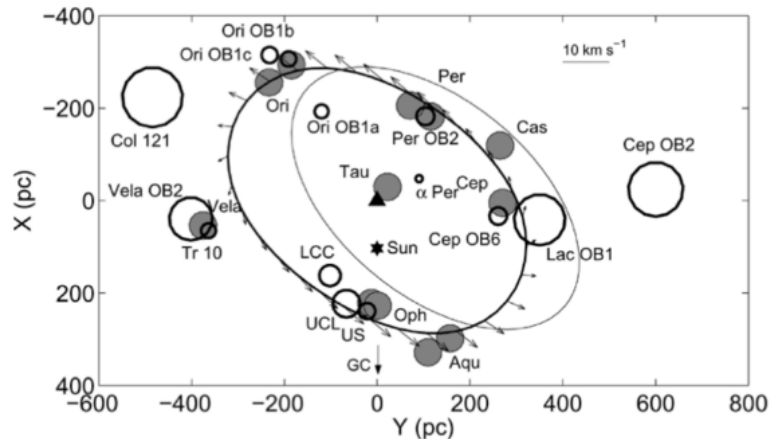
Figure 1.3 A cartoon showing the position of ρ Ophiuchi and Serpens clouds within Gould's Belt, and relative to the Sun. Aqu represents the position of Serpens, which is located in the Aquila Rift (Perrot & Grenier 2003).

Both young clusters have been observed by numerous surveys ranging in wavelength from X-ray to submillimeter. As part of the Spitzer Space Telescope's Legacy
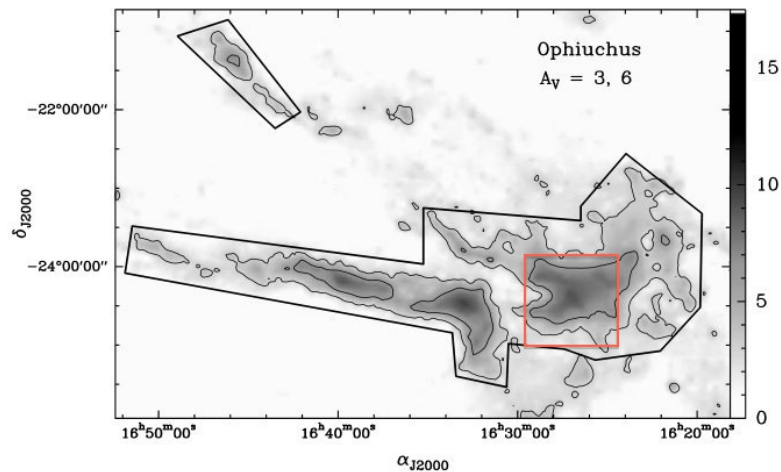
Figure 1.4 An extinction map of ρ Ophiuchi. The red box is approximately our field of view. The contour levels are A$_v$=3 and A$_v$= 6 magnitudes. This map was created using background star counts at red wavelengths (7000 Å. Taken from André & Saraceno (2007) originally from Cambrésy (1999).)

programs, about 106 objects in ρ Ophiuchi were identified as YSOs due to infrared excess in the mid- and far- infrared (Allen et $al.$, unpublished data). This study was biased towards stars in the earliest stages of star formation, which are still encompassed by gas and dust. X-ray studies have also been conducted of the region with ROSAT, XMM- Newton, ASCA and Chandra (Grosso et $al.$ 2000; Gagné, Skinner, & Daniel 2004; Ozawa, Grosso & Montmerle 2005). These surveys have targeted more evolved PMS stars with magnetic surface activity. Due to the highly variable nature of X-ray emission, YSOs with little or no circumstellar dust have been undersampled. Optical spectroscopic surveys have been conducted of ρ Ophiuchi, however these studies have been biased towards objects with X-ray emission or towards stars with suspected Hα emission (Bouvier & Appenzeller 1992, Martín et $al.$ 1998, Wilking et $al.$ 2005).
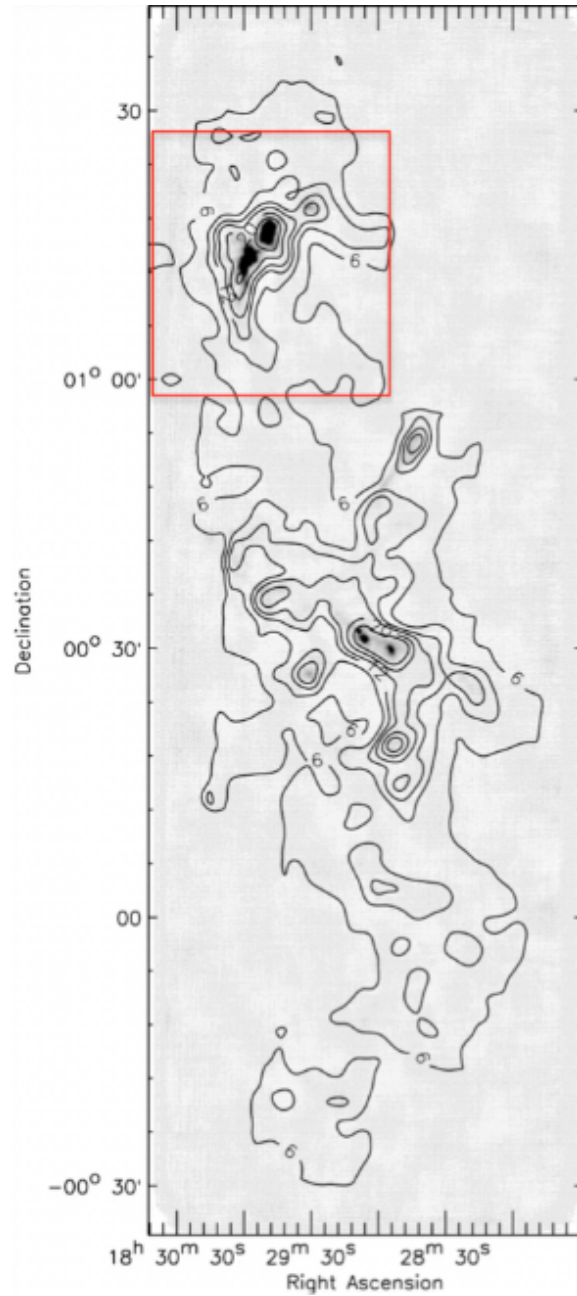
Figure 1.5 An extinction map of Serpens. The red box is a portion of our field of view, the east edge of our survey area is off the left edge of the image. Contours are A_v= 6, 9, 12, 15, 20, and 25 magnitudes. The contours are calculated from c2d Spitzer maps. The grey scale image is 1.1 mm continuum emission from cold dust. Taken from Enoch *et al.* (2007).

The Spitzer Space Telescope has studied Serpens, identifying 235 YSOs with infrared excesses using observations obtained in both the mid- and far- infrared (Harvey *et al.* 2006; Winston *et al.* 2007; Winston *et al.* 2009). X-ray surveys have also been done, using Chandra and XMM - Newton (Preibisch 2003; Giardino *et al.* 2007; Winston *et al.* 2007). These surveys suffer from the same shortcomings as the infrared and X-ray surveys done in ρ Ophiuchi. As in ρ Ophiuchi, recent spectroscopic optical surveys of Serpens have been biased, focusing on objects with infrared excesses (Oliveira *et al.* 2009; Winston *et al.* 2009).

1.6 OBJECTIVES AND METHOD

The objectives of this study are (1) to determine the star-forming history providing insight into possible triggering events or lack thereof, (2) to infer an initial mass function (IMF) for comparison with the field and other star-forming regions, and (3) to characterize disk evolution setting limits on disk timescales for young clusters in both the Serpens and ρ Ophiuchi molecular clouds. To this end, optical spectra for an unbiased sample of candidate YSOs in both the ρ Ophiuchi and Serpens regions have been obtained. These spectra were used to confirm youth, determine effective temperatures and bolometric luminosities, and when compared with theoretical models, estimate the ages and masses (see sections I.2, I.3 (ρ Ophiuchi) and II.2 II.3 (Serpens)). Optical images taken in R and I (ρ Ophiuchi) and V and R (Serpens) bands have been used to create color-magnitude diagrams. These color magnitude diagrams were then used to select sample candidate YSOs (see sections I.2.1 (ρ Ophiuchi) and II.2.1 (Serpens)). Cluster membership was established by the presence of lithium absorption at 6707 Å and/or Hα in emission. Youth was also confirmed via the presence of X-ray emission and/or an infrared excess, determined from previous studies. Additionally, a diagram similar to a Wolf diagram was used to ascertain cluster membership by plotting the extinction versus distance assuming

the objects (eliminating giants) are on the main sequence. Objects above a certain extinction (e.g., in ρ Ophiuchi the criteria was anything 1.5 magnitudes or higher) that appear to be closer than the cloud distance are too extincted to be foreground objects and too luminous to be on the main sequence. They are likely pre-main sequence members (see sections I.4.2 (ρ Ophiuchi) and II.3.2 (Serpens)). These data have been combined with other optical, and infrared surveys to form an extinction-limited sample of YSOs, reconstruct the star-forming history, estimate disk survival times and the onset of planet formation, as well as to begin investigations into the IMFs. The derived IMFs were compared to the field star IMF as well as the IMFs of other young clusters such as IC 348 (Luhman *et al.* 1998; Luhman *et al.* 2003), Taurus (Briceño *et al.* 2002; Luhman 2004) and the Orion Nebula Cluster (Hillenbrand 1997; Slesnick, Hillenbrand, & Carpenter 2004) to give insight into the dependence of the IMF on temperatures and pressures of the gas in which stars are born (Kroupa 2001)(see sections I.4.6.2 (ρ Ophiuchi) and II.3.8 (Serpens)).

As a cluster ages, encounters between stars cause lower mass stars to migrate outward; this process is known as mass segregation. In younger clusters, mass segregation has not yet occurred to a large extent and YSOs are still bound by the molecular gas. Therefore any differences in mass distributions between young clusters are likely due to differences in the physical conditions of the cloud from which the stars were created (Bonnell & Davies 1998). However recent simulations have found that the timescale for dynamical mass segregation could be shorter than previously predicted (Moeckel & Bonnell 2009; Allison *et al.* 2009; Bastian, Covey, & Meyer 2010) therefore, it is unclear if the presence of mass segregation is primordial or not. There are two timescales that are important to this process: the crossing time and the relaxation time. The crossing time is the time required for a star to move from one side of a cluster to the other, assuming it is traveling at the typical random speed of objects in the cluster. This is the shortest timescale over which significant dynamical

events can occur and the timescale for the cluster to be virialized:

$$\tau_{cross} = \frac{2R}{v} \qquad (1.6)$$

where R is the radius of the cluster and v is the typical speed as measured by the velocity dispersion of objects in the cluster. The relaxation time is the time for a star to be significantly perturbed by other objects in the cluster i.e., the time required for a star to lose all memory of its initial orbit:

$$\frac{\tau_{relax}}{\tau_{cross}} \approx \frac{0.1N}{\ln N} \qquad (1.7)$$

where is N is the number of stars in a cluster (Lada & Lada 2003). Unless Mass segregation is primordial, it is expected to occur in about the relaxation time, and likely takes place in a longer time than the crossing time (Mouri & Taniguchi 2002). Spatial and temporal studies remain important for understanding the physics for how and why stars end up with their observed mass (Lada & Lada 2003).

Circumstellar disks are important in both star and planet formation. It is believed that matter is accreted onto PMS stars through disks, and that these disks are also the sites of planet formation (Strom *et al.* 1989; Fang *et al.* 2009). Dust emission from the circumstellar disks surrounding YSOs are the cause of infrared emission excess over that from the stellar photosphere. Disk evolution can be studied by looking at the magnitude of an infrared excess as a function of age and mass. Disk lifetimes can be inferred by the fraction of sources with disk signatures as a function of age. Disk lifetimes seem to be inversely correlated to stellar mass (Hernandez 2007). Studies indicate that the inner disk close to the star dissipates faster than the cooler outer disk (Strom *et al.* 1989; Hillenbrand 2002; Mamajek *et al.* 2004; Carpenter *et al.* 2005; Fang *et al.* 2009). Objects displaying evidence of an disk inner hole may be sites of planet formation (Strom *et al.* 1989; Fang *et al.* 2009).

These disks are called transition disks. The disk frequency of a young cluster can be obtained by plotting the number objects versus the magnitude of an infrared excess. Transition disk objects were identified by comparing the 24-μm excess to the 3.6-μm excess using Spitzer Space Telescope studies (Allen *et al.* 2011) (see sections I.4.6.1 (ρ Ophiuchi) and II.3.6 (Serpens)).

REFERENCES

Allen, L.E., Megeath, T., Padgett, D., Wilking, B. A., Gagné M., *et al.* 2011, in preparation.

Allison, R., Goodwin, S., Parker, R., *et al.* 2009, ApJ, 700, L99

André, P. 1994, Observations of Protostars and Protostellar Stages in "The Cold Universe," eds. T. Montmerle, C.J.Lada, I.F.Mirabel, & J.Tran Thanh Van, Editions Frontiéres, p.179

André, P. & Saraceno, P., 2007, Probing the origin of the stellar initial mass function A wide-field Herschel photometric survey of nearby star-forming cloud complexes in a Proposal for a SPIRE/PACS GT Key Project.

Ballesteros-Paredes J., Klessen R.S., & Vazquez-Semadeni E. 2003, ApJ, 592, 188

Bastian, N., Covey, K.R., & Meyer, M.R. 2010, ARA&A, 48, 339

Bonnell, I. A & Davies, M. 1998, MNRAS, 295, 691

Bonnell, I. A., Larson, R. B., & Zinnecker, H. 2007, in Protostars and Planets V, ed. B. Reipurth, D. Jewitt, & K. Keil (Tucson, AZ: Univ. Arizona Press), p. 149

Bouvier, J. & Appenzeller, I. 1992, A&AS, 92, 481

Briceño, C., Preibisch, T., Sherry, W.H., *et al.* 2007, Protostars and Planets V, 345

Briceño, C., Luhman, K. L., Hartmann, L., Stauffer, J. R., & Kirkpatrick, J. D. 2002, ApJ, 580, 317

Briceño, C., Hartmann L.W., Stauffer J., Gagné M., Stern R., & Caillault J. 1997, AJ, 113, 740

Cambrésy, L., 1999, A& A, 345, 965

Carpenter, J. M., Wolf, S., Schreyer, K., Launhardt, R., & Henning, T. 2005, AJ, 129, 1049

Chabrier, G. 2003, PASP, 115, 763

Chabrier, G. 2005 in The Initial Mass Function 50 Years Later, ed. E. Corbelli, F. Palla, & H. Zinnecker (Astrophysics and Space Science Library, Vol. 327; Dordrecht: Springer), 41

Dzib, S., Loinard, L., Mioduszewski, A. J., *et al.* 2010, ApJ, 718, 610

Eiroa, C., Djupvik, A, & Casali, M. 2008 in Handbook of Star Forming Regions Vol.II, Ed. B. Reipurth, (ASP: San Francisco), 693

Elmegreen B.G. 2000, ApJ, 530, 277

Elmegreen B.G., & Lada, C. 1977, ApJ, 214, 725

Evans, N.L., Dunham, M.M., Jorgensen, J.K., *et al.* 2009, ApJS, 181, 321

Fang, M., van Boekel, R., Wang, W., Carmona, A., Sicilia-Aguilar, A., & Henning, Th. 2009, A&A, 504, 461

Gagné, M., Skinner, S., & Daniel, K. 2004, ApJ, 613, 393

Giardino, G, Favata, F., Micela, G., Sciortino, S., & Winston, E. 2007, A& A, 463, 275

Grosso, N., Montmerle, T., Bontemps, S., André, Ph., & Feigelson, E. 2000, A& A, 359, 113

Hartmann, L. 2001, AJ, 121, 1030

Hartmann, L., Ballesteros-Paredes, J., & Bergin, E.A. 2001, ApJ, 562, 852

Harvey, P., Chapman, N., Lai, S.-P., *et al.* . 2006, ApJ, 644, 307

Hernandez, J., Calvet, N., Briceño, C. *et al.* 2007, ApJ, 671, 1784

Hillenbrand, L. 1997, AJ, 113, 1733

Hillenbrand, L. A. 2002, arXiv Astrophysics e-prints astro-ph/0210520

Hillenbrand, L.A, Bauermeister, A., & White, R. 2007 in Cool Stars, Stellar Systems, and the Sun XIV: ASP Conference Series, Vol. XX

Hillenbrand, L. A., & White, R. J. 2004, ApJ, 604, 741

Kroupa, P. 2001, MNRAS, 322, 231

Lada, C. 1987 in Star Forming Regions, edited by M. Peimbert & J. Jugaku, p. 1

Lada, C. 1999 in The Origin of Stars and Planetary Systems, edited by C. Lada &
     N. Kylafis, p. 143

Lada, E., Lada, C., & Muench A. 1998 in The Stellar Initial Mass Function, edited
     by G. Gilmore and D Howell, Vol 142

Lada, E., & Lada, C. 1995, AJ, 109,1682

Lada, C., & Lada, E. 2003, ARA& A, 41, 57

Larson, R. B. 2003, Reports on Progress in Physics, 66, 1651

Loren, R. B. 1989, ApJ, 338, 925

Luhman, K. L. 2004, ApJ, 617, 1216

Luhman, K. L., Rieke, G. H., Lada, C. J., & Lada, E. A. 1998, ApJ, 508, 347

Luhman, K.L., Stauffer, J. R., Muench, A. A., *et al.* 2003, ApJ, 593, 1093

Mamajek, E. E., Meyer, M. R., Hinz, P. M., *et al.* 2004, ApJ, 612, 496

Martín, E. L., Montmerle, T., Gregorio-Hetem, J., & Casanova, S. 1998, MNRAS,
     300, 733

Meyer, M. R., Adams, F. C., Hillenbrand, L. A., Carpenter, J. M., & Larson, R.
     B., 2000 in Protostars and Planets IV, ed. V. Mannings, A. P. Boss, & S. S.
     Russell (Tucson, AZ: Univ. Arizona Press), 121

Miller, G., & Scalo, J. 1979, ApJS, 41, 513

Moeckel, N., & Bonnell, I. 2009, MNRAS396, 1864

Mouri, H., & Taniguchi, Y. 2002, ApJ, 580, 844

Mouschovias T. Ch. 1991, ApJ, 646, 1043

Nakano T. 1998, ApJ, 494, 587

Nutter, D.J., Ward-Thompson, D.,& André, P. 2006, MNRAS, 368, 1833

Oliveira, I., Merin, B., Pontoppidan, K. M., *et al.* 2009, ApJ, 691, 672

Ozawa, H., Grosso, N., & Montmerle, T. 2005, A&A, 429, 963

Perrot & Grenier, A&A, 2003, 404, 519

Preibisch, T. 2003, A&A, 410, 951

Ruden, S. 2009 in The Origin of Stars and Planetary Systems, edited by C. Lada & N. Kylafis, p. 143

Salpeter, E. 1955, ApJ, 121, 161

Scalo, J. 1986 in The Stellar Initial Mass Function, edited by G. Gilmore & D Howell, p. 1

Shu F.H, Adams F.C, & Lizano S. 1987, ARA&A, 25, 23

Slesnick, C. L., Hillenbrand, L. A. & Carpenter, J. M. 2004, ApJ, 610, 1045

Slesnick, C. L., Hillenbrand, L. A. & Carpenter, J. M. 2008, ApJ, 688, 377

Strom, K. M., Strom, S. E., Edwards, S., Cabrit, S., & Skrutskie, M. F. 1989, AJ, 97, 1451

Ward-Thompson, D., André, P., Crutcher, R., Johnstone, D., Onishi, T., *et al.* 2007, in Protostars and Planets V, ed. B. Reipurth, D. Jewitt, & K. Keil, p. 33

Wilking, B. A., Meyer, M. R., Robinson, J. G., & Greene, T. P., 2005, AJ, 130, 1733

Wilking, B. A., Gagné, M., & Allen, L. E., 2008 in Handbook of Star Forming Regions Vol.II, ed. B. Reipurth (San Francisco, CA: ASP), 351

Winston, E., Megeath, S. T., Wolk, S. J., *et al.* 2007, ApJ, 669, 493

Winston, E., Megeath, S. T., Wolk, S. J., *et al.* 2009, AJ, 137, 4777

Paper I
The Initial Mass Function and Disk Frequency of the ρ Ophiuchi Cloud:
An Extinction-Limited Sample

Kristen L. Erickson [1]

Department of Physics and Astronomy, University of Missouri-St. Louis
1 University Boulevard, St. Louis, MO 63121
kle6x2@mail.umsl.edu

Bruce A. Wilking [1]

Department of Physics and Astronomy, University of Missouri-St. Louis
1 University Boulevard, St. Louis, MO 63121
bwilking@umsl.edu

Michael R. Meyer

Institute for Astronomy Swiss Federal Institute of Technology
Wolfgang-Pauli-Strasse 27, CH-8093 Zurich Switzerland
mmeyer@phys.ethz.ch

John G. Robinson [2]

Department of Physics and Astronomy, University of Missouri-St. Louis
1 University Boulevard, St. Louis, MO 63121
jrobinson@gmail.com

and

Lauren N. Stephenson [1]

Department of Physics and Astronomy, University of Missouri-St. Louis
1 University Boulevard, St. Louis, MO 63121
lnafff@mail.umsl.edu

ABSTRACT

We have completed an optical spectroscopic survey of an unbiased, extinction-limited sample of candidate young stars covering 1.3 deg^2 of the ρ Ophiuchi star forming region. While infrared, X-ray, and optical surveys of the cloud have identified many young stellar objects (YSOs), these surveys are biased towards particular stages of stellar evolution and are not optimal for studies of the disk frequency and initial mass function. We have obtained over 300 optical spectra to help identify 135 association members based on the presence of Hα in emission, lithium absorption, X-ray emission, a mid-infrared excess, a common proper motion, reflection nebulosity, and/or extinction considerations. Spectral types along with R and I band photometry were used to derive effective temperatures and bolometric luminosities for association members to compare with theoretical tracks and isochrones for pre-main-sequence stars. An average age of 3.1 Myr is derived for this population which is intermediate between that of objects embedded in the cloud core of ρ Ophiuchi and low mass stars in the Upper Scorpius subgroup. Consistent with this age we find a circumstellar disk frequency of 27% $\pm$ 5%. We also constructed an initial mass function for an extinction-limited sample of 123 YSOs (A$_v \leq$ 8 mag), which is consistent with the field star initial mass function for YSOs with masses >0.2 M$_\odot$. There may be a deficit of brown dwarfs but this result relies on completeness corrections and requires confirmation.

Subject headings: stars: formation – stars: pre-main-sequence – ISM: individual (ρ Ophiuchi cloud) – open clusters and associations: individual (Upper Scorpius)

1. Introduction

An important question in the theory of star formation is whether the initial mass function (IMF) of stars is universal. Variations in the IMF from region to region may hold clues to the roles of accretion, fragmentation, and ejection in producing the stellar mass spectrum (e.g., Bonnell *et al.* 2007). One of the best places to investigate the IMF is in molecular clouds with active star formation since cluster membership is

well-determined, low mass stars have had a limited amount of time to segregate, and one can associate variations in the IMF to the physical conditions of the cloud. Due to large columns of dust obscuring all but the brightest objects in the cloud, IMF studies of young clusters require unbiased, extinction limited spectroscopic surveys (e.g., Bastian *et al.* 2010).

The ρ Ophiuchi molecular cloud complex is a well-studied, nearby region of active star formation (see Wilking *et al.* 2008 for review). Located at 130 pc from the Sun (Mamajek 2008), its proximity guarantees access to the broadest range of luminosity and mass. Most recently, the Spitzer Space Telescope surveyed ρ Ophiuchi in the mid- and far-infrared as part of the Legacy and guaranteed time programs. About 292 young stellar objects (YSOs) were identified with infrared excesses due to circumstellar disks (Evans *et al.* 2009) over a field of view of 6.8 square degrees. X-ray studies have also been conducted of the region with ROSAT, XMM-Newton, ASCA, and Chandra revealing more evolved YSOs with magnetic surface activity (Grosso *et al.* 2000; Gagné *et al.* 2004; Ozawa *et al.* 2005). But for studies of the IMF, one must sample all phases of pre-main-sequence (PMS) evolution from heavily embedded YSOs in their main accretion phase, to classical T Tauri stars (CTTS), to weak-emission T Tauri stars (WTTS) with little or no circumstellar dust. Optical spectroscopic surveys targeting CTTS and WTTS have been conducted of this region, however these studies have been biased toward objects with X-ray emission or YSOs with suspected Hα emission (Bouvier & Appenzeller 1992; Martin *et al.* 1998; Wilking *et al.* 2005). Wilking *et al.* (2005, hereafter Paper I) obtained 136 spectra from 5820Å- 8700Å at a resolution of 2.9 Å and identified 88 cluster members in the main L 1688 cloud of the Ophiuchus complex. The members had a median age of 2.1 Myr and included 39 CTTS. However, their survey had a selection bias toward YSOs with Hα emission.

In this paper, we present the results of a new optical spectroscopic survey

which, when combined with data from Paper I, enables us to construct an unbiased, extinction-limited sample of YSOs in the L 1688 cloud. Section 2 describes this new spectroscopic survey, which covered the wavelength range 6249Å-7657Å with a resolution of 1.4 Å that enabled us to resolve Li in absorption, an indicator of youth. The analysis of the spectra to derive spectral types and exclude background giants is described briefly in Section 3. Section 4 discusses the results of our analysis including the identification of association members, their spatial distribution, their placement in a Hertzsprung-Russell (H-R) diagram relative to several theoretical models and their age distribution. The Section concludes by defining an extinction-limited sample and the resulting disk frequency and distribution of masses in this subsample for comparisons with other star-forming regions. Finally, Section 5 compares low-extinction YSOs in L 1688 with those in Upper Scorpius and explores the relationship between star formation in Upper Scorpius, the surface population in L 1688, and that in the cloud core.

2.   Observations and Data Reduction

Over 200 moderate resolution spectra were obtained for 184 stars identified through R and I band photometry as candidate YSOs. Fifty-two of these stars had spectral classifications reported in Paper I, allowing us to refine our previous spectral classifications. Newly observed YSO candidates numbered 133. These observations are described in detail in the following sections.

2.1.   Sample Selection

Candidate YSOs were selected from an I vs. (R-I) color magnitude diagram. R and I band photometry were obtained from short (5 minute) exposure images obtained with the 0.6 m Curtis-Schmidt Telescope located at Cerro Tololo Inter-American Observatory in 1995 March (see also Wilking *et al.* 1997 for description). The CCD

images covered a $67' \times 68.5'$ area centered on RA(2000) = $16^h\ 27^m\ 14.7^s$, decl.(2000) = $-24°30'06''$ with a scale of $2.03''$ pixel^{-1}. The survey area is shown in Figure 1 relative to the distribution of molecular gas. Photometry was performed using an $8.1''$ diameter aperture optimized for the $4''$ full width at half-maximum of the point-spread function (Howell 1989) with local sky background measured in an annulus $10 - 20''$ in diameter. Zero-points were computed in the Kron-Cousins photometric system using standard star fields established by Landolt (1992). Completeness limits were estimated by adding artificial stars in half magnitude intervals to the images and extracting them using DAOFIND in the Image Reduction and Analysis Facility (IRAF).[1] Recovery of $\geq 90\%$ of the artifical stars occurred for R$\leq$18.1 mag and I$\leq$17.0 mag. Photometry was not reliable for stars with R$\leq$12.4 mag and I$\leq$11.8 due to saturation of the CCD.

An I vs. (R-I) diagram for over 2500 stars is presented in Figure 2. The ordinate is the absolute I magnitude assuming a distance of 130 pc. For stars saturated in our images, R and I band photometry was adopted from the studies of Chini (1981), Gordon and Strom (1990, unpublished data), Bouvier & Appenzeller (1992), or Walter *et al.* (1994). Photometry from Chini was transformed into the Kron-Cousins system using the relations derived by Fernie (1983). The diagram is complete for the brightest stars which are candidate YSOs except for RXJ 1624.9-2459, ROXR1-4/SR-8, SR 24n, HD 148352, and ROXR2-15 for which previous photometry was not available. For comparison, PMS isochrones and the zero-age main sequence (ZAMS) derived from the models of D'Antona & Mazzitelli (1997) are shown (see Section 4.4). One of the known association members, WL 18, has strong Hα emission (EW = 96 Å) relative to the R band continuum which may explain its position below the ZAMS.

From this diagram, we have drawn a sample for spectroscopic follow-up of stars

---

[1]IRAF is distributed by the National Optical Astronomy Observatory, which is operated by the Association of Universities for Research in Astronomy, Inc., under cooperative agreement with the National Science Foundation.

which are on or above the 10^7 year isochrone and brighter than our completeness limits. Samples selected from this region of the color magnitude diagram should be representative for stars earlier than M6 with $A_v \leq 3$ mag and ages $\leq 10^7$ years.

Accurate positions ($<0.5''$) for these stars were obtained using the ASTROM program distributed by the Starlink Project and a set of secondary astrometric standards. The secondary position references were 27 Hα emission line stars with accurate positions determined relative to SAO stars in a 5 square degree region on the Red Palomar Sky Survey plate (Wilking *et al.* 1987). These positions were compared to counterparts from the Two Micron All Sky Survey (2MASS); matches were found within a radius of 2 $''$Positions were then shifted by $+0.2$ s in right ascension to bring them into agreement with the 2MASS coordinate system (Cutri *et al.* 2003).

2.2. Hydra Observations

Optical spectra were obtained for stars located over a 1.3 deg^2 area centered on L 1688 using Hydra, the multi-fiber spectrograph, on two different telescopes. Fiber configurations were designed to observe the maximum number of candidate YSOs; crowding at the edges of our field restricted the number of sources that could be observed. The first set of observations were made using Hydra on the Blanco 4-m telescope at Cerro Tololo Inter-American Observatory on 2003 August 10-12. The Bench Schmidt camera with the SiTe 2kx4k CCD gave a 40$'$ field of view. The 2 $''$ diameter fibers coupled with the 790 lines mm^{-1} KPGLD grating yielded a wavelength coverage of 6275-7975 Å centered near 7125 Å. The spectral dispersion was 0.90 Å pixel^{-1} giving an effective resolution of 2.7 Å. The resolution at the central wavelength was $\lambda/\Delta\lambda$=2600. The second set of observations utilized Hydra on the WIYN 3.5m telescope on 2006 June 15-17[2]. The Bench Spectrograph Camera was used with the

---

[2]The WIYN Observatory is a joint facility of the University of Wisconsin-Madison, Indiana University, Yale University, and the National Optical Astronomy Observatory.

T2KA CCD which gave a 1° field of view. The red fiber cable (2 ″ diameter) and the 1200 lines mm^{-1} grating with a blaze angle of 28.7° were combined with the GG-495 filter to cover the range of 6250-7657 Å centered near 6960 Å. The spectral dispersion was 0.68 Å pixel^{-1} giving an effective resolution of 1.4 Å. The resolution at the central wavelength was $\lambda/\Delta\lambda$=5000. Three fiber configurations were observed at each telescope, set to observe overlapping regions of the 1.3 square degree target field.

The spectra were reduced using IRAF. Images were processed for bias and dark corrections using CCDPROC. Multiple exposures of a given field were median-combined and then reduced with IRAF's DOHYDRA package. The images were flat-fielded using dome flats obtained for each fiber configuration. Sky subtraction was accomplished using the median of 7-10 sky spectra distributed across the field for each configuration. The spectra were wavelength calibrated using 5 s exposures of the PENRAY (CTIO: He, Ne, Ar, Xe) or CuAr (WIYN) lamps taken in each fiber configuration. Scattered light corrections were not made and no flux calibration was performed. In Table 1, we summarize the observations by presenting for each field the observation date and telescope, pointing center, number of candidate YSOs observed, number of exposures, and the total integration time. The typical signal-to-noise ratio for stars with R=16 mag was 30 for the CTIO spectra and 20 for the WIYN spectra as measured by line free regions of the continuum.

3. Analysis of the Spectra

As in Paper I, spectral types were derived from visual classification (visual pattern matching of our smoothed program star spectra with standard star spectra) supported by quantitative analysis of some spectral indices. For the purposes of matching spectral features with those of standard stars, our Hydra spectra were smoothed using a Gaussian filter to the resolution of the standard stars used for direct comparison.

All spectra have been normalized to 1 by dividing out a fit to the continuae, carefully excluding regions with emission lines or broad absorption due to TiO. Normalized spectra were smoothed to a resolution of 5.7 Å for comparison with the spectral standards of Allen & Strom (1995). For giants and later type dwarfs (M5V - M9V), optical spectra from the study of Kirkpatrick *et al.* (1991) were used with an effective resolution of either 8 or 18 Å. The relative strength of absorption due to Hα and a blend of Ba II, Fe I, and Ca I centered at 6497 Å is the most sensitive indicator of spectral type for F-K stars and the depth of the TiO bands for K-M stars.

A rough estimate of the surface gravity of an object is important in distinguishing PMS stars from background giants. The primary gravity-sensitive absorption feature available for analysis in our spectra was the CaH band centered at 6975 Å. This band is evident in the spectra of dwarf stars with spectral types later than K5. Following Allen (1996), we have calculated a CaH index as the ratio of the continuum at 7035±15 Å to the flux in the CaH absorption band at 6975±15 Å and a TiO index (primarily temperature sensitive for stars $\geq$ K5) as the ratio of the continuum at 7030±15 Å to the flux in the TiO absorption band at 7140±15 Å from the unsmoothed, normalized spectrum of each program object. In Figure 3, we plot the CaH index versus TiO index for 136 program objects. Error bars are computed based on the one-sigma error in the mean in flux averages and propagated to the ratios. The solid lines represent first- or second-order fits to the standard star spectra.

4. Results

Spectral types were determined for 174 of 184 stars in this study. These data are presented in Table 2 along with any previous source names, X-ray associations, RA and decl. in J2000, the (R-I) color indices, I magnitudes, and previous spectral classifications. The presence of lithium absorption at 6707 Å and the equivalent width of Hα are also given (emission shown as a negative value). Based on the CaH

index, we have identified nine background giants and seven possible dwarfs. Spectral classifications agree well with optical and infrared spectral types previously published by Bouvier & Appenzeller (1992), Martin *et al.* (1998), Luhman & Rieke (1999), Cieza *et al.* (2010), as well as those in Paper I. A notable exception is WLY 2-48/ISO-Oph 159. Geers *et al.* (2007) report an optical spectral type of M0 while Luhman & Rieke (1999) classify it as earlier than F3. Our spectrum shows broad Hα absorption partially filled in with emission as well as an absorption line from OI at 7774 Å characteristic of early-type stars. The strength of the latter plus the absence of an absorption line due to the blend at 6497 Å (Ba II, Fe I, Ca I) leads us to a spectral classification of A0. This spectral classification is in agreement with that derived by McClure *et al.* (2010).

When combined with the results of Paper I, optical spectra have been obtained for 87% of the stars in the M(I) vs. (R-I) diagram that fell above our completeness limit and on or above the 10^7 year old isochrone. A reanalysis of the R and I band photometry has led us to revise some of the magnitudes published in Paper I. The revised photometry is presented in Table 4 in the Appendix and used to derive the stellar parameters in this paper.

4.1. Emission-line Spectra

In our previous study, 39 of 131 sources (30%) were found to have strong Hα emission characteristic of CTTS. In this sample, which was not biased toward the detection of Hα emission, 15 sources were found to have EW(Hα) > 10 Å. All of these are newly identified CTTS using this coarse criterion (Herbig & Bell 1988). An additional 17 objects showed weaker Hα emission (10 Å > EW(Hα) > 5 Å) with all but one having an M spectral type. The variable nature of Hα emission is evident when comparing stars observed days apart and stars observed in this study and in Paper I.

4.2. Identification of Pre-main-sequence Association Members

Identification of 35 new PMS objects was accomplished using the same membership criteria as in Paper I with some additional criteria as described below. An additional 13 YSOs with optical spectral types were taken from the literature. Combined with the 87 association members from Paper I, there are a total of 135 objects with optical spectral types that meet one or more of these criteria. These objects are listed in Table 3.[3] Ninety percent of the YSOs in our sample have K or M spectral types.

The criteria include the following:

- Hα in emission with EW > 10 Å during at least one observation, characteristic of CTTSs. Fifty-three objects fit this criterion.

- Association with X-ray emission is a signpost of youth and has been observed in 82 stars in our sample.

- The presence of lithium absorption is an indicator of youth for stars with spectral type K0 and cooler and clearly resolved in the spectra of 46 stars.

- A mid-infrared excess as observed by Infrared Space Observatory (ISO) with a spectral index from 2.2-14 μm (Bontemps *et al.* 2001) or the Spitzer Space Telescope from 3.6-24 μm (Wilking *et al.* 2008) indicative of a circumstellar disk. Thirty-eight objects display a mid-infrared excess.

- A proper motion in common with the association mean as noted by Mamajek (2008). In addition, we include Object 1-3 from this study as a common proper motion member based on data from the UCAC3 catalog.

---

[3]One object, [WMR2005] 3-17, was removed as an association member from Paper I since one could not rule out that it is a background giant.

- Two early-type stars, HD 147889 and Source 1, are associated with reflection nebulosity in the R and I band images.

- Finally, 100 objects (excluding giants identified in Section 3) that are too luminous to be main sequence objects at the distance to ρ Oph *and* have an estimate for A_v too high to be foreground to the cloud ($A_v > 1.5$ mag).

We have noted in Table 3 objects with near-infrared variability from the study of Alves de Oliveira & Casali (2008) but do not require this for association membership. Only one of the objects classified as a possible dwarf based on the CaH index, Object 4-52, displayed a criterion for association membership and is included in Table 3.

Mamajek (2008) has noted that proper motion data for two of the objects in Table 3, X-ray sources GY 280 and HD 148352, are discordant and are possible foreground objects. Despite this fact, we include them in Table 3 but note that X-ray emission alone may not be sufficient to identify YSOs.

4.3.   Distribution of Association Members

The distribution of the 135 association members identified by this study is shown in Figure 1 relative to contours of ^{13}CO column density which delineate the cloud boundaries (Loren 1989). Star symbols mark the locations of the multiple B star ρ Oph and the three most massive members of the L 1688 embedded cluster: HD 147889, Source 1, and SR 3. While the association members are concentrated toward the molecular gas, there is marked lack of association members in the direction of the cold, dense cores B and E. A comparison of this distribution with that of association members identified at all wavelengths (Wilking *et al.* 2008) confirms that we are missing the youngest and most highly obscured YSOs in the cloud.

4.4. Hertzsprung-Russell Diagram

To derive luminosities, we began by dereddening sources using the $(R - I)$ color index assuming the reddening law derived by Cohen *et al.* (1981) in the Kron-Cousins system:

$A_v = 4.76$ E(R-I), Sp Ty $< A0$ (early-type) (1)

$A_v = 6.25$ E(R-I), Sp Ty $\geq A0$ (late-type) (2)

where R $= 3.2$ for early-type stars and 3.8 for late-type stars. R and I band data were taken from this study except where noted in Column 6 of Table 3. For five sources, R and I band data were not available and sources were dereddened using J and H band data from the 2MASS survey (Cutri *et al.* 2003) and transformed into the CIT photometric system using the relationships derived by Carpenter (2001). A sixth source (WL 18) was dereddened using J and H magnitudes since strong Hα emission distorts its R band magnitude. In these latter cases, we used the relation for the CIT photometric system

$A_v = 9.09$ E(J-H) (Cohen *et al.* 1981). (3)

In a few instances, the errors in the photometry and/or spectral classifications yielded negative values for the extinction of a few tenths and an extinction of 0.0 was assumed.

Effective temperatures were derived from the spectral classifications with typical uncertainties of ± 150 K for K-M stars. We note that the assumption of dwarf, rather than subgiant, surface gravities will *overestimate* T_{eff} for stars with spectral types of G5-K5 by <250 K and *underestimate* T_{eff} for stars with spectral types of M2-M8 by <200 K (e.g., Drilling & Landolt 2000). Intrinsic colors and bolometric corrections for dwarf stars were taken from the works of Schmidt-Kaler (1982) for B8-K5 stars and from Bessell (1991) for K5-M7 stars. For the three B stars, we adopted the intrinsic colors, bolometric magnitudes, and temperatures from Drilling & Landolt

(2000), converting the colors into the Kron-Cousins system. For the M8 brown dwarf candidates, we assumed values of T_{eff} = 2400, $(R - I)_0$ = 2.5, and BC(I) = -1.7 (Dahn *et al.* 2002; Hawley et al. 2002).

The absolute I magnitude, M(I), was computed given the extinction and assuming a distance of 130 pc. We then derived the bolometric magnitude and luminosity given:

$$M_{bol} = M(I) + BC(I) \ (4),$$

and

$$\log(L_{bol}/L_{\odot}) = 1.89 - 0.4 \ M_{bol} \ , \ M_{bol}(\odot) = 4.74. \ (5)$$

In the situations where J and H were used to deredden, M(J) is recorded in Column 7 of Table 3 and was used along with BC(J) to derive M_{bol}. The median error in log(L) is computed to be 0.14 dex by adding quadratically errors in the R and I photometry, an uncertainty in the distance modulus of 0.17 mag corresponding to a depth of 10 pc, and an uncertainty 0.03 mag in the intrinsic color and 0.1 mag in the bolometric correction due to spectral type errors. In most cases the dominant error was the uncertainty in the distance modulus.

H-R diagrams for 135 association members were made using tracks and isochrones from D'Antona & Mazzitelli (1997, DM) F. D'Antona & I. Mazzitelli (1998, private communication), Palla & Stahler (1999, PS99), and Siess *et al.* (2000). Despite the differences in treatments of the equation of states as a function of mass and of convection, the models give very similar results for our sample. The diagrams for the former two are shown in Figure 4 as they represent the broadest range in mass. The masses and ages interpolated from the DM models are given in Table 3. Since most of the objects lie on convective tracks, uncertainties in the mass *relative to the DM models* were estimated from the errors in the spectral classifications and uncertainties in the age from errors in the luminosities. Uncertainties in the mass for objects in the

range of 0.08-1.3 $M_\odot$ were typically 16%-30%, with the higher value corresponding to the lower mass objects. Uncertainties in the log(age) were 0.17-0.25 dex relative to DM models with the greater uncertainty for the higher mass objects. We note that uncertainties in the absolute masses and ages will be larger with theoretical mass tracks underpredicting absolute stellar mass by 30% - 50% (Hillenbrand 2009). No age or mass estimate was possible for RXJ 1624.9-2459 as it fell below the 10^8 year isochrone.

4.5. Age Distribution

The values for log(age) derived from the DM models are consistent with a normal distribution with an average log(age) of 6.49$\pm$0.05 (3.1 Myr). Ages derived from the PS99 models agree surprisingly well while the Siess *et al.* models yield systematically older ages for log(age)$\leq$7.0; the difference can be as much as 0.4 dex for a DM age of 1 Myr. Given the large areal coverage of our survey (1.3 deg^2 or 6.8 pc^2), which must include members of the Upper Sco subgroup, an age spread in our sample would not be unexpected. However, simulations do not suggest an *intrinsic* age spread. Assuming Gaussian-distributed errors in log T and log L and using the DM models for 3 Myr, a Monte Carlo simulation derived values of log T and log L for over 12,000 samples in the mass range of 0.12 - 1.0 $M_\odot$ weighted by the Chabrier (2003) system mass function. While the simulated age distribution appears somewhat narrower than what we observe, a Kolmogorov-Smirnov (K-S) test cannot reject the null hypothesis that the two samples are drawn from the same parent population at the 3% level. Lack of strong evidence for a large age spread is consistent with what is found in other young clusters or associations (e.g., Hillenbrand 2009; Slesnick *et al.* 2008) and supports the idea of rapid star formation (Hartmann 2001).

The average age for this sample is somewhat older than the average of 0.3 Myr derived from more obscured sources in the core using the DM models and dereddened

using JHK photometry (e.g., Greene & Meyer 1995; Luhman & Rieke 1999; WGM99; Natta *et al.* 2002). However, we note that there are systematic differences in our derived luminosities, and hence ages, when (J-H) photometry is used to deredden sources instead of (R-I). Using (J-H) colors from 2MASS yields systematically higher values for A_v and hence L_{bol}. As a consequence, the average log(age) for our sample dereddened with (J-H) colors is 6.14±0.05 (1.4 Myr) compared to 6.49±0.05 (3.1 Myr) when (R-I) is used. Indeed, a K-S test applied to both versions of our age distributions suggests that the difference is significant. The reason for this discrepancy is not understood but could involve the adopted reddening law (Cohen *et al.* 1981), surface gravity effects, or possible excess emission in the J and H bands from optically-thick disks. J and H band excesses will overestimate the luminosity which leads to an underestimate of ages (Cieza *et al.* 2005). Regardless, the older average age for our sample relative to the more obscured sources is significant when both samples are dereddened using (J-H) (1.3 Myr vs. 0.3 Myr) even considering that the previous studies used the pre-Hipparcos distance of 160 pc.

4.6. An Extinction-limited Sample

To explore the frequency of circumstellar disks and the IMF, we considered 123 objects that formed an extinction-limited sample with $A_v \leq 8$ mag. This sample is representative for objects with $M \geq 0.2$ $M_\odot$ for an age of 3 Myr using the DM models.

4.6.1. Disk Frequency

Using published data from the ISO (Bontemps *et al.* 2001) and the Spitzer Space Telescope (Evans *et al.* 2009), we can look for a mid-infrared excess relative to the photosphere using the spectral index from 2.2-14 μm or 3.6-24 μm, respectively. The spectral index is defined as

$$\alpha = dlog\lambda F_\lambda / dlog\lambda$$

A mid-infrared excess is defined as $\alpha \geq$ -1.60 which is characteristic of an optically-thick disk (e.g., Greene *et al.* 1994). This results in 33 of the 123 sources, or 27% $\pm$ 5%, showing evidence for a circumstellar disk lacking a large inner hole (see Table 3) with the uncertainty estimated assuming Poisson statistics (Gehrels 1986). We adopt this disk frequency estimated over near- to mid-infrared wavelengths as the most reliable disk indicator. The sample size is not sufficient to investigate possible variations in the disk frequency with spectral type.

As a check, we can use the slope of the 3.6-8.0 μm flux densities from the Spitzer Space Telescope to assess the fraction of sources with mid-infrared excesses. A linear least squares fit was made to the flux densities for each source compiled from the Spitzer c2d catalog available in NASA/IPAC Infrared Science Archive. Following Lada *et al.* (2006), disk models suggest that $\alpha \geq$ -1.80 over this wavelength range is indicative of an optically thick disk. The distribution of spectral indices as a function of spectral type is shown in Figure 5. For the 122 sources for which data were available, 40 or 33% $\pm$ 5% showed evidence for an optically thick disk consistent with our previous estimate. We can compare this disk frequency to that derived by Lada *et al.* for the IC 348 cluster who considered 299 YSOs, most of which reside in area completely sampled for M > 0.3 $M_\odot$ and A_v <4 mag (Luhman *et al.* 2003). Their value of 30% $\pm$ 4% for IC 348 is consistent with our disk frequency which is not surprising given the similarity in the cluster's estimated age of 2-3 Myr (Herbst 2008).

With knowledge of the spectral types, we can also look for evidence of even smaller infrared excesses from the inner disk in the K band. Using data from the 2MASS survey, we transformed the magnitudes into the CIT system and dereddened them using Equation (3). Assuming that the excess at J was zero, the difference of

the dereddened (J-H) color to the intrinsic color was then used to estimate

$$r_H = F_{H_{ex}}/F_H$$

where $F_{H_{ex}}$ is the broadband flux from circumstellar emission and F_H is the expected stellar flux at 1.6 μm. This was then used to estimate the excess at K:

$$r_K = F_{K_{ex}}/F_K = (1 + r_H)(10^{[(H-K)-(H-K)_0-0.065A_v]/2.5} - 1).$$

Values of ΔK = log(1 + r_K) were computed and those that equaled or exceeded 0.20 were associated with an optically-thick inner disk (Skrutskie *et al.* 1990). We note that three sources with an apparent K-band excess did not display a mid-infrared excess; all three have values close to ΔK=0.20 and may be identified as excess sources due to photometric errors. Twenty-three of 123 sources, or 19% ± 4%, showed evidence for an optically thick inner disk. While the assumption of no excess emission at J could underestimate ΔK, the higher percentage of mid-infrared excess sources is typical of young clusters and likely reflects the greater sensitivity of mid-infrared photometry to disk emission (e.g., Meyer *et al.* 1997; Haisch *et al.* 2000). The dispersal of the inner disk by accretion, stellar winds, and/or planet formation could also contribute to the lower disk frequency derived from the K-band. Candidate transition disk objects with a mid-infrared excess and ΔK≤0.10 include WSB 18, ISO-Oph 1, WSB 52, ISO-Oph 195, and Object 2-57, SR 21, DoAr 25, SR 9, and WMR 2-37. The latter four have been confirmed as transition disk objects through modeling of their spectral energy distributions from optical through millimeter wavelengths (Eisner *et al.* 2009; Cieza *et al.* 2010; Andrews *et al.* 2011).

4.6.2. Initial Mass Function

Previous investigations of the IMF in ρ Ophiuchi have produced diverse results. Luhman & Rieke (1999) used K band spectra for approximately 100 stars; mass

estimates for 36 plus completeness corrections were used to construct an IMF. Their IMF is roughly flat from 0.05-1 $M_\odot$ and peaks at $\sim$0.4 $M_\odot$. de Marchi *et al.* (2010) use these data and fit it to a tapered power-law, and derive a characteristic mass of 0.17 $M_\odot$. Marsh *et al.* (2010) also derive an IMF for ρ Ophiuchi which continues to rise into the brown dwarf regime, however this study was completely photometric in nature.

We divided the 123 YSOs that formed an extinction-limited sample ($A_v \leq 8$ mag) into mass bins with a width in log(mass) of 0.4 dex. No correction was made for close binaries. A plot of the resulting mass function, shown in Figure 6, displays a peaks and turns over at 0.13 $M_\odot$. [4] The last three mass bins are not complete for $A_v = 8$ mag, so completeness corrections were made assuming an age of 3 Myr. To this end, the maximum visual extinction to which a source could be observed, $A_{v_{max}}$, was estimated for a source in the center of each mass bin using the DM models and assuming an I band limiting magnitude of 15.9. This value, estimated from Figure 2, is where the 3 Myr isochrone intersects our completeness limit. To account for variations in extinction within the region, we used the extinction maps from Ridge et al. (2006) with an effective resolution of 3′. The fractional area of our survey box with A_v=0-2, 2-4, 4-6, 6-8, and >8 mag was estimated to be 0.09, 0.32, 0.24, 0.14, and 0.21, respectively. We then estimated the number of missing sources for each extinction interval assuming a uniform stellar surface density weighted by the fractional area. For the three lowest mass bins, the number of sources would increase by a factor of 1.04, 1.43, and 3.32. While our completeness corrections are dependent on the choice of PMS model and reddening law, the use of other models instead of DM does not significantly change these corrections.

For comparison with our IMF, the lognormal system mass function derived by

---

[4]Objects in mass function with known subarcsecond companions include GSS 5, HD 147889, WLY 2-2, WSB 38, SR 12, SR 9, VSSG 14, SR 24N, ROX 31, SR 20, and SR 13 (see Barsony *et al.* 2003, and references therein).

Chabrier (2003) for field stars with M≤1.0 $M_\odot$ is shown in Figure 6 integrated over our mass bins and normalized to the observed number of objects in the 0.08-0.20 $M_\odot$ mass bin. For M> 1.0 $M_\odot$, a power law of the form $\zeta(\log m) \propto m^{-1.3}$ was used. Error bars plotted in Figure 6 were calculated using the methods of Gehrels (1986) and multiplied by our completeness corrections. In order to make an overall (large scale) comparison of the IMF with other regions and the field star IMF, we computed the ratio of high (1 - 10 $M_\odot$) to low (0.1 - 1 $M_\odot$) mass stars. For our sources, this ratio is R = 0.12 and 0.10 when including our completeness corrections with an uncertainty of ±0.04 calculated using the methods of Gehrels (1986). Our value of R is in agreement with values found for ρ Ophiuchi and other young embedded clusters (Meyer *et al.* 2000). The ratio of high-to-low mass stars for a Chabrier system IMF is 0.16, hence we conclude that coarsely our mass function is consistent with that of the field star IMF. To make a more detailed comparison, a K-S test was performed over the mass ranges for which no completeness corrections were necessary (M>0.2 $M_\odot$). We cannot reject the null hypothesis that the samples were drawn from the same parent population with a probability of 40%, suggesting that the IMF of ρ Ophiuchi is not significantly different from the field star IMF over this mass range.

When examined in more detail, there might be subtle differences between our mass function and the field star IMF. Chabrier's (2003) lognormal IMF underestimates the number of objects in the mass bin centered at 0.13 $M_\odot$. In Chabrier (2003), a characteristic mass of 0.22 $M_\odot$ was derived for the field star IMF, however we find that our most frequently occurring mass is 0.13 $M_\odot$. Moreover we note that our lowest mass bin, which is made up of brown dwarfs, has fewer objects than predicted by the model. These differences may be artifacts of methods used to derive our IMF. To quantify the possible deficit, we calculated the ratio of low mass stars (0.08 - 1 $M_\odot$) to brown dwarfs (≤ 0.08 $M_\odot$). Using our completeness corrected sample, we derive a ratio of 9.1 (+3.3,-2.6) with errors calculated using methods of Gehrels (1986). While this value is within the range found by Andersen *et al.* (2008) for

other star forming regions, it is higher than values derived for ρ Ophiuchi by other studies (Geers *et al.* 2011; Alves de Oliveira *et al.* 2010). We note that both of these studies were biased toward finding brown dwarfs and only a small subset of their data was confirmed spectroscopically. However as shown in Figure 6, when the errors in our completeness corrected values are taken into account, this deficit may not be significant. We conclude that the turnover in our IMF is real, but it is uncertain if there is a real deficit of brown dwarfs compared to the field star IMF. Given the difficulty of estimating completeness corrections for the brown dwarf regime, more sensitive spectroscopic surveys are needed to sample completely this population.

Finally, we compare our IMF to that derived for other star forming regions, noting that it is dubious to compare directly IMFs which have been derived using different methods. The IMF in the Taurus star-forming cloud differs from most other star-forming regions in that it displays a higher characteristic mass ($\sim$0.8 M$_\odot$) as well as a corresponding deficit of brown dwarfs (Briceno *et al.* 2002; Luhman 2004). The IMFs derived for the Orion Nebula Cluster (ONC), IC 348 cluster, and Upper Scorpius are more similar to that in L 1688. While all show a turnover at low mass (Slesnick *et al.* 2004; Luhman *et al.* 1998; Slesnick *et al.* 2008), a somewhat higher characteristic mass of approximately 0.2 M$_\odot$ is reported for the ONC and IC 348. Our peak mass of 0.13 M$_\odot$ is very similar to that reported by Slesnick, Hillenbrand, & Carpenter (2008) for Upper Scorpius, but unlike our study, they report an *excess* of brown dwarfs relative to the field.

5.   Temporal Relationship with Upper Sco

Given the larger data set for YSOs distributed in the low extinction regions of the L 1688 cloud, we revisited the relationship between star formation in this extended region (6.8 pc^2) to that in the L 1688 cloud core and in the Upper Scorpius subgroup of the Sco-Cen OB association. As noted in Paper I and Section 4.5,

spectroscopic studies of embedded sources in the 1 pc x 2 pc centrally condensed core have consistently yielded ages between 0.1-1 Myr when using the D'Antona & Mazzitelli tracks and isochrones, with a median age of 0.3 Myr. The median age for the distributed population is significantly older than that in the higher extinction cloud core.

In Paper I we compared our H-R diagram for 88 association members in L 1688 with that of the 252 members of the Upper Scorpius subgroup compiled by Preibisch *et al.* (2002) and noted there were no significant differences in age between the two samples. However, comparisons with the Upper Scorpius sample are more complicated since Preibisch *et al.* derived temperatures and luminosities in a different manner. For example, R and I band photometry was obtained from the UKST Schmidt plates, intrinsic colors from Hartigan *et al.* (1994), and the reddening law from Herbig (1998) plus a combination of evolutionary models were used (but primarily those of Palla & Stahler 1999). To ease the comparison between the two samples, we compiled (J-H) photometry for sources in both samples from the 2MASS catalog (Cutri *et al.* 2003), transformed it to the CIT system, and derived extinctions and luminosities as described in Section 4.4. A dwarf temperature scale was used to relate spectral types in both samples to effective temperatures. We note that a distance of 130 pc was used for L 1688 and 145 pc for Upper Sco (de Zeeuw *et al.* 1999). The H-R diagram for the Upper Sco sample is shown in Figure 7 relative to the theoretical tracks and isochrones from D'Antona & Mazzitelli. Ages were interpolated for sources in both samples using the DM models. The average log(age) for the Upper Sco sample is 6.43 (2.7 Myr) compared to 6.14 (1.4 Myr) for L 1688. A K-S test applied to both samples suggests that they are not drawn from the same parent population. Hence in this reanalysis, the low mass objects distributed across the L 1688 cloud appear intermediate in age between low mass stars in Upper Sco and YSOs embedded in the centrally condensed core. Consistent with this picture is the lower fraction of K0-M5 stars in Upper Sco with optically-thick disks (19%; Carpenter *et al.* 2006) compared

to ∼30% from this study.

Do the timescales involved allow the formation of the distributed population of L 1688 to be triggered by events in Upper Sco? If a supernova helped power an expanding HI shell originating in Upper Sco and moving at ∼15 km s^{-1} as proposed by de Geus (1992), then in 1 Myr it would move about 15 pc and barely cover the distance in the plane of the sky between the center of Upper Sco and L 1688. A triggering event from Upper Sco would be consistent with the average age difference of ∼1.3 Myr between low mass stars in Upper Sco and L 1688. By retracing the motions of high proper motion objects, Hoogerwerf *et al.* (2001) suggest that a supernova in a binary system occurred in Upper Sco about 1 Myr ago that produced the runaway star ζ Oph and the pulsar PSR J1932+1059. But this would have been too recent for a shock wave to cross the 15 pc expanse between the two regions and initiate the formation of low mass YSOs in L 1688 with an average age of 2-3 Myr, thus requiring an earlier event.

6.   Summary

Over 200 moderate resolution optical spectra were obtained for candidate YSOs in a 1.3 deg^2 area centered on L 1688. When combined with the 136 spectra obtained in our initial spectroscopic study in Paper I, 135 objects with optical spectral types are now identified as association members based on the presence of Hα in emission, X-ray emission, lithium absorption, a mid-infrared excess, a common proper motion, reflection nebulosity, or extinction considerations. Fifteen of these display Hα in emission consistent with being newly identified CTTS.

Masses and ages were derived for association members using several theoretical models. Using the tracks and isochrones from D'Antona & Mazzitelli (1997) and F. D'Antona & I. Mazzitelli (1998), we derive an average age of 3.1 Myr for this distributed population. We find a circumstellar disk frequency of 27% ± 5% for

our sample, consistent with our derived age and results from other studies. Nine sources are identified as candidate transition disk objects with mid-infrared excesses and no significant K band excess; four of these have been confirmed by recent studies. When compared to simulations, our data are consistent with sampling a single age, artificially spread by uncertainties in the distance, spectral type, and surface gravity suggesting any intrinsic age spread is small. The age of 3.1 Myr for this surface population is intermediate between that of YSOs embedded in the cloud core of ρ Ophiuchi and low mass stars in Upper Sco.

We also constructed an IMF for an extinction-limited sample of 123 YSOs ($A_v \leq$ 8 mag), which is a significant increase in sample size and mass range over previous studies. The resulting IMF is consistent with the field star IMF for YSOs with mass >0.2 $M_\odot$. However it may be inconsistent for masses below 0.2 $M_\odot$. We find that our sample has a lower characteristic mass ($\sim$0.13 $M_\odot$) than the field star IMF as well as a possible deficit of brown dwarfs.

A.   Photometry Revised from Paper I

A reanalysis of the R and I band photometry presented in Table 2 of Paper I necessitated some revisions. These revisions, presented in Table 4, are due in large part because of saturation problems with some of the brighter association members. In these cases, photometry was adopted from other studies as noted.

REFERENCES

Allen, L.E. 1996, Ph.D. thesis, University of Massachusetts

Allen, L.E. & Strom, K.M. 1995, AJ, 109, 1379

Alves de Oliveira, C., & Casali, M. 2008, A&A, 485, 155

Alves de Oliveira, C., Moraux, E., Bouvier, J., *et al.* 2010, A&A, 515, A75

Andersen, M., Meyer, M., Greissl, J., & Aversa, A. 2008, ApJ, 683, L183

Andrews, S. M., Wilner, D. J., Espaillat, C., *et al.* 2011, ApJ, 732, 42

Barsony, M., Koresko, C., & Matthews, K. 2003, ApJ, 591, 1064

Bastian, N., Covey, K.R., & Meyer, M.R. 2010, ARA&A, 48, 339

Bessell, M.S. 1991, AJ, 101, 662

Bonnell, I. A., Larson, R. B., & Zinnecker, H. 2007, in Protostars and Planets V, ed. B. Reipurth, D. Jewitt, & K. Keil (Tucson, AZ: Univ. Arizona Press), 149

Bontemps, S., André, P. Kaas, A., *et al.* 2001, A&A, 372, 173

Bouvier, J. & Appenzeller, I. 1992, A&AS, 92, 481

Briceno, C., Luhman, K. L., Hartmann, L., Stauffer, J. R., & Kirkpatrick, J. D. 2002, ApJ, 580, 317

Carpenter, J.M. 2001, AJ, 121, 2851

Carpenter, J.M., Mamajek, E. E., Hillenbrand, L. A., & Meyer, M. R. 2006, ApJ, 651, L49

Casanova, S., Montmerle, T., Feigelson, E. D., *et al.* 1995, ApJ, 439, 752

Casassus, S., Dickinson, C., Cleary, K., *et al.* 2008, MNRAS, 391, 1075

Chabrier, G. 2003, PASP, 115, 763

Chini, R. 1981, A&A, 99, 346

Cieza, L. A., Kessler-Silacci, J. E., Jaffe, D. T., Harvey, P. M., Evans, N. J., II, 2005, ApJ, 635, 422

Cieza, L. A., Schreiber, M. R., Romero, G. A., *et al.* 2010, ApJ, 712, 925

Cohen, J.G., Frogel, J.A., Persson, S.E., & Elias, J.H. 1981, ApJ, 249, 481

Cohen, M. & Kuhi, L. V. 1979, ApJS, 41, 743

Cutri, R.M., et al., 2003, 2MASS All Sky Catalogue of Point Sources (The IRSA 2MASS All-Sky Point Source Catalog, NASA/IPAC Infrared Science Archive.)

D'Antona, F. & Mazzitelli, I. 1997, Mem. Soc. Astron. Ital., 68, 807

Dahn, C. et al. 2002, AJ, 124, 1170

de Geus, E. J. 1992, A&A, 262, 258

de Marchi, G., Paresce, F., & Portegies Zwart, S. 2010, ApJ, 718, 105

de Zeeuw, P. T., Hoogerwerf, R., Bruijne, J. H. J., Brown, A. G. A., & Blaauw, A. 1999, AJ, 117, 354

Dolidze, M. V. & Arakelyan, M. A. 1959, Soviet Astron., 3, 434

Drilling, J. S. & Landolt, A.U. 2000, in Astrophysical Quantities, ed. A. Cox (4th ed.; New York: AIP Press), 381

Eisner, J. A., Monnier, J. D., Tuthill, P., & Lacour, S. 2009, ApJ, 698, L169

Elias, J. H. 1978, ApJ, 224, 453

Evans, N. J., II, Dunham, M. M., Jorgenson, J. K., *et al.* , 2009, ApJS, 181, 321

Fernie, J. D. 1983, PASP, 95, 782

Gagné, M., Skinner, S., & Daniel, K. 2004, ApJ, 613, 393

Geers, V. C., Pontoppidan, K. M., van Dishoeck, E., *et al.* 2007, A&A, 476, 279

Geers, V.C., Scholz, A., Jayawardhana, R., *et al.* 2011, ApJ, 726, 23

Gehrels, N. 1986, ApJ, 303, 336

Grasdalen, G. L., Strom, K. M., Strom, S. E. 1973, ApJ, 184, L53

Greene, T. P. & Meyer, M. R. 1995, ApJ, 450, 233

Greene, T. P., Wilking, B. A., André, Ph., Young, E. T., & Lada, C. J. 1994, ApJ, 434, 614

Greene, T. P. & Young, E T. 1992, ApJ, 395, 516

Grosso, N., Montmerle, T., Bontemps, S., André, Ph., & Feigelson, E. 2000, A&A, 359, 113

Haisch, K. E., Lada, E. A., & Lada, C. J. 2000, AJ, 120, 1396

Hartigan, P., Strom, K. M., & Strom, S. E. 1994, ApJ, 427, 961

Hartmann, L. 2001, AJ, 121, 1030

Hawley, S. et al. 2002, AJ, 123, 3409

Herbig, G. H. 1998, ApJ, 497, 736

Herbig, G. H. & Bell, K. R. 1988, Third Catalog of Emission-Line Stars of the Orion Population (Lick Obs. Bull. No. 1111; Santa Cruz, CA: Lick Observatory)

Herbst, W. 2008, in Handbook of Star Forming Regions Vol.I, ed. B. Reipurth (San Francisco, CA: ASP), 372

Hillenbrand, L. A. 2009, in IAU Symp. 258, The Ages of Stars, ed. E. E. Mamajek, D. R. Soderblom, & R. Wyse (Cambridge: Cambridge Univ. Press), 81

Hoogerwerf, R., de Bruijne, & de Zeeuw 2001, A&A, 365, 49

Houk, N. & Smith-Moore, M. 1988, Michigan Catalog of Two-Dimensional Spectral Types for the HD Stars, Vol. 4 (Ann Arbor, MI: Univ. Michigan)

Howell, S. B. 1989, PASP, 101, 616

Imanishi, K., Koyama, K., & Tsuobi, Y. 2001, ApJ, 557, 747

Kirkpatrick, J.D., Henry, T.J., & McCarthy, D.W. 1991, ApJS, 77, 417

Lada, C. J., Muench, A. A., Luhman, K. L., *et al.* 2006, AJ, 131, 1574

Landolt, A.U. 1992, AJ, 104, 340

Loren, R. B. 1989, ApJ, 338, 925

Luhman, K. L. 2004, ApJ, 617, 1216

Luhman, K. L. & Rieke, G. H. 1999, ApJ, 525, 440

Luhman, K. L., Rieke, G. H., Lada, C. J., & Lada, E. A. 1998, ApJ, 508, 347

Luhman, K.L., Stauffer, J. R., Muench, A. A., *et al.* 2003, ApJ, 593, 1093

Mamajek, E., 2008, Astron. Nachr., 329, 10

Marsh, K., Plavchan, P., Kirkpatrick, J., *et al.* 2010, ApJ, 719, 550

Martín, E. L., Montmerle, T., Gregorio-Hetem, J., & Casanova, S. 1998, MNRAS, 300, 733

McClure, M. K., Furlan, E., Manoj, P., *et al.* 2010 ApJ, 188, 75

Meyer, M. R., Adams, F. C., Hillenbrand, L. A., Carpenter, J. M., & Larson, R. B., 2000, in Protostars and Planets IV, ed. V. Mannings, A. P. Boss, & S. S. Russell (Tucson, AZ: Univ. Arizona Press), 121

Meyer, M. R., Calvet, N., & Hillenbrand, L. A. 1997, AJ, 114, 288

Montmerle, T., Koch-Miramonde, L., Falgarone, E., *et al.* 183, ApJ, 269, 182

Natta, A., Testi, L., Comerón, F., *et al.* 2002, A&A, 393, 597

Ozawa, H., Grosso, N., & Montmerle, T. 2005, A&A, 429, 963

Palla, F., & Stahler, S.W 1999, ApJ, 525, 772

Prato, L. 2007, ApJ, 657, 338

Preibisch, T., Brown, A. G. A., Bridges, T., Guenther, E., & Zinnecker, H. 2002, AJ, 124, 404

Preibisch, T. & Zinnecker, H. 1999, AJ, 117, 2381

Ridge, N. A., Di Francesco, J., Kirk, H., *et al.* 2006, AJ, 131, 2921

Schmidt-Kaler, Th. 1982, in Landolt-Bornstein New Series, Numerical Data and Functional Relationships in Science and Technology, Group 4, Vol. 2b, ed. K. Schaffers & H.H. Voigt (New York: Springer), 451

Siess, L., Dufour, E., & Forestini, M. 2000, A&A, 358, 593

Skrutskie, M. F. et al 1990, AJ, 99, 1187

Slesnick, C. L., Hillenbrand, L. A. & Carpenter, J. M. 2004, ApJ, 610, 1045

Slesnick, C. L., Hillenbrand, L. A. & Carpenter, J. M. 2008, ApJ, 688, 377

Struve, O. & Rudkjobing, M. 1949, ApJ, 109, 92

Torres, C. A. O., Quast, G. R., da Silva, L., *et al.* 2006, A&A, 460, 695

Vrba, F. J., Strom, S. E., Strom, K. M. 1976, AJ, 81, 958

Vrba, F. J., Strom, K. M., Strom, S. E., *et al.* 1975, ApJ, 197, 77

Walter, F. M. et al. 1994, AJ, 107, 692

Wilking, B. A., Gagné, M., & Allen, L. E., 2008, in Handbook of Star Forming Regions Vol.II, ed. B. Reipurth (San Francisco, CA: ASP), 351

Wilking, B. A. & Lada, C. J. 1983, ApJ, 274, 698

Wilking, B. A., Lada, C. J., & Young, E. T. 1989, ApJ, 340, 823

Wilking, B. A., Meyer, M. R., Robinson, J. G., & Greene, T. P., 2005, AJ, 130, 1733 (Paper I)

Wilking, B. A., Schwartz, R. D., & Blackwell, J. H. 1987, AJ, 94, 106

Wilking, B. A., Schwartz, R. D., Fanetti, T., & Friel, E. 1997, PASP, 109, 549

Zacharias, N., Finch, C., Girard, T., *et al.* 2009, VizieR On-Line Data Catalog: I/315

L1688
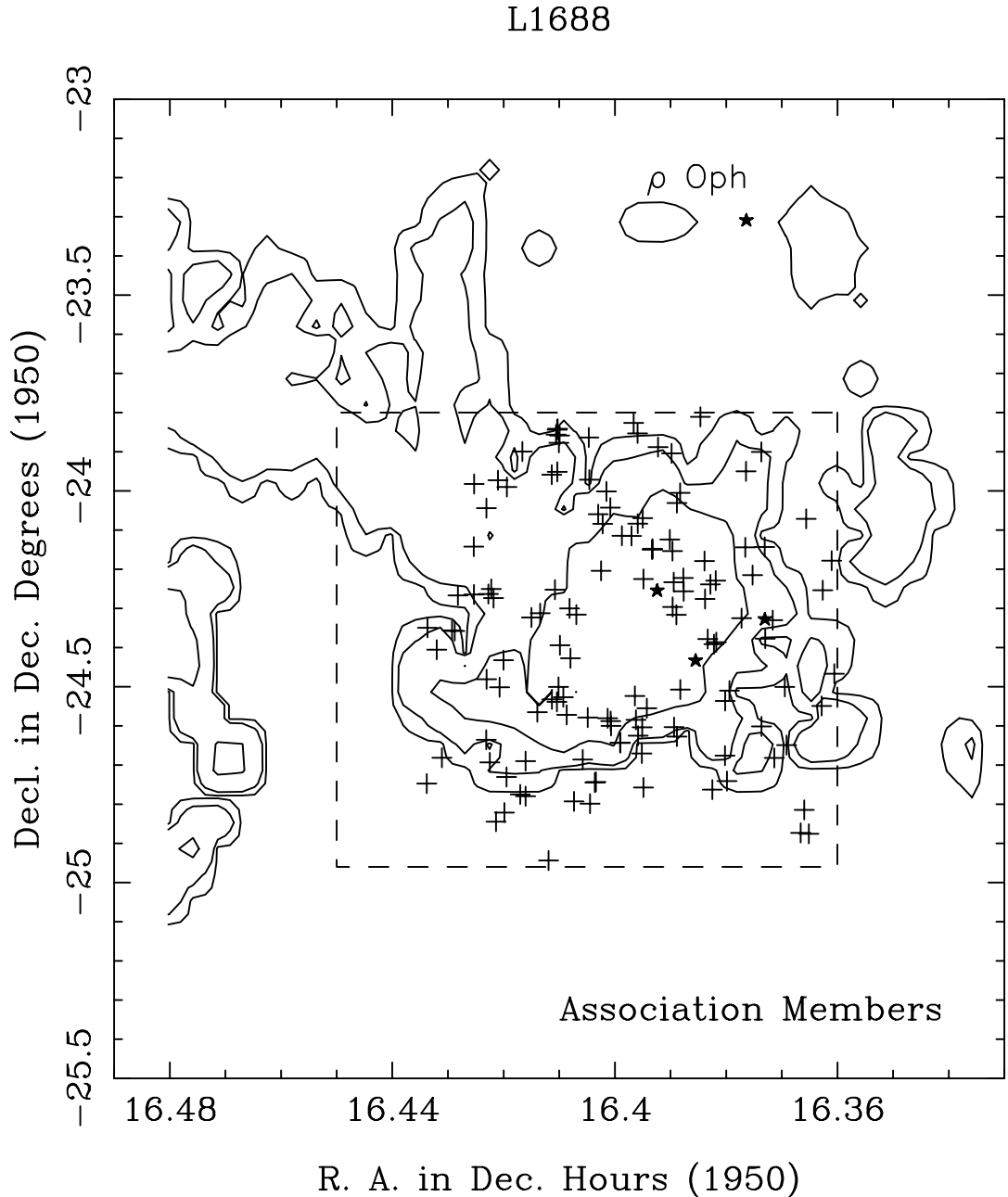
Fig. 1.— Distribution of association members is shown relative to contours of ^{13}CO column density. The contours were computed from Loren (1989) assuming LTE and T_{ex} = 25 K. The values of the contours in units of cm^{-2} are 6×10^{14}, 3×10^{15}, and 1.5×10^{16}; the lowest contour delineates the outer boundary of the dark cloud. The dashed box outlines the field included by our Hydra observations. Star symbols mark the locations of the star ρ Oph A (labeled) and the association members Oph S1, SR 3, and HD 147889 in the L 1688 core.
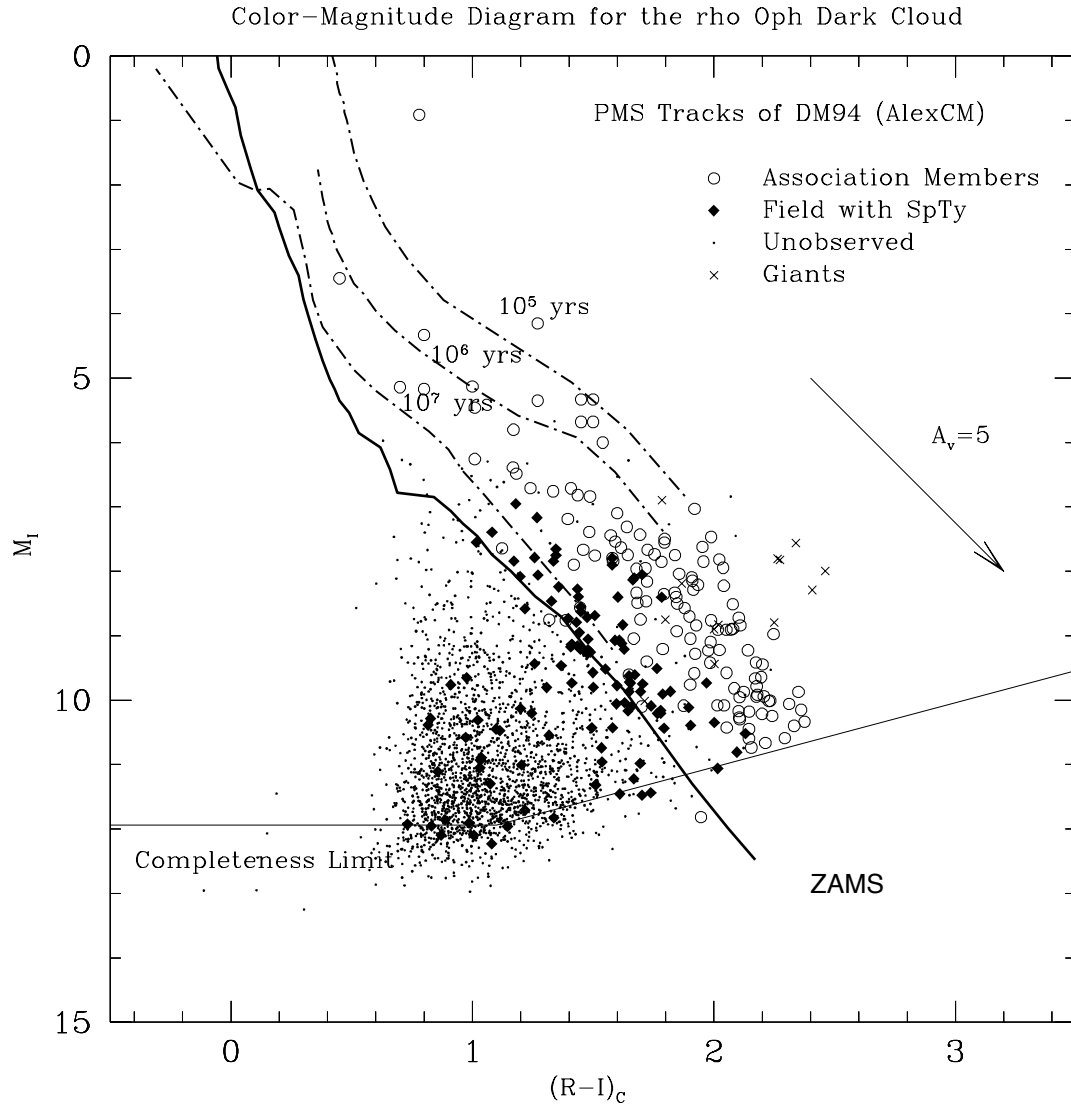
Fig. 2.— I vs. (R-I) color-magnitude diagram from our R and I band images. The ordinate is the absolute I magnitude assuming a distance of 130 pc and with no correction for reddening. Objects observed spectroscopically are shown by open circles (association members), diamonds (field stars), or "x"s (giants). Isochrones and the ZAMS from the DM models are shown for comparison.
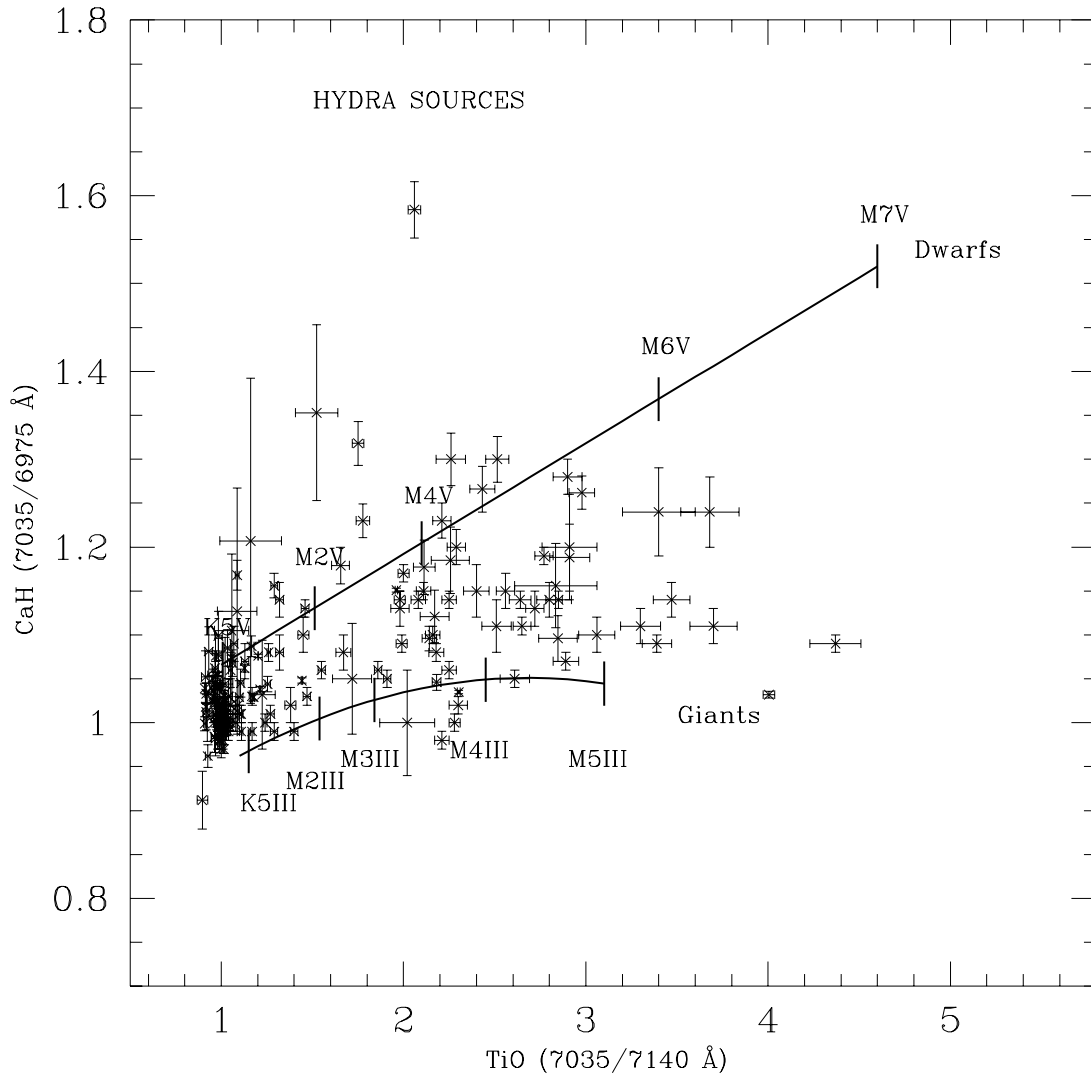
Fig. 3.— Plot of the CaH vs. TiO indices as defined in the text for 136 program objects. The solid lines were derived from fits to dwarf and giant spectral standards. For the dwarf standards from K5-M7, the fit was $y = 0.126x + 0.940$ with a correlation coefficient of r=0.94. We note that for spectral types later than M7, both indices decrease in response to an overall depression of the continuum so that an M8 V star has a CaH index similar to that of an M4 V star. For the giant standards from K5-M5, the fit gave $y = -0.0357x^2 + 0.191x + 0.795$ with a correlation coefficient of r=0.82.
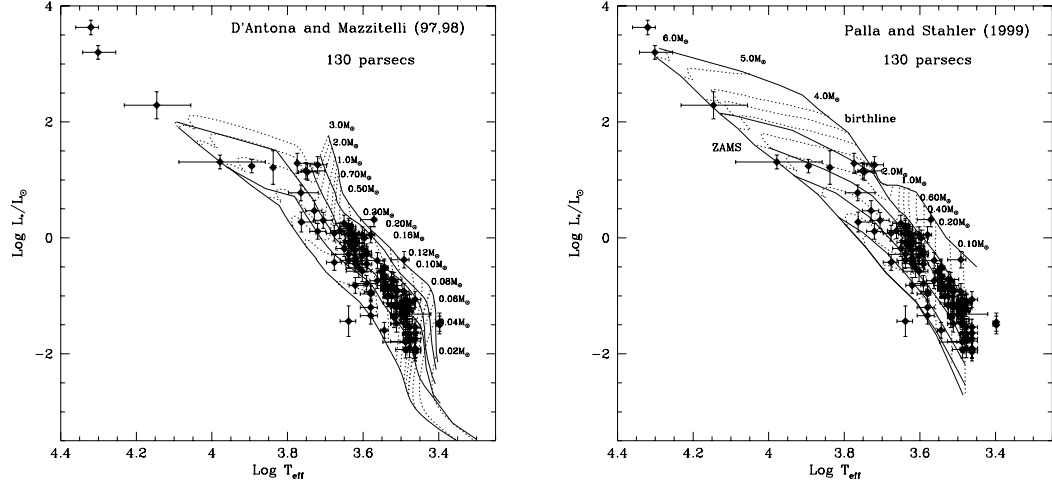
Fig. 4.— Hertzsprung-Russell diagrams for the ρ Oph association members with optically-determined spectral types assuming a distance of 130 pc. The solid diamonds mark the positions of YSOs relative to the theoretical tracks and isochrones of D'Antona & Mazzitelli (1997,1998) in Figure 4a or Palla & Stahler (1999) in Figure 4b. Error bars in Log T_{eff} were estimated from uncertainties in the spectral type and surface gravity. Error bars in Log L_{bol} were estimated from errors in the photometry and uncertainties in the distance modulus and bolometric correction. In Figure 4a, isochrones shown as solid lines are 10^5, 3×10^5, 10^6, 3×10^6, 10^7, and 10^8 years. Evolutionary tracks from 0.02 $M_\odot$ to 2.0 $M_\odot$ are shown by dashed lines. The bold dashed line marks the evolutionary track for a star at the hydrogen-burning limit. In Figure 4b, the birthline is shown as a solid line followed by isochrones for 10^6, 3×10^6, 10^7, and 10^8 years and the ZAMS. Evolutionary tracks from 0.1 $M_\odot$ to 6.0 $M_\odot$ are shown by dashed lines.
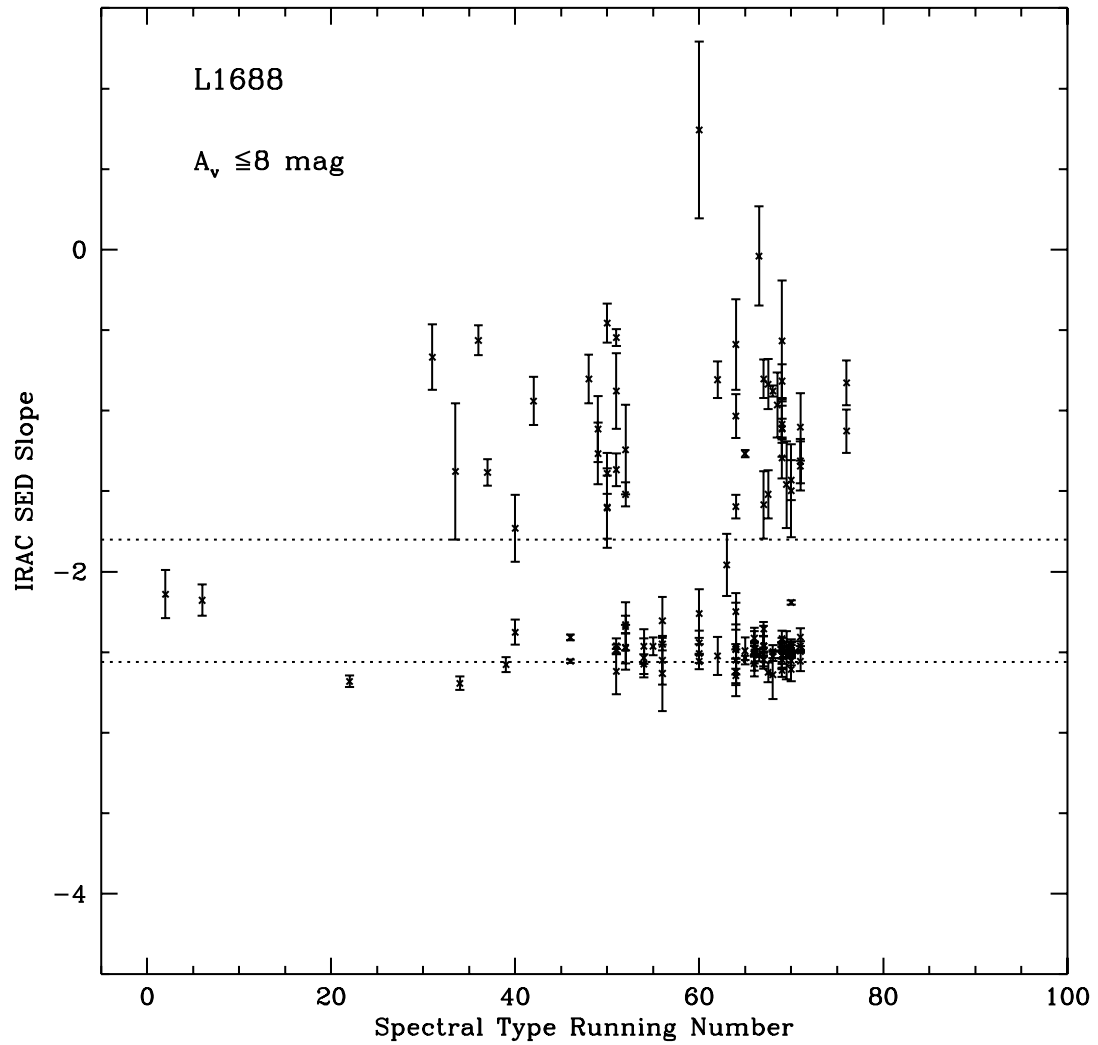
Fig. 5.— Spectral indices using the IRAC flux densities as a function of spectral type. The spectral index was computed using a linear least-squares fit to the 3.6-8.0 μm flux densities. Error bars were calculated from the fit given the statistical uncertainties in the flux densities.
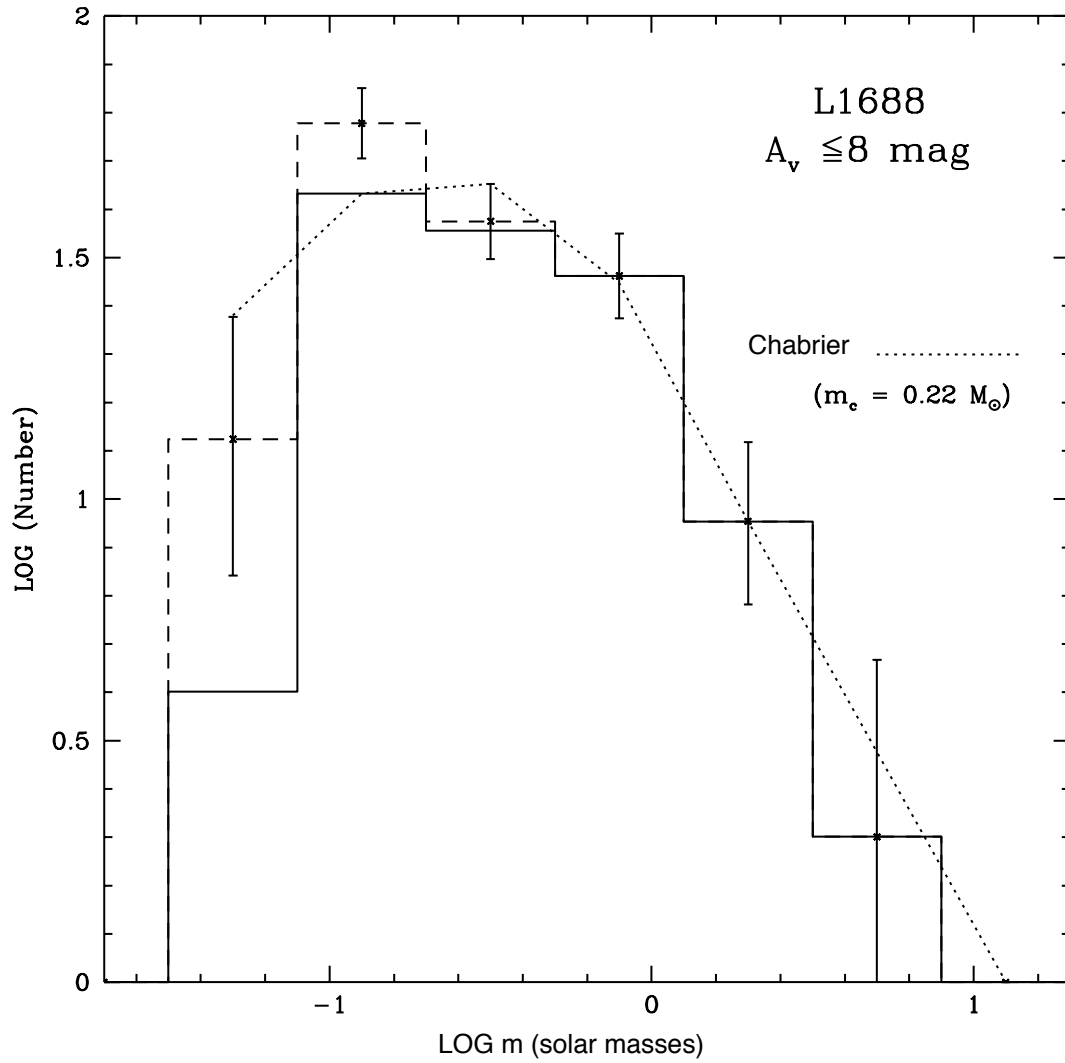
Fig. 6.— Initial mass function for our extinction-limited sample. Dashed lines show the members added from the completeness corrections described in Section 4.6.2. The dotted line is the Chabrier (2003) system mass function which is lognormal for M<1.0 $M_\odot$ and a power law for M>1.0 $M_\odot$.
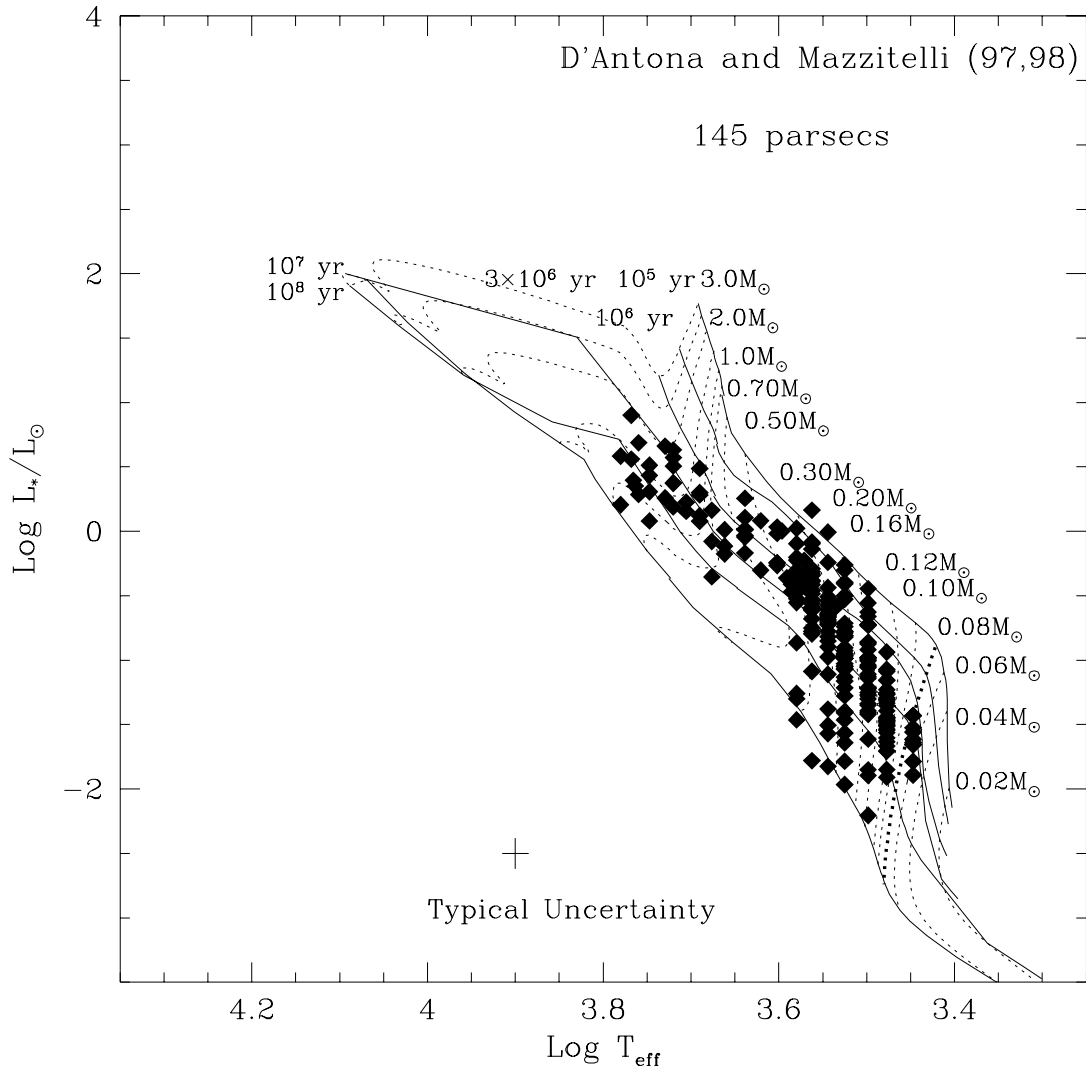
Fig. 7.— Hertzsprung-Russell diagram for 252 low-mass objects in Upper Sco from the study of Preibisch & Zinnecker (1999) relative to the DM97 models. Bolometric luminosities were derived using (J-H) colors from the 2MASS survey (see the text).

Table 1. Summary of Hydra Observations

Field No.	Date (YYMMDD)	Telescope	Position (J2000.0)	Sources	No. of Exp.	Int. Time (minutes)
1	030810	Blanco	16:27:05.4 -24:45:09	24	5	135
2	030811	Blanco	16:28:15.2 -24:14:04	47	5	135
3	030812	Blanco	16:26:01.9 -24:14:23	48	5	135
4	060615	WIYN	16:25:47.2 -24:41:00	32	10	240
5	060616	WIYN	16:28:21.6 -24:28:00	42	10	240
6	060617	WIYN	16:27:22.9 -24:09:00	30	10	240

Table 2.   Optical Properties of Candidate Young Stellar Objects

F	Ap.[a]	Names(s)[b]	X-Ray ID[c]	RA(J2000) (h:m:ss.s)	decl.(J2000) (° ′ ″)	Li?	EW(Hα)	I	(R-I)[d] (mag)	Prev Sp. Ty.[e] (mag)	Sp. Ty.	Adopt	Notes
3	39			16 24 39.3	-24 07 10	…	1.1	15.31	1.41	…	K0-K2	K1	
4	40			16 24 39.7	-24 35 08	…	-9.2	15.87	2.11	…	M4.5	M4.5	
4	13			16 24 40.5	-24 43 09	…	<0.3	15.96	1.90	…	G5-K6	K0:	
3	11			16 24 40.7	-24 21 40	…	0.90	14.83	1.49	…	K0-K2	K1	
4	29			16 24 41.1	-24 17 49	…	> -0.4	15.15	2.05	…	M1-M3	M2	
4	99			16 24 43.9	-24 47 53	…	0.70	14.64	1.61	…	K3	K3	
4	14			16 24 44.8	-25 00 18	…	-3.5	15.74	1.64	…	M2-M4	M2	Poss. dwarf
3	37			16 24 46.9	-24 22 21	…	0.90	13.61	1.86	…	K6-M0	K7	
4	72			16 24 46.9	-24 22 02	…	<0.8	13.70	1.66	…	K2-K5	K4	
4	2	UCAC3		16 24 47.7	-24 52 58	…	1.0	13.41	1.17	…	G2-G5	G5	
4	42			16 24 48.1	-24 40 04	…	> -0.4	14.80	2.14	…	M3.5-M7	M4.5	
4	85			16 24 49.3	-24 28 12	…	1.0	14.20	1.45	…	K0-K5	K3:	
3	10			16 24 50.2	-24 35 39	…	1.3	15.39	1.66	…	G5-K5	U	
3	4			16 24 51.6	-24 17 21	…	0.9	14.69	1.62	…	K1-K3	K2	
3	12			16 24 55.7	-24 09 15	…	2.0	15.01	1.26	…	G2-G5	G4	
3	90	UCAC3		16 24 55.8	-24 53 34	…	1.1	…	…	…	K3-K6	K6	
3	58			16 24 57.3	-24 11 23	Yes	-3.0	13.72	1.91	…	M3-M4	M3.5	
4	59	WSB 18		16 24 59.7	-24 55 59	Yes:	-87	13.78	1.93	M3.5 (WMR)	M2.5-M4.5	M3.5	
4	82	WSB 19/UCAC3		16 25 02.0	-24 59 30	…	-40	13.12	1.80	…	M3-M5.5	M4.5	
3	28			16 25 03.8	-24 22 24	…	2.5	14.64	1.59	…	F6-G4	G0	
4	88	UCAC3		16 25 05.0	-24 41 09	…	0.80	13.47	1.58	…	K3-K5	K4	
3	42			16 25 05.6	-24 03 11	…	0.90	15.58	1.71	…	K6-M0	K7III	Giant
3	14			16 25 07.2	-23 59 48	…	3.7	16.04	1.11	…	F2-F5	F3	
3	44			16 25 07.9	-23 58 03	…	1.2	14.78	1.45	…	G5-K0	G9	
4	38			16 25 10.9	-24 46 03	…	-10	15.78	2.20	…	M4-M6	M5	
4	32			16 25 11.9	-24 37 07	…	0.80	14.78	1.79	…	K5-K6	K6	
3	31			16 25 12.3	-23 58 31	…	0.80	14.71	1.41	…	K1-K3	K2	
3	17			16 25 16.8	-24 04 41	…	0.80	15.37	1.50	…	K3	K3	
3	27			16 25 17.0	-24 11 44	…	0.80	14.36	2.25	…	M3-M4.5	M4.5III	Giant
4	52			16 25 18.9	-24 47 59	Yes:	-12	14.98	2.17	…	M2-M4	M3	Poss. dwarf

Table 2—Continued

F	Ap.[a]	Names(s)[b]	X-Ray ID[c]	RA(J2000) (hhmmss.s)	decl.(J2000) (° ′ ″)	Li?	EW(Hα)	I	(R-I)[d] (mag)	Prev Sp. Ty.[e] (mag)	Sp. Ty.	Adopt	Notes
4	91	UCAC3		16 25 22.9	-24 57 18	...	0.70	12.74	1.27	...	K3-K5	K3	
4	26			16 25 23.1	-24 42 08	...	0.95	14.79	1.46	...	K1-K5	K3	
3	6			16 25 23.6	-24 22 54	...	1.6	15.61	1.63		G4-G9	G5	
3	35			16 25 24.1	-23 56 56	...	-1.6	15.18	1.67	M3 (WMR)	M3-M4	M3.5	Poss. dwarf
3	34			16 25 25.6	-24 07 28	...	1.2	15.19	1.65	...	G9-K0	K0	
6	42	Same as 3-34				...	<2						
3	30			16 25 26.3	-24 23 56	...	1.3	15.67	1.66		G5-K5	G7	
3	45			16 25 26.3	-24 01 06	...	0.90	14.50	1.85	...	K7-M0	K7	
3	3	UCAC3		16 25 26.7	-23 56 53	...	0.90	14.28	1.48	...	K0-K2	K2	
3	2			16 25 27.0	-24 20 50	...	0.70	15.66	1.74	...	K3-K4	K4	
6	76	UCAC3		16 25 28.8	-24 22 59	...	<0.1	15.14	1.51	M3.25 (WMR)	U	M3.25	Poss. dwarf
4	65	UCAC3		16 25 29.9	-24 39 14	...	-0.30	14.15	1.22	M2 (WMR)	M1-M3	M2	
4	62			16 25 31.6	-24 21 22	...	<0.2	17.03	1.61	K1.5 (WMR)	<M0	K1.5	
4	17			16 25 32.3	-24 19 59	...	>-3.5	15.63	1.60	...	K7-M3	M0	
4	58			16 25 34.1	-24 36 32	...	<0.5	14.81	1.45	...	U	U	
3	50	GSS 15		16 25 35.6	-24 34 00	...	0.80	13.39	2.27	...	M3-M4.5	M4III	Giant
4	98	UCAC3		16 25 36.1	-25 00 26	...	>-0.2	13.65	1.20	...	K2-K6	K5	
3	5			16 25 36.2	-24 04 04	...	0.90	15.15	1.92	...	K5.5-K8	K6:	
3	56	ISO-Oph 1/WLY 2-2/UCAC3		16 25 36.8	-24 15 42	Yes	-2.8	13.36	1.58	K3.5 (LR)	K3-K5	K4	
1	49			16 25 37.8	-24 13 43	...	<0.2	13.57	2.46	M4.25III (WMR)	M3.5-M5	M4.25III	Giant
3	29			16 25 37.9	-24 43 05	...	0.70	14.71	1.41	...	K2-K4	K3	
1	40			16 25 44.2	-24 33 02	...	>-0.5	16.09	2.13	...	K2-K4	K3	
1	16	UCAC3	ROX3	16 25 49.6	-24 51 30	Yes	-2.4	11.03	1.01	K3/M0 (BA)	K6-M1	K8	
1	3	UCAC3		16 25 50.5	-24 47 34	...	1.0	13.47	1.42	...	G9-K0	K0	
6	28	Same as 1-28				...	<0.2				K4		
1	44			16 25 51.0	-24 34 55	...	>-0.4	16.38	2.10	...	<K6	K4	
1	5			16 25 52.5	-24 04 19	Yes:	0.70	16.02	1.10	F9.5 (WMR)	G5-K5	G9	
1	33			16 25 57.5	-24 42 07	...	1.0	14.40	1.62	...	K0-K2	K2	
1	15			16 25 57.6	-24 41 00	...	0.70	15.34	1.60	...	K0-K2	K1	
1	16			16 25 58.9	-24 52 47	Yes:	-7.3	13.86	1.92	M4.5 (WMR)	M2-M4	M4	

Table 2 —Continued

F	Ap.[a]	Names(s)[b]	X-Ray ID[c]	RA(J2000) (hhmmss.s)	decl.(J2000) (° ′ ″)	Li?	EW(Hα)	I	(R-I)[d] (mag)	Prev Sp. Ty.[e] (mag)	Sp. Ty.	Adopt	Notes
3	9			16 26 02.2	-24 02 04	...	0.60	13.76	1.87	...	M2.5-M4	M3III	Giant
3	53			16 26 03.0	-24 08 48	...	3.7	14.73	1.44	...	F2-F4	F3	
3	20	UCAC3		16 26 09.1	-24 01 29	...	1.0	13.81	1.36	...	K0-K3	K2	
4	11	UCAC3		16 26 10.9	-24 52 14	...	1.0	12.52	1.18		G9-K3	K1	
3	10	UCAC3		16 26 16.9	-24 00 07	...	1.0	13.36	1.26	...	K0-K3	K2	
3	43	GSS 29	ROXC J162616.8	16 26 16.9	-24 22 23	Yes:	-2.6	15.23	2.17	K6 (LR)	K5-K6	K6	
4	93	Same as 3-43				Yes	>-2.5				K5-K6		
6	2	Same as 3-43				Yes	-0.50				K6		
3	15	UCAC3	RXJ1626.3-2407?	16 26 18.7	-24 07 19	Yes	-3.0	13.07	1.80	M3.25 (WMR)	M3-M3.5	M3.25	
3	29			16 26 18.8	-24 12 25	...	1.1	15.44	1.82	...	K1-K3	K2	
6	39			16 26 22.5	-23 58 19	...	>-1.0	16.12	1.32	K4 (WMR)	K6	K6	
3	23	GSS 32/Source 2	ROXC J162624.0	16 26 24.1	-24 24 48	...	-7.6	15.58	2.23	K8 (LR)	K5-K6	K5	
4	51			16 26 24.3	-24 01 16	...	-11	15.84	2.11	M4.5 (WMR)	M3-M5.5	M4.5	
4	31			16 26 29.2	-24 48 15	...	1.3	16.46	1.04	G0 (WMR)	F6-G3	G0	
1	25			16 26 35.5	-24 55 58	...	>-0.4	16.00	1.58	...	K1-K3	K3	
3	16	ISO-Oph 51	ROXC J162636.8	16 26 37.0	-24 15 52	Yes:	-9.6	15.67	1.70	...	K7-M1	M0	
3	26	AOC 88		16 26 37.5	-24 08 42	...	0.80	16.01	1.79	...	K2-K4	K3	
3	18	GSS 37/VSSG 2	ROXC J162642.8	16 26 42.9	-24 20 30	...	-10	14.33	1.99	K6 (MMGC), M0 (LR)	K7-M2	M1	
3	33	UCAC3	ROXC J162643.2	16 26 43.1	-24 11 09	Yes	-1.0	13.32	1.51	K8 (WMR)	K7-M0	K8	
1	21			16 26 43.5	-24 52 23	...	0.80	14.33	1.39	...	K6-K7	K6	
1	22		ROXN 6	16 26 44.4	-24 47 13	Yes	-4.0	13.92	1.79	M4.5 (WMR)	M3-M4	M4	
3	36			16 26 46.1	-23 58 10	...	-3.8	15.53	2.11	M3 (WMR)	M2-M4	M3	
1	8		ROXN 9	16 26 48.2	-24 42 03	...	-9.1	15.58	2.23	M3.75 (WMR)	M5-M6	M5	
4	34	Same as 1-8				...	-3.4				M4-M6		
2	56	AOC 64		16 26 50.5	-24 13 52	Yes	-6.2	14.79	2.02	M4.5 (WMR)	M3-M4	M3.5	
3	21	Same as 2-56				Yes	-5.8				M3-M4		
6	10			16 26 53.2	-24 05 58	...	> -0.4	16.92	1.48	K0.5 (WMR)	U	K0.5	
3	24			16 26 53.7	-24 01 55	...	1.6	15.78	1.77	...	G5-K2	G9	
6	85	Same as 3-24				...	>-3.0				U	U	
2	60	UCAC3		16 26 55.0	-24 10 16	...	0.2	13.84	1.44	M3 (WMR)	M2-M4	M3	

Table 2 —Continued

F	Ap.[a]	Names(s)[b]	X-Ray ID[c]	RA(J2000) (hhmmss.s)	decl.(J2000) (° ′ ″)	Li?	EW(Hα)	I	(R-I)[d] (mag)	Prev Sp. Ty.[e] (mag)	Sp. Ty.	Adopt	Notes
1	1			16 26 57.4	-24 49 48	...	0.70	15.78	1.78	...	K4-K5	K5	
4	4			16 26 57.8	-24 52 37	...	<0.5	17.48	0.98	K5 (WMR)	G2-K6	K5	
2	32		ROXC J162704.0	16 27 04.2	-24 09 32	Yes	-4.1	14.06	1.68	M2 (MMGC)	M0-M2	M1	
3	7	Same as 2-32		16 27 04.5	-24 03 28	Yes	-5.2				M0-M2		
2	51					...	0.90	13.97	1.60		K0-K3	K2.5	
3	41	Same as 2-51				...	0.90				K1-K3		
1	5	ISO-Oph 97/GY 194	ROXRF 9	16 27 04.6	-24 42 13	Yes:	-2.6	15.66	1.88	...	K8-M0	M0	
5	67			16 27 04.6	-24 42 58	Yes	-3.5	14.97	1.72	...	K6-M1	K8	
2	29			16 27 06.6	-24 07 03	...	-4.3	15.36	2.18	M4.5 (WMR)	M3-M5	M4.5	
3	46	Same as 2-29				...	-12				M3-M5.5		
3	57	ISO-Oph 106		16 27 09.1	-24 12 01	...	-12	16.16	2.29	M2.5 (WMR)	U	M2.5	Poss. dwarf
5	81	Same as 3-57				...	-5.0				M2-M3		
2	23		ROXC J162711.8	16 27 12.0	-24 10 31	Yes	-0.50	15.33	1.90	M0: (MMGC)	K4-K5	K6	
3	54	Same as 2-23				Yes:	>-1.5				K4-K6		
5	58	Same as 2-23				Yes	>-1.0				K6-M2		
6	38	Same as 2-23				...	-1.7				K6		
1	6	WSB 47		16 27 17.0	-24 47 11	...	0.70	15.08	1.76	K1 (WMR)	K2-K5	K2	
5	14	Same as 1-6				...	0.70				K4-K6		
2	61	UCAC3		16 27 17.1	-24 06 48	...	0.90	13.67	1.67	...	K1-K3	K3	
3	22	Same as 2-61				...	0.80				K2-K3		
6	62			16 27 18.0	-23 58 46	...	0.80	13.20	1.62	...	K7-K8	K8	
5	82			16 27 18.1	-24 53 16	...	-9.0	16.63	2.02	M2.5 (WMR)	M0-M5	M2.5	Poss. dwarf
6	17			16 27 20.4	-23 58 42	...	>-0.2	17.40	1.34	U (WMR)	M0-M3	M1	
6	21			16 27 25.2	-23 55 54	...	1.0	13.41	1.34	...	K2-K3	K2	
2	40			16 27 28.9	-24 09 38	...	2.8	14.85	1.48	...	F2-F4	F3.5	
3	38	Same as 2-40				...	2.9				F2-F5		
1	13	ISO-Oph 149	ROXRF 26	16 27 30.9	-24 47 26	...	-7.2	16.17	2.15	...	M1-M2	M1	
6	44	UCAC3		16 27 31.3	-23 59 09	...	0.30	13.12	1.02	M1 (WMR)	M0-M1	M1	Poss. dwarf
1	17	ISO-Oph 155/GY 292	[IKT2001] 69	16 27 33.2	-24 41 14	...	-60	15.65	2.01	K8 (LR)	K5-K6	K6	
5	59	Same as 1-17				...	-80				K6-M0		

Table 2—Continued

F	Ap.[a]	Names(s)[b]	X-Ray ID[c]	RA(J2000) (hhmmss.s)	decl.(J2000) (° ′ ″)	Li?	EW(Hα)	I	(R-I)[d] (mag)	Prev Sp. Ty.[e] (mag)	Sp. Ty.	Adopt	Notes
1	7	GY 297		16 27 36.5	-24 28 33	…	<0.2	13.32	1.35	M2 (WMR)	M2-M3.5	M3	
2	46	Same as 1-7				…	<0.2				M2-M3		
5	88	Same as 1-7				…	0.30				M3-M4		
6	18	Same as 1-7				…	0.40				M2-M3		
2	7	WLY 2-48/ISO-Oph 159		16 27 36.9	-23 58 27	Yes:	-10	16.02	2.15	…	M4-M5.5	M4.5	
1	9			16 27 37.3	-24 30 34	…	10+em	14.67	1.99	M0 (G)	B5-F2	A0	
2	35	UCAC3		16 27 38.0	-23 57 24	Yes	-2.8	13.73	1.72	M2.5 (WMR)	M1-M3	M2.5	
1	31		ROXC J162738.2	16 27 43.6	-24 04 02	…	-1.4	13.41	1.58	…	K5-K6	K5.5	
1	31			16 27 45.2	-24 51 25	Yes	1.0	14.26	1.51	…	K1-K2	K2	
1	14			16 27 49.3	-25 03 33	…	-5.7	14.07	1.85	M4.5 (WMR)	M3-M5	M3.5	
6	79			16 27 54.4	-23 56 09	…	<0.8	16.50	1.04	G2.5 (WMR)	F6-K0	G2.5	
5	28	UCAC3		16 27 59.7	-24 51 60	…	0.70	13.63	1.27	…	K3-K5	K4	
6	23			16 28 00.8	-23 57 16	…	>-0.4	17.01	1.74	M0 (WMR)	K8-M0	M0	
2	30			16 28 01.4	-24 00 52	Yes	-3.8	13.90	1.84	M3 (WMR)	M2	M2	
2	27			16 28 02.2	-24 02 11	…	1.1	14.62	1.48	…	G5-K0	G9	
1	4			16 28 03.4	-24 19 05	…	3.3	15.31	1.66	…	F1-F3.5	F2	
6	11			16 28 04.9	-24 53 22	Yes	-9.2	14.41	2.11	…	M5-M6	M5.5	
2	78			16 28 05.9	-23 56 08	…	1.1	17.28	1.22	K5 (WMR)	G5-K2	G9	
2	21			16 28 06.6	-24 29 12	…	0.90	15.48	1.79	…	K0-K2	K1	
2	12			16 28 08.1	-24 18 55	…	2.4	14.79	1.48	…	F7-G4	G0	
5	43	UCAC3		16 28 09.9	-24 04 49	…	0.80	13.36	1.58	K4.5 (WMR)	K1-K4	K3	
2	41			16 28 11.0	-24 48 48	…	>-0.4	16.68	0.86	…	K0-K5	K4.5	
5	98			16 28 11.1	-24 55 57	…	>-0.4	15.92	2.00	…	K0-K5	K3:	
2	18			16 28 11.2	-24 06 18	Yes	-6.3	14.29	2.10	M3.75 (WMR)	M3-M4.5	M3.75	
2	22			16 28 12.3	-24 29 19	…	0.80	15.44	1.70	…	G9-K0	G9	
2	62				-24 09 28	…	0.90	13.37	2.26	…	M2.5-M4	M3.5III	Giant
5	17	Same as 2-62				…	1.2				M2.5-M4.5		
6	34	Same as 2-62				…	1.2				M3-M4		
1	24	ISO-Oph 194	ROXC J162813.7	16 28 13.9	-24 32 49	…	-11	15.72	2.36	…	M3-M4.5	M4	
5	73			16 28 13.9	-24 56 10	Yes	-3.5	14.13	1.45	…	K7-M0	M0	

Table 2 —Continued

F	Ap.[a]	Names(s)[b]	X-Ray ID[c]	RA(J2000) (hhmmss.s)	decl.(J2000) (° ′ ″)	Li?	EW(Hα)	I	(R-I)[d] (mag)	Prev Sp. Ty.[e] (mag)	Sp. Ty.	Adopt	Notes
6	27			16 28 14.4	-23 57 52	…	>1.4	17.53	1.12	G7 (WMR)	G0-K5	G7	
2	26	AOC 7		16 28 14.9	-24 23 22	…	-2.3	15.32	1.71	…	G9-K2	K0:	
2	39			16 28 15.8	-24 09 32	…	1.1	15.73	1.78	…	G9-K2	K0	
5	94			16 28 16.6	-24 07 36	…	>2.0	16.79	1.67	U (WMR)	U	M0	
6	7	Same as 5-94				…	<0.3				K6-M1		
1	10	ISO-Oph 195	RXJ 1628.2-2405	16 28 16.9	-24 05 15	Yes	<-3.4	13.91	1.68	K5 (MMGC)	K5-K6	K6	
5	32	Same as 1-32		16 28 17.6	-24 33 54	…	1.0	15.30	1.97	…	K3-K5	K3	
6	49	Same as 1-32				…	<0.1				U		
2	53			16 28 18.8	-24 20 15	…	<0.2	15.01	2.00	…	M0-M5	MIIII	Giant
5	62	Same as 2-53				…	0.90				K7-M2		
5	29			16 28 20.0	-24 26 11	…	>-0.2	15.70	1.20	G5 (WMR)	U	G5	
2	59			16 28 20.1	-24 23 18	…	-4.2	15.65	2.04	M3.5 (WMR)	M3-M4	M3.5	
5	16			16 28 21.5	-24 48 15	…	0.70	15.09	1.55	…	K5-K6	K5	
2	6		ROXC J162821.5	16 28 21.6	-24 21 55	Yes	-3.3	14.99	1.98	M2.5 (WMR)	M2-M3	M2.5	
1	41			16 28 21.7	-24 17 45	…	1.5	15.29	1.65	…	F9-G4	G1	
2	10			16 28 23.0	-24 48 28	…	-14	15.74	2.10	…	M3.5-M5	M5	
6	9			16 28 24.8	-24 08 14	…	1.2	16.53	1.54		K4-K6	K4:	
1	33	Same as 2-9				Yes:	>-0.1				K3-K5		
5	26			16 28 24.9	-24 35 43	…	-9.0	14.80	1.98	M5 (WMR)	M3.5-M5	M5	
5	12			16 28 28.3	-24 52 22	…	0.50	15.03	1.37	K6 (WMR)	K5-K6	K6	
5	21			16 28 28.3	-23 58 51	…	<2.0	17.04	1.31	U (WMR)	U	U	
6	49			16 28 29.4	-24 31 21	…	<0.1	16.57	1.20	K0 (WMR)	G9-K5	K0	
2	37	Same as 5-49		16 28 31.2	-24 02 34	…	0.6	14.41	1.93	…	K3-K5	K5:	
2	44			16 28 32.4	-24 05 49	…	-6.4	15.44	2.35	…	M3-M4	M3.5	
2	45			16 28 32.6	-24 15 24	…	-11	15.97	2.33	M3.5 (WMR)	M3-M4	M3.5	
5	84			16 28 36.3	-24 00 43	…	<1.0	16.31	1.53	K1 (WMR)	G5-K6	G5:	
6	56	Same as 5-84				…	1.6				F6-K0		
2	16		ROXC J162843.1	16 28 43.1	-24 22 52	Yes:	-6.8	14.47	2.07	M4.75 (WMR)	M3-M5	M4	

Table 2 —Continued

F	Ap.[a]	Names(s)[b]	X-Ray ID[c]	RA(J2000) (hhmmss.s)	decl.(J2000) (° ′ ″)	Li?	EW(Hα)	I	(R-I)[d] (mag)	Prev Sp. Ty.[e] (mag)	Sp. Ty.	Adopt	Notes
5	51			16 28 43.5	-24 52 18	...	1.3	12.97	1.08	...	K0-K4	K2	
5	44			16 28 43.6	-24 04 44	...	1.7	15.77	1.25	G0 (WMR)	F6-K0	G0	
2	47	AOC 27		16 28 43.9	-24 06 41	...	0.9	14.32	1.80	...	K6-M0	M0III	Giant
5	7			16 28 47.2	-24 28 13	...	-190	16.00	2.05	...	M3.5-M5.5	M4.5	
5	74			16 28 48.6	-24 04 41	...	<0.6	14.74	1.41	...	F0-G9	G0:	
		Same as 5-74				...	1.9:				F6-G9		
6	50			16 28 49.8	-23 55 08	...	>0.5	15.17	1.65	...	M3-M4	M3.5	
2	54	Same as 2-54				...	>0.2				M3-M4		
6	25			16 28 51.6	-24 06 11	...	1.9	15.37	1.31	...	G2-G4	G3	
2	97	UCAC3		16 28 52.1	-24 47 39	...	0.80	13.62	1.70	...	K3-K5	K2	
5	20	AOC 73		16 28 56.9	-24 38 10	...	1.0	15.44	1.65	...	K3-K6	K3:	
5	4	AOC 40	ROXC J162856.8	16 28 57.1	-24 31 09	...	-52	15.39	2.08	...	M5-M6	M5.5	
2	50	WSB 65		16 28 58.9	-24 04 23	...	1.5	14.52	1.44	...	G3-G5	G4	
5	93			16 28 59.2	-24 05 16	...	> -0.4	17.05	1.69	G2.5 (WMR)	F1-K5	G2.5	
6	9	Same as 5-93				...	>-1.0				U		
6	4			16 29 00.0	-24 26 39	...	<1.0	15.24	0.96	G9 (WMR)	U	G9	
2	36			16 29 02.0	-23 56 23	...	<0.4	14.46	2.00	...	M3-M3.5	M3.5III	Giant
5	53			16 29 02.0	-24 31 11	...	>0.2	17.43	0.89	G7.5 (WMR)	G9-K6	K0	
2	57			16 29 03.1	-24 27 49	...	-12	13.19	1.95	...	M3.5-M5.5	M5	
6	31	Same as 2-57				Yes	-17				M3-M5		
5	96			16 29 03.7	-24 30 02	...	<0.5	16.55	1.70	...	M2-M4	M3	
6	6	UCAC3		16 29 06.9	-23 55 16	...	1.6	13.97	1.44	...	K1-K3	K2	
6	25	Same as 5-25		16 29 11.6	-24 22 15	...	>0.1	17.79	1.09	G0.5 (WMR)	F0-K5	G0.5	
6	77					...	>-1.0				K0-K6		
2	42			16 29 14.3	-24 25 42	...	2.2	15.96	0.82	...	F9-G3	G1	
2	19			16 29 14.4	-24 11 53	...	0.80	15.68	1.90	...	K3-K4	K4	
5	87			16 29 20.1	-24 21 32	...	-7.0	17.67	1.01	U (WMR)	K6-M2	M0	
5	71	UCAC3		16 29 21.7	-24 45 09	...	0.80	13.23	1.35	...	K3	K3	
5	33			16 29 23.5	-24 27 51	...	>-0.8	17.52	0.83	K1 (WMR)	U	K1	
5	35			16 29 23.8	-24 43 54	...	0.90	14.03	1.33	...	K0-K4	K1	

Table 2—Continued

F	Ap.[a]	Names(s)[b]	X-Ray ID[c]	RA(J2000) (hhmmss.s)	decl.(J2000) (° ′ ″)	Li?	EW(Hα)	I	(R-I)[d] (mag)	Prev Sp. Ty.[e] (mag)	Sp. Ty.	Adopt	Notes
5	34	UCAC3		16 29 23.9	-24 29 11	...	<0.2	16.15	0.97	G5 (WMR)	U	G5	
5	24			16 29 24.5	-24 30 55	...	>-0.3	17.66	0.87	G2.5 (WMR)	G0-M0	G2.5	
2	8			16 29 24.6	-24 09 01	...	0.90	14.36	1.43	...	G8-K0	G9	
2	33	UCAC3		16 29 24.8	-24 06 48	...	1.0	14.12	1.45	...	K0-K2	K1	
5	31			16 29 25.6	-24 39 35	...	1.0	13.97	1.78	...	K1-K5	K3	
2	14			16 29 27.2	-24 23 18	...	<0.2	16.00	1.49	...	M2-M3	M3	
2	17			16 29 28.7	-24 21 26	...	2.1	15.85	0.83	...	F7-G4	G0	
2	49			16 29 32.2	-24 05 49	...	0.80	14.30	1.40	...	K1-K3	K3	
5	77			16 29 32.5	-24 36 06	...	<0.2	14.78	1.63	...	K4-K5	K5	

[a]HYDRA field and aperture number of observation.

[b]Sources names from optical or infrared studies by (GSS, Source 2) Grasdalen et al. 1973; (VSSG) Vrba et al. 1975; (VSS) Vrba et al. 1976; (WSB) Wilking et al. 1987; (WLY) Wilking et al. 1989; (GY) Greene & Young 1992; (ISO-Oph) Bontemps et al. 2001; (AOC) Alves de Oliveira & Casali 2008; and (UCAC3) Zacharias et al. 2009.

[c]X-ray source association from the EINSTEIN survey by (ROX) Montemerle et al. (1983), the ROSAT surveys by (RXJ) Martín et al. (1998) and (ROXRF) Grosso et al. (2000), the Chandra surveys by ([IKT2001]) Imanishi et al. (2001) and (ROXC) N. Grosso (2005, private communication), or the XMM-Newton survey by (ROXN) Ozawa et al. (2005).

[d]R and I band photometry from this study except for ROX 3 which are from Gordon & Strom (1990, unpublished data).

[e]References for spectral types: (BA) Bouvier & Appenzeller 1992; (MMGC) Martín et al. 1998; (LR) Luhman & Rieke 1999; (WMR) Wilking et al. 2005; (G) Geers et al. 2007.

Table 3.   Association Members with Optical Spectra

F	Ap.	Names(s)[a]	WMR[b]	Sp. Type[c]	A_v[d] (mag)	M(I) (mag)	$\log T_{eff}$ (K)	$\log(L/L_\odot)$	M_*[e] ($M_\odot$)	Log(age) (yr)	Criteria[f]	Notes[g]
4	40			M4.5	2.1	9.03	3.488	-1.79	0.15	7.18	ext	
4	29			M2	5.6	6.23	3.544	-0.82	0.32	6.46	ext	
3	37			K7	6.8	3.96	3.602	0.06	0.42	5.65	ext	
4	42			M4.5	2.3	7.83	3.488	-1.31	0.16	6.57	ext	
		RXJ 1624.9-2459		K5 (MMGC)	0.3 (2M)	6.91	3.638	-1.44	...	...	pm,x	(1)
3	58		2-15	M3.5	2.6	6.60	3.512	-0.90	0.19	6.23	ext,li	
4	59	WSB 18		M3.5	2.7	6.58	3.512	-0.89	0.19	6.23	ext,ha,IRX	(4)
4	82	WSB 19		M4.5	0.2	7.46	3.488	-1.16	0.16	6.38	ha,IRX	
4	38			M5	1.8	9.13	3.477	-1.78	0.12	7.01	ext,ha	
4	32			K6	7.0	5.03	3.621	-0.40	0.73	6.61	ext	
4	52			M3	5.0	6.40	3.525	-0.85	0.23	6.27	ext,ha	
		GSS 5		G9 (TQ)	0.6 (GS)	3.08	3.729	0.47	1.7	6.65	pm,x	(4)
			2-10	M5	0.7	8.51	3.477	-1.53	0.14	6.75	ha	
		SR 22	1-7	M4.5	0.0 (GS)	7.31	3.488	-1.10	0.16	6.31	ha,pm,x	
		HD 147889		B2 (HS)	4.4 (C)	-1.76	4.320	3.63	8.3	zams?	pm,ref. neb.	(2)
3	45	ROXR1-4/SR 8		K7	6.7	4.89	3.602	-0.32	0.55	6.24	ext	
				K7 (MMGC)	1.6 (2M)	3.81	3.602	-0.18	0.49	5.98	ext,pm,x	
4	17			M0	4.3	7.49	3.580	-1.34	0.52	7.98	ext	
3	5			K6:	7.8	4.92	3.621	-0.35	0.70	6.51	ext	
3	56	WLY 2-2		K4	6.7	3.79	3.662	0.12	0.80	6.08	ext,IRX,li	(4)
		WLY 2-3	3-15	M2	4.8	6.42	3.544	-0.90	0.32	6.58	ext,ha,IRX,x	
			2-32	M3.5	2.5	7.20	3.512	-1.14	0.21	6.54	ext,li,x	
4	16	ROX 3		K8	1.1 (GS)	4.82	3.591	-0.28	0.47	6.06	li,pm,x	
		VSS 23	1-22	K5.5	5.0	3.81	3.630	0.10	0.56	5.78	ext,pm,x	
1	3			K0	6.6	3.96	3.720	0.11	1.3	6.95	ext,pm	
		WLY 2-11	2-25	M5	2.1	7.71	3.477	-1.22	0.14	6.39	ext,ha,x	
		SR 4	1-29	K4.5	2.8 (BA)	3.45	3.650	0.25	0.66	5.75	ext,ha,IRX,li,pm,x	
		GSS 20	1-38	K5.5	5.9	3.92	3.630	0.05	0.57	5.85	ext,pm,x	
1	16	Chini 8	3-14	M4	1.8	7.22	3.498	-1.12	0.18	6.40	ext,li	
			2-1	M5.5	0.0	7.47	3.462	-1.06	0.12	6.09	ha,li,x	

Table 3—Continued

F	Ap.	Names(s)[a]	WMR[b]	Sp. Type[c]	A_v[d] (mag)	M(I) (mag)	log T_{eff} (K)	log(L/L$_\odot$)	M_*[e] (M$_\odot$)	Log(age) (yr)	Criteria[f]	Notes[g]
			4-28	M3	5.2	6.33	3.525	-0.82	0.23	6.24	ext,x	
		GSS 23	1-13	K0 (MMGC)	7.1 (BA)	1.09	3.720	1.26	2.9	5.69	ext,pm,x	(4)
		VSSG 19	2-19	M2	3.3	5.43	3.544	-0.50	0.29	6.00	ext,x	
		SR 3		M4.5	1.7	7.21	3.488	-1.06	0.16	6.27	ext,ha,li	
3	43	GSS 29		B6 (EL)	6.5 (C)	0.28	4.146	2.28	3.8	6.13	pm	(3)
		GSS 29	1-5	K6	9.3	4.06	3.621	0.00	0.54	5.86	ext,IRX,li	
3	15	GSS 28	4-39	K4.5	2.9	4.54	3.650	-0.18	0.85	6.52	ext,ha,IRX,li,pm,x	
			2-11	M3.25	2.3	6.14	3.519	-0.73	0.20	6.09	ext,li	
				M4.75	0.0	7.75	3.482	-1.25	0.15	6.46	li,x	
		WSB 28	1-25	M2	2.7	5.92	3.544	-0.70	0.36	7.99	ext,ha,pm,x	
		GY 5	4-16	M5.5	2.0	9.15	3.462	-1.74	0.11	5.06	ext,ha,IRX,x	
		GY 3	4-41	M8	0.0	10.1	3.398	-1.45	0.04	5.43	ha,IRX,x	
		GSS 31	1-30	G6	7.6 (GS)	1.41	3.752	1.16	2.8	6.23	ext,IRX,pm,x	
		DoAr 25	1-28	K5	3.6 (GS)	3.65	3.638	0.16	0.60	5.76	ext,ha,IRX,li,pm,x	
		EL 24	2-27	K5.5	7.6	3.86	3.630	0.08	0.57	5.81	ext,ha,IRX,x	
3	23	GSS 32/Source 2		K5	10	3.90	3.638	0.06	0.63	5.92	ext,IRX,x	
3	51		4-18	M4.5	2.1	9.01	3.488	-1.78	0.15	7.17	ext,ha	
			4-25	M5.5	1.1	9.57	3.462	-1.90	0.08	6.87	x	
		WSB 34	2-36	M4.5	0.7	8.16	3.488	-1.44	0.16	6.75	ha	
		Source 1	1-2	B3	13	-0.77	4.301	3.20	6.0	zams?	ext,ref. neb.,x	(3)(4)
3	16	ISO-Oph 51		M0	4.9	7.13	3.580	-1.20	0.57	7.73	ext,IRX,li,x	
			4-4	M5	1.9	8.83	3.477	-1.66	0.13	6.89	ext,ha,x	
		WSB 37	2-29	M5	0.7	7.40	3.477	-1.09	0.14	6.24	ha,IRX,li,x	
3	18	GSS 37/VSSG 2		M1	6.1	5.13	3.562	-0.39	0.36	5.99	ext,ha,IRX,li,x	
3	33		1-21	K8	4.2	5.25	3.591	-0.45	0.56	6.40	ext,li,pm,x	
1	21			K6	4.4	6.09	3.621	-0.82	0.72	7.51	ext	
		GY 112	1-20	M3	2.2	6.34	3.525	-0.82	0.23	6.24	ext,pm,x	
1	22		3-22	M4	1.0	7.74	3.498	-1.33	0.18	6.68	li,x	
3	36	WSB 38	4-13	M3	4.6	7.20	3.525	-1.16	0.25	6.73	ext	
			1-36	G3.5	7.4	2.38	3.765	0.78	1.8	6.78	ext,ha,IRX,li,pm,x	(4)

Table 3—Continued

F	Ap.	Names(s)[a]	WMR[b]	Sp. Type[c]	A_v[d] (mag)	M(I) (mag)	$\log T_{eff}$ (K)	$\log(L/L_\odot)$	M_*[e] ($M_\odot$)	Log(age) (yr)	Criteria[f]	Notes[g]
1	8		4-30	M4.5	2.7	8.04	3.488	-1.40	0.16	6.68	ext,li,var,x	
			4-59	M5	2.0	8.80	3.477	-1.65	0.13	6.88	ext,x	
		WSB 40	1-32	K5.5	5.3	4.20	3.630	-0.06	0.61	6.04	ext,ha,pm	
		WL 18	4-53	K6.5	12 (2M)	4.63	3.612	-0.52	0.74	6.78	ext,ha,IRX,x	
2	56		2-38	M3.5	3.3	7.26	3.512	-1.16	0.21	6.58	ext,li,var	
			4-46	K7	8.7	5.54	3.602	-0.57	0.71	6.80	ext,ha,IRX,x	
		SR 24s	1-37	K1	6.2	3.45	3.705	0.30	1.5	6.52	ext,ha,IRX,pm,x	
		SR 24n		M0.5 (CK)	8.9 (2M)	2.32	3.571	0.32	0.47	<6.0	ext,ha,IRX	(3)(4)
2	32			M1	4.1	6.00	3.562	-0.74	0.45	6.61	ext,li,x	
5	67			K8	5.5	6.09	3.591	-0.79	0.71	7.15	ext,li	
1	5	GY 194		M0	6.0	6.47	3.580	-0.93	0.64	7.26	ext,li,x	
		GY 204	4-65	M5.5	0.4	9.63	3.462	-1.93	0.08	6.88	ha,IRX,var,x	
2	29		4-63	M4.5	2.5	8.26	3.488	-1.48	0.16	6.80	ext,ha	
5	81	ISO-Oph 106	4-37	M2.5	6.4	6.74	3.535	-1.01	0.28	6.61	ext,ha,IRX	
		SR 21		G1 (MMGC)	7.6 (GS)	1.12	3.774	1.29	2.9	6.26	ext,IRX,pm,x	
2	23			K6	7.7	5.16	3.621	-0.46	0.77	6.72	ext,li,x	
		WSB 45	3-44	M4.5	0.0	7.75	3.488	-1.29	0.16	6.52	li,pm,x	
		WSB 46	1-9	M2	0.5	6.41	3.544	-0.89	0.32	6.57	pm,x	
			4-10	M3.5	4.3	7.37	3.512	-1.20	0.21	6.65	ext,ha,x	
6	62			K8	4.9	4.72	3.591	-0.24	0.46	5.99	ext	
		WSB 48	1-6	M3.75	0.0	7.66	3.491	-1.31	0.17	6.59	ha,IRX,pm	
		SR 12		M0	2.3 (GS)	4.00	3.580	0.05	0.33	5.46	ext,pm,x	(4)
		WSB 49	3-6	M4.25	0.3	7.53	3.493	-1.22	0.17	6.49	ha,IRX,li,pm,x	
		GY 264	4-45	M8	0.0	10.2	3.398	-1.50	0.04	5.47	ha,var,x	
			3-7	M4.75	0.0	8.75	3.482	-1.65	0.14	6.95	x	
		GY 280	2-20	M2	1.0	8.16	3.544	-1.59	0.36	7.73	x	(5)
		GY 284	4-22	M3.25	4.9	7.75	3.519	-1.37	0.24	6.98	ext,IRX,x	
		GY 292		K5 (LR,GS)	8.9	4.77	3.638	-0.28	0.80	6.58	ext,IRX,x	
		WSB 50	2-6	M4.5	1.9	7.36	3.488	-1.12	0.16	6.33	ext,li,x	
2	7			M4.5	2.3	9.04	3.488	-1.80	0.15	7.19	ext,ha,li:	

Table 3—Continued

F	Ap.	Names(s)[a]	WMR[b]	Sp. Type[c]	A_v[d] (mag)	M(I) (mag)	log T_eff (K)	log(L/L_⊙)	M_*[e] (M_⊙)	Log(age) (yr)	Criteria[f]	Notes[g]
1	9	ROX 30A		K3 (GS)	4.1	5.19	3.676	-0.42	0.90	7.25	ext,x	
2	35	WLY 2-48/ISO-Oph 159		A0	12	1.68	3.979	1.31	2.1	7.53	ext,IRX	
			4-54	M2.5	2.9	6.44	3.535	-0.89	0.27	6.43	ext,li	
		WLY 2-49	4-24	K5.5	9.6	4.16	3.630	-0.04	0.61	6.01	ext,ha,IRX,x	
2		WSB 51	2-35	K6	4.1	4.29	3.621	-0.10	0.57	6.01	ext,ha,li,pm,x	
2	31			K5.5	5.9	4.29	3.630	-0.09	0.63	6.10	ext,li,x	
		WSB 53	1-31	K5.5	3.4	4.43	3.630	-0.15	0.66	6.21	ext,ha,pn	
		WSB 52	3-5	K5	7.0	4.26	3.638	-0.08	0.69	6.18	ext,ha,IRX,li,x	
		SR 9	1-26	K5	1.3 (BA)	3.57	3.638	0.20	0.59	5.71	ha,IRX,li,pm,x	(4)
			2-34	M2	3.9	5.52	3.544	-0.54	0.29	6.04	ext,x	
		GY 326	4-64	M2	9.6 (2M)	5.01	3.544	-0.77	0.31	6.38	ext,IRX,x	
1	14		3-21	M3.5	2.2	7.20	3.512	-1.14	0.21	6.54	ext,li	
		VSSG 14	1-14	A7	9.1	1.48	3.895	1.24	2.1	6.76	ext,pm,x	
		ROX 31	1-10	K7.5	5.0	4.12	3.597	0.00	0.41	5.68	ext,x	(4)
		SR 10	1-24	M2	0.0	6.36	3.544	-0.87	0.32	6.54	ha,IRX,pm,x	(4)
		WSB 58	3-34	M4.75	0.7	7.41	3.482	-1.12	0.15	6.31	x	
			3-31	M5	0.8	7.47	3.477	-1.12	0.14	6.28	ha,li,x	
2	30		2-3	M2	4.2	5.79	3.544	-0.65	0.30	6.20	ext,li	
1	11			M5.5	0.3	8.66	3.462	-1.54	0.10	6.59	li	
2	18		2-21	M3.75	3.4	6.70	3.491	-0.92	0.16	6.14	ext,li	
		ROX 32	3-11	M3	3.4	6.08	3.525	-0.72	0.22	6.12	ext,li,x	
5	73			M0	3.4	6.55	3.580	-0.97	0.63	7.33	ext,li	
1	24	ISO-Oph 194		M4	4.6	7.41	3.498	-1.19	0.18	6.50	ext,ha,IRX,x	
		WSB 60	3-20	M4.5	1.9	7.73	3.488	-1.27	0.16	6.51	ext,ha,IRX	
2	10	ISO-Oph 195		K6	6.3	4.57	3.621	-0.21	0.63	6.23	ext,IRX,li,x	
			3-12	M3	1.9	6.80	3.525	-1.01	0.24	6.49	ext	
2	59		4-3	M3.5	3.4	8.05	3.512	-1.48	0.22	7.07	ext,IRX,li,x	
2	6		2-37	M2.5	4.5	6.72	3.535	-1.00	0.28	6.61	ha	
1	10			M5	1.2	9.45	3.477	-1.91	0.11	7.13	ext,IRX,li,x	
			2-30	K5	6.7	5.03	3.638	-0.39	0.86	6.80	ext,ha,IRX,x	

Table 3—Continued

F	Ap.	Names(s)[a]	WMR[b]	Sp. Type[c]	A_v[d] (mag)	M(I) (mag)	log T_{eff} (K)	log(L/L$_\odot$)	M_*[e] (M$_\odot$)	Log(age) (yr)	Criteria[f]	Notes[g]
1	26		2-4	M2	4.6	6.26	3.544	-0.83	0.32	6.48	ext,x	
		HD 148352	3-39	M5	0.4	8.98	3.477	-1.72	0.13	6.95	li	
		HD 148352		F2 (HS)	0.0 (2M)	1.18	3.838	1.21	2.1	6.71	x	(5)
2	44		4-57	M3.5	5.3	6.68	3.512	-0.93	0.20	6.27	ext	
2	45			M3.5	5.2	7.28	3.512	-1.17	0.21	6.59	ext,ha	
		SR 20	1-35	G7	7.0 (GS)	1.46	3.747	1.14	2.8	6.22	ext,ha,pm,x	(4)
2	16		2-23	M4	2.8	7.25	3.498	-1.13	0.18	6.41	ext,li,x	
		SR 13	1-15	M3.75	0.0 (BA)	5.33	3.491	-0.38	0.14	4.77	ha,IRX,pm,x	(4)
5	7			M4.5	1.8	9.36	3.488	-1.93	0.14	7.34	ext,ha,var	
		WSB 63	3-43	M1.5	3.9	5.61	3.553	-0.58	0.35	6.20	ext,ha,li,x	
5	4			M5.5	0.2	9.73	3.462	-1.97	0.08	6.91	ha,IRX,var,x	
2	57			M5	0.3	7.46	3.477	-1.12	0.14	6.28	ha,IRX,li	
			3-37	M5.5	0.0	8.91	3.462	-1.64	0.10	6.67	li	
		ROX 35A		K3 (BA)	2.1 (W)	3.93	3.676	0.08	1.0	6.36	ext,li,x	
		ROX 35B		G4 (BA)	2.5 (GS)	3.64	3.763	0.27	1.2	7.22	ext,x	

[a]Sources names from optical or infrared studies noted in Table 2 plus: (SR) Struve & Rudkjøbing 1949; (DoAr) Dolidze & Arakelyan 1959; (EL) Elias 1978; (Chini) Chini 1981; (WL) Wilking & Lada 1983; and (ROXR1) Casanova et al. 1995.

[b]Source name from Wilking et al. (2005).

[c]Optical spectral types from this study or Wilking et al. (2005) except where noted: (EL) Elias 1978; (CK) Cohen & Kuhi 1979; (HS) Houk & Smith-Moore 1988; (GS) Gordon & Strom 1990, private communication; (BA) Bouvier & Appenzeller 1992; (TQ) Torres et al. 2006; and (MMGC) Martín et al. 1998.

[d]R and I band magnitudes used to compute A_v and L_{bol} are from this study except where noted: (C) Chini 1981; (GS) Gordon & Strom 1990, private communication; (BA) Bouvier & Appenzeller 1992; and (W) Walter et al. 1994. (2M) denotes J and H band data from 2MASS were used to compute A_v and L_{bol} and M(J) replaces M(I) in Column 7.

[e]Masses and ages estimated from the tracks and isochrones of D'Antona & Mazzitelli (1997) and F. D'Antona & I. Mazzitelli (1998, private communication) except where noted in the last column.

[f]Association membership established through location above the main sequence and A_v > 1.5 mag (ext), the presence of Hα emission EW > 10 Å (ha), an infrared excess (IRX), lithium absorption (li), proper motion (pm), reflection nebulosity (ref. neb.), near-infrared variability (var), or X-ray emission (x). See the text for details.

[g]Notes: (1) sits below main sequence, possible foreground star; (2) spectroscopic binary Casassus et al. 2008; (3) mass and age derived from the tracks and isochrones of Palla & Stahler 1999; (4) subarcsecond companion observed in infrared and treated as a single object (Barsony et al. 2003, Prato 2007); (5) discordant proper motion (Mamajek 2008).

Table 4. Revised Photometry from Paper I

Name	I	(R-I)	Reference
$[WMR\ 2005]1-29$	10.7	1.0	Bouvier & Appenzeller (1992)
$[WMR\ 2005]1-30$	11.57	1.54	Gordon & Strom (1990, private communication)
$[WMR\ 2005]1-28$	11.37	1.17	Gordon & Strom (1990, private communication)
$[WMR\ 2005]4-66$	17.85	$\cdots$	This study
$EM*SR\ 12$	10.92	1.27	Gordon & Strom (1990, private communication)
$[WMR\ 2005]1-26$	9.9	0.8	Bouvier & Appenzeller (1992)
$[WMR\ 2005]3-19$	$\cdots$	$\cdots$	Edge of image: this study
$[WMR\ 2005]1-35$	11.25	1.45	Gordon & Strom (1990, private communication)
$[WMR\ 2005]1-15$	10.9	1.45	Bouvier & Appenzeller (1992)
$[WMR\ 2005]4-56$	17.04	1.70	This study
$[WMR\ 2005]1-3$	$\cdots$	$\cdots$	Saturated: this study

Paper II
A Spectroscopic Survey of the Serpens Main Cluster

Kristen L. Erickson[2]

Department of Physics and Astronomy, University of Missouri-St. Louis

1 University Boulevard, St. Louis, MO 63121

kle6x2@umsl.edu

Bruce A. Wilking[2]

Department of Physics and Astronomy, University of Missouri-St. Louis

1 University Boulevard, St. Louis, MO 63121

bwilking@umsl.edu

Michael R. Meyer

Institute for Astronomy, Swiss Federal Institute of Technology

Wolfgang-Pauli-Strasse 27

CH-8093 Zurich, Switzerland

mmeyer@phys.ethz.ch

Jinyoung Serena Kim

Steward Observatory, University of Arizona

933 North Cherry Avenue

Tucson, AZ 85721

serena@as.arizona.edu

William Sherry

National Optical Astronomy Observatories

950 North Cherry Avenue

Tucson, AZ 87719

wsherry@noao.edu

and

Matthew Freeman

Department of Physics and Astronomy, University of Missouri-St. Louis

1 University Boulevard, St. Louis, MO 63121

mlf72c@umsl.edu

ABSTRACT

We have completed an optical spectroscopic survey of an unbiased sample of candidate young stars in the Serpens Main star-forming region selected from deep B, V, and R band images. While infrared, X-ray, and optical surveys of the cloud have identified many young stellar objects (YSOs), these surveys have been biased toward particular stages of pre-main sequence evolution. We have obtained over 700 optical spectra that, when combined with published data, have led to the identification of 63 association members based on the presence of Hα in emission, lithium absorption, X-ray emission, a mid-infrared excess, and/or reflection nebulosity. Twelve YSOs are identified based on the presence of lithium absorption alone. An additional 16 possible association members have been singled out for further study. Spectral types along with V and R band photometry were used to derive effective temperatures and bolometric luminosities for association members to compare with theoretical tracks and isochrones for pre-main sequence stars. An average age of 2 Myr is derived for this population with an age spread of 1-5 Myrs. We are unable to determine if this age spread is intrinsic or a result of a very large spread in distance of individual sources. Modeling of the spectal energy distributions from optical though mid-infrared wavelengths has revealed three new transition disk objects, making a total of six in the cluster. Echelle spectra for a subset of these sources enabled estimates of $v \sin i$ and surface gravity values for 12 association members. Surface gravities are found to be consistent with dwarf or sub-gaint stars.

Subject headings:

1. Introduction

Young clusters provide a valuable test bed for star formation theories since large numbers of stars have formed out of the same molecular cloud under the same conditions. Measurement of the age distribution within a cluster places limits on star formation time scales and processes. To understand more clearly the star formation process, measurement of characteristics such as age, mass function, and disk frequency are necessary. These characteristics can be most fully studied by unbiased spectroscopic surveys (Bastian, Covey & Meyer 2010). The Serpens Molecular cloud is an ideal region for studies of young clusters as it contains objects in all stages of evolution from protostars to pre-main sequence stars (see Eiroa, Djupvik, & Casali 2008 for review). The Spitzer Space Telescope has studied Serpens in the mid- and far-infrared as part of the Legacy programs. About 235 objects were identified as YSOs due to infrared excesses in two main concentrations (Harvey *et al.* 2006; Winston *et al.* 2007; Winston *et al.* 2009). The best-studied concentration is the Serpens Main region which contains two dense cores hosting an infrared cluster centered on SVS 20 (Eiroa & Casali 1992) along with numerous submillimeter sources (Testi & Sargent 1998; Testi *et al.* 2000; Davis *et al.* 1999; Hogerheijde *et al.* 1999). Most of these sources are not visible at optical wavelengths. X-ray studies have also been conducted of this region with XMM- Newton and Chandra (Preibish 2003; Winston *et al.* 2007; Giardino *et al.* 2007). These surveys have targeted more evolved pre-main sequence stars with magnetic surface activity and trace an older, more distributed population surrounding the core of more embedded infrared sources (Kaas *et al.* 2004). The second concentration, dubbed Serpens South, is located about 3 degrees south of Serpens Main. While less well-studied, it is a cluster rich in protostars embedded in a dense filamentary cloud (Harvey *et al.* 2006; Gutermuth *et al.* 2008).

Estimates for the distance to the Serpens Main cloud have varied considerably over the years and they are complicated by its location toward the Aquila Rift (Dzib et al. 2010). Initial estimates of 440 pc were based on the spectroscopic parallax of the B star HD 170634 (BD+01 3694) which lies about 6′ east of the dense molecular core and illuminates S 68 (Racine 1968; Strom, Grasdalen, & Strom 1974). Later estimates using a Wolf diagram technique that measured extinction vs. distance to background stars yielded distances of 200-260 pc (Straižys et al. 1996, 2003; Knude 2011). However most recently, Dzib et al. (2010, 2011) used the VLBA to measure parallaxes for both components of EC 95, a YSO binary system embedded in the Serpens Main molecular core. Their estimate of 429±2 pc suggests that Wolf diagram techniques are encountering foreground clouds associated with the Aquila Rift. We adopt 429 pc as the distance to the Serpens Main cloud which is consistent with distance estimates to S 68. We note that the presence of foreground clouds raises the possibility that there could be YSOs in our sample foreground to the Serpens cloud for which we would be overestimating their luminosities and underestimating their ages.

To gain a complete picture of the star-forming history of a region, all phases of pre-main-sequence (PMS) evolution must be studied. But due to the highly variable nature of X-ray emission, YSOs with little or no circumstellar dust have been under sampled in the Serpens Main cluster. Optical spectroscopic surveys have been conducted of this region, however these studies have been biased towards objects with X-ray emission (Wilking *et al.* 2008) or towards stars with infrared excesses (Winston *et al.* 2009, Oliveira *et al.* 2009). We present the results of a new optical spectroscopic survey of 346 candidate YSOs over a 0.25 square degree region centered on Serpens Main which provides an unbiased sample of optically-visible YSOs in the Serpens Main cloud. Section 2 describes B, V, and R band imaging plus both intermediate and high resolution spectroscopic observations. Data reduction techniques including analysis of spectra to derive spectral types and surface gravities are also described.

Section 3 discusses the results of our analysis including the identification of association members and their spatial distribution, placement in a Hertzsprung-Russell (H-R) diagram relative to several theoretical models, age distribution, disk frequency, and accretion and rotation rates. Modeling of the spectral energy distributions from optical through mid-infrared wavelengths is described. Section 4 compares Serpens to other star forming regions and explores the possibility of an age spread.

2.   Observations and Data Reduction

Over 700 moderate resolution spectra were obtained for 346 stars selected from a (V-R) vs. V color-magnitude diagram as candidate YSOs. These observations and the data reduction are described in detail in the following sections.

2.1.   B, V, and R Photometry and Sample Selection

B, V, and R band images were obtained on 25 May 2007 through light cirrus with the 90prime wide-field camera on the 2.3 meter Bok Telescope (Williams *et al.* 2004). Using one of the four CCDs, the images covered a $30.7'$ x $30.7'$ area with a scale of $0.45''$ pixel^{-1} centered on the Serpens Main cluster, $RA(2000) = 18^h\ 29^m\ 56.7^s$, decl.(2000) $= +01°12'24''$. In order to sample the brightest and faintest sources, four dithered exposures with integration times of 4 sec and 80 sec were obtained plus several 0.2 sec exposures. Each frame was dark subtracted and flat-fielded using twilight flats. Image distortion due to the wide field of view was corrected via re-sampling of the data using astrometric standards from the USNO survey.

Aperture photometry was performed using the *phot* task in IRAF[1]. An aperture radius of r=5 pixels ($2.25''$) was used for the 4 sec and 80 sec exposures that matched

---

[1]IRAF is distributed by the National Optical Astronomy Observatory, which is operated by the Association of Universities for Research in Astronomy, Inc., under cooperative agreement with the National Science Foundation.

the full width at half maximum of the point-spread function (Howell 1989). Local sky background was measured in an annulus of radius 15-25 pixels. An aperture radius of r=7 pixels (3.15″) was used for the brightest stars in 0.2 sec exposures to capture the entire point spread function. Statistical errors were measured in IRAF which assumes a Poisson detection model. The final instrumental magnitudes were weighted averages of those from the dithered images.

The primary photometric calibration was established from seven bright stars in the field (SCB 41, 43, 47, 60, 67, 70, 72; Straižys *et al.* 1996). Magnitudes were kindly provided by Richard D. Schwartz from observations in June and July of 2009 at the Galaxy View Observatory in Sequim, WA. A number of Landolt standards in the Johnson-Cousins system covering a wide range of colors and airmasses were observed throughout the night to obtain coefficients for extinction, instrumental transformations, and zero points. Considering all sources of photometric errors, the B, V, and R magnitudes have 1% uncertainties. These sources were used to calibrate the brightest stars in the 0.2 sec exposures (R<9.6) and the 4 sec exposure frames (R<12.6). Considering calibration and statistical errors, minimum uncertainties in the B, V, and R band photometry were (0.03, 0.05, and 0.05 mags) at 0.2 sec and (0.08, 0.09, and 0.03 mags) at 4 sec. A group of bright, unsaturated sources with R=12.6-16.0 mag were used as secondary standards in the 80 sec images, yielding uncertainties due to calibration of (0.08, 0.10, and 0.04 mag). Photometric uncertainties for sources fainter than B∼21, V∼20, R∼18.5 mags are dominated by sky noise. Completeness limits at V and R of 20.25 mag and 18.75 mag, respectively, were estimated from the turnover in a plot of the number of stars vs. magnitude.

2.2. Spectroscopy

Candidate YSOs were selected for spectroscopic observations from a V vs. (V-R) color magnitude diagram (Fig. 1). Targets were located on or above the ZAMS with

V magnitudes brighter than 20.0. The sample includes objects with masses $\geq$0.5 M$_\odot$ and A$_v$ < 3.4 mag. Optical spectra were obtained using several instruments; Hydra, Hectospec, a Boller and Chivens (B&C) spectrograph, and the Magellan Inamori Kyocera Echelle (MIKE) spectrograph, on the WIYN, MMT, Bok and Magellan Clay telescopes, respectively. For multi-fiber instruments (Hydra and Hectospec), fiber configurations were designed to observe the maximum number of candidate YSOs; crowding at the edges of our field restricted the number of sources that could be observed. Observing parameters are detailed in Table 1. For all spectral observations, scattered light corrections were not made and no flux calibration was performed. All spectra were bias and dark corrected using the *ccdproc* routine in IRAF unless otherwise specified. The typical signal-to-noise ratio was 20 - 100 as measured by line-free regions of the continuum. Spectra were normalized and smoothed for comparison with dwarf standard stars.

In June and September of 2008, the brightest objects in our sample were observed on the Bok 2.3 meter telescope using the B&C spectrograph. In June, objects were observed at red wavelengths (5954 -7115 Å) in first order. In September, objects were observed at blue wavelengths (3850 -5566 Å) in second order with a copper sulfate filter used to block first order light. All spectra taken on the Bok telescope were extracted using the *apall* routine in IRAF. This routine also performs sky subtraction of the data. Dome flats were used to correct for pixel-to-pixel variations in responsivity of the CCD. A HeArNe lamp was used to wavelength calibrate the data.

Spectra were obtained on the WIYN[2] 3.5 meter telescope using Hydra in 2006, 2009, and 2010. Spectra were extracted with IRAF's *dohydra* package using dome flats obtained for each fiber configuration. Sky spectra were taken by placing fibers on random positions distributed across each field. Sky subtraction was accomplished

---

[2]The WIYN Observatory is a joint facility of the University of Wisconsin-Madison, Indiana University, Yale University, and the National Optical Astronomy Observatory.

using the median of 10-15 sky spectra. A CuAr lamp was used for wavelength calibration.

In July of 2010 and September of 2011, objects were observed on the MMT 6.5 meter telescope using Hectospec. Spectra observed in 2010 were reduced using E-SPECROAD created by Juan Cabanela. Dome flats were acquired for flat-field corrections. The E-SPECROAD pipeline extracts spectra, applies bias, dark, and flat-field corrections and performs the wavelength calibration. Sky subtraction was achieved using sky spectra taken by offsetting the telescope. For spectra where this was unsuccessful, sky spectra taken by placing fibers on random positions distributed across each field were used. Spectra observed in 2011 were reduced at the OIR Telescope Data Center using the SPECROAD pipeline, supported by the Smithsonian Astrophysical Observatory (Fabricant et al. 2005; Mink et al. 2007). Spectra in 2011 were corrected to remove atmospheric water vapor absorption bands at 6870-6955 Å and 7680-7730 Å. All the spectra were wavelength calibrated using exposures from a HeNeAr lamp.

Objects observed using the red and blue path on the Magellan Clay 6.5 meter telescope using MIKE had 33 orders and 32 orders, respectively. All data taken on MIKE were reduced using the IRAF *mtools* package created by Jack Baldwin, along with standard IRAF routines. *mtools* extracts "tilted" spectra, performs sky subtraction, and removes cosmic rays. Dome flats were used to correct for pixel-to-pixel variations in responsivity of the CCD. These spectra were wavelength calibrated using exposures of a ThAr lamp.

2.3. Spectral Classification

Spectral classifications were derived for each spectrum. Table 2 presents the results using the moderate resolution spectra from the B&C, Hydra, and Hectospec spectrographs. As shown in the last column of Table 2, many sources were observed

multiple times in blue and red wavelength bands. When spectral classifications for a given source did not agree between observations, all spectra were compared and a final spectral type and range determined with the highest weight given to spectra with the highest signal-to-noise. In general, there was very good agreement in spectral classifications between observations. Table 3 presents the results from the echelle spectra obtained with MIKE. The spectral typing procedures are described below.

2.3.1. Moderate Resolution Spectra

Spectral types were first derived from visual pattern matching of absorption features in our program star spectra with those in dwarf standard star spectra. In order to match spectral features between standard stars and target objects, all of our spectra were smoothed using a Gaussian filter to the resolution of the standard stars. Depending on the wavelength coverage of the spectra, normalized spectra were smoothed to a resolution of 5.7 Å, 4.5 Å, or 3 Å for comparison with spectral standards of Allen & Strom (1995), Jacoby, Hunter & Christian (1984), or Le Borgne *et al.* (2003), respectively. Spectra at red wavelengths were pattern matched using the Na I doublet at 5893 Å, Ca I at 6122 Å and 6162 Å for G, K, and M stars, as well as the TiO bands for stars later than K5 (Torres-Dodgen & Weaver 1993). For stars with no indicator of youth, the relative depth of Hα to the blend of Ba II, Fe I, and Ca I at 6497 Å was also used. Spectra at blue wavelengths were pattern matched using the Ca H and K lines at 3969 Å and 3934 Å, the Ca I line at 4226 Å, and the Fe I line at 4271 Å. For stars cooler than F5, the G-band around 4300 Å was used and for stars cooler than K5, the Mg I b band around 5200 Å and MgH band around 4750 Å were also employed (Gray & Corbally 2009).

Classifications were also made using the program SPTCLASS written by Jesus Hernandez (Hernandez *et al.* 2005). The program was written to determine spectral classifications for stars from B2 to M9.5 using numerous spectral features and is

optimized for spectra obtained with Hectospec with the 270 g mm^{-1} grating. As our 2011 data were the only data with this observing setup, it is the only set of data confirmed using this program. The SPTCLASS spectral types agreed with our visual classifications within 3 subclasses.

A rough estimate of the surface gravity of an object is important in distinguishing pre-main sequence stars from background giants or field dwarfs. The primary gravity-sensitive absorption feature available for analysis in our spectra was the CaH band centered at 6975 Å. A CaH index was calculated as the ratio of the continuum at 7035 $\pm$15 Å to the flux in the CaH absorption band at 6975 $\pm$ 15 Å and a TiO index as the ratio of the continuum at 7030 $\pm$ 15 Å to the flux in the TiO absorption band at 7140 $\pm$ 15 Å from the unsmoothed, normalized spectrum of each science object. These indices were then plotted against each other. For objects with multiple observations, values are an average weighted by the noise. Dwarfs and giants define distinct curves on the plot with sub-giants falling between. In both sets of Hectospec spectra, the strength via visual comparison with standard stars of the sodium doublet at 5893 Å and Ca II triplet at 8660 Å were also used to determine which sources were giants (Torres-Dodgen & Weaver 1993).

2.3.2. Echelle Spectra

Spectral classifications for data taken with MIKE were accomplished using visual comparisons with standard stars retrieved from the ELODIE archive at Observatoire de Haute-Provence with similar spectral resolution to our data (Moultaka *et al.* 2004). For all spectral types, initial classifications were made employing hydrogen lines from Hα to Hγ along with Ba II, Ti I, Fe I and Ca I around 6497 Å (which are not blended at this resolution). For B stars, He I lines at 4143 Å and 4417 Å, as well as the Ca II line at 4267 Å, were employed. For A stars and later, Ca I at 4226.7 Å was also available. For F and G type stars, Fe I at 4383.5, 4325.7, and 4045.8 Å were used as

additional criteria. Spectral types from these high resolution spectra generally agreed with those from our moderate resolution spectra within 2 subclasses. The range of adopted spectral types are given in columns 5 and 6 of Table 3.

The echelle spectra are well-suited to estimate surface gravity due to a number of available gravity-sensitive lines (Ginestet et al. 1994; Gray & Corbally 2009). The procedure for estimating log g was as follows. Equivalent widths of various lines depending on spectral type were measured and plotted versus temperature from synthetic spectra from the POLLUX database[3](Palacios *et al.* 2010) with log g values of 4.5, 4.0, and 3.5. In order to obtain a full range of temperatures and surface gravities, synthetic spectra were created using both ATLAS and MARCS model atmospheres. For sources with spectral types between B6 and A7, equivalent widths of $H\alpha$, $H\beta$, $H\gamma$, and $H\delta$ were used (Palacios *et al.* 2010). These lines may be somewhat filled in with emission, so the values presented for sources in this spectral range were viewed as lower limits. For the B stars, we then checked that the He I lines at 4009, 4026, 4121, 4144, 4387 and 4471 Å were in agreement with the temperature and log g values. This was done by visual comparison with standard stars from the ELODIE spectral database with dwarf, sub-giant and giant luminosity classes. For the A stars, the fit was checked using the Ca I line at 4226 Å and the Fe I lines at 4271, 4046, and 4383 Å. For sources with spectral types A1-F7, the equivalent widths of the Ca II lines at 8498 and 8542 Å were plotted as described above, with the addition of log g values of 3.0. Line ratios of the Fe II and Ti II blend at 4400 and 4395 Å to Fe I lines at 4271 and 4383 Å and Ca I at 4226 Å were also plotted and used as above. For sources with spectral types from F5 to K1, the equivalent widths of Ca II at 8498 and 8542 Å, Fe I at 8621 and 8688 Å, and Ti I at 8435 and 8426 Å, as well as the ratio between Y II at 4376 Å and Fe I at 4383 Å were plotted as above, with the addition of log

---

[3]This research was achieved using the POLLUX database (http://pollux.graal.univ-montp2.fr/), operated at LUPM (Universite Montpellier II - CNRS, France) with the support of the PNPS and INSU.

g values of 2.0. The range of values for log g was then determined, and matched to luminosity classes V, IV and/or III. These values represent a limit, and not a firm determination of log g. It is also important to note that for stars hotter than about F5 there is little difference in temperatures and log g values for dwarfs, giants and sub-dwarfs, making it difficult to differentiate between these.

Using our echelle spectra, esimates for $v \sin i$ were made by convolving the synthetic spectrum of a standard to match the line widths observed in our spectra. Our main assumptions were that rotation was the dominant source of line broadening and that this was significantly larger than the source of broadening in the synthetic spectra. Synthetic spectra were taken from the POLLUX database (Palacios et $al.$ 2010) which assumed microturbulent broadening of 1-2 $\mathrm{km\,sec^{-1}}$. Synthetic spectra selected to match the spectral types and surface gravities of our objects were convolved using the $gauss$ package in IRAF. $v \sin i$ for each object was derived from the average of the individual $v \sin i$ values measured from the widths of the convolving gaussians needed to match the full width at half maximum for ~ 10 metal lines distributed over the entire spectrum. In most cases, the value of $v \sin i$ for a given object did not vary significantly with surface gravity; the average values are presented in Table 3 except for SCB 40 for which a range is given. To check the validity of our technique, we selected 6 stars with high signal-to-noise spectra in the ELODIE database with published values of $v \sin i$: HD 187642 (α Aquili, A7V), HD 58946 (F0V), HD 70958 (F3V), HD 111456 (F6V), HD 176303 (F8V), and HIP 106231 (K3V) (Glebocki et $al.$ 2005, White, Gabor, & Hillenbrand 2007; Schroeder, Reiners, & Schmitt 2009; Lopez-Satiago et $al.$ 2010). With our method, we were able to reproduce the published values for $v \sin i$ to within 10%.

3. Results

Optical spectra have been obtained for 86% of the stars in the V vs. (V-R) diagram (Fig. 1) that fell above V=18.5 and (V-R) =1.8.

3.1. Spectral Classifications and Surface Gravities

Spectral types were determined for 336 of 346 stars; 7 of these were adopted from the literature. These data are presented in Table 2 along with previous source names, RA and decl. in J2000, some observing details, V magnitudes, and the (B-V) and (V-R) color indices. For 6 sources with optical spectral types, (V-R) color indices were not available, so (J-H) values from 2MASS are presented. The presence of lithium absorption at 6707 Å and the equivalent width of Hα are also indicated (emission shown as a negative value). Based on surface gravity indicators (see Sec. 2.4), twelve background giants have been identified. The possible range of surface gravities were estimated for objects with echelle spectra and are listed in column 7 of Table 3. The majority are consistent with dwarf or subgiant surface gravities, although as alluded to earlier, log g values do not vary greatly with luminosity class for stars hotter than F5 which dominate this sample.

Two sources are of particular interest: KOB 370 and J183037.5+0117581. KOB 370 is a known double with both sources reported to have Hα in emission (Kaas *et al.* 2004). The sources are not spatially resolved in our moderate resolution spectra and show Hα in emission with the EW(Hα) varying from -2.4 to -9.5 Å. However our MIKE spectrum does not show Hα in emission. This could be due to the variable nature of Hα emission. The X-ray source J183037.5+0117581 has hydrogen lines that do not match any of the standard stars. The echelle spectrum shows that hydrogen absorption lines and the Ca II triplet are filled in with emission, making the spectral type for this source more uncertain. Accounting for this fact, we revised the spectral

classification derived from moderate resolution spectra from K5 to K0.

Thirty of our sources had optical and infrared spectral types previously published by Winston *et al.* (2009) and Oliveira *et al.* (2009). Our spectral classifications agree well with those previously published with two exceptions; WMW 124 and WMW 220. Winston *et al.* (2009) report spectral types of K6.5 and A3, respectively. Strong H absorption lines with broad wings in the blue and red, the absence of He I at 4387 Å, a weak blend of Ba II, Ti, Fe I and Ca I at 6497 Å, and the lack of TiO bands led to our classification of A2 for WMW 124. It is worth noting that our position and the position reported by Winston are different by 1.6″, so it is possible that these may be different sources, however no source appears that close in our R band image. The strength of Ca I at 4226 Å and Fe I at 4383 Å relative to the G band at 4300 Å, the absence of the MgH bands, and the strength of the Mg I triplet at 5167, 5172, and 5183 Å led to our K1 classification for WMW 220.

3.2. Association Membership

Fifteen new pre-main sequence objects were identified using the same criteria of Erickson *et al.* (2011) with one exception; proper motions were unknown and not used as a criterion. These criteria include, Hα in emission with EW > 10 Å during at least one observation, X-ray emission, the presence of lithium absorption for stars with spectral type K0 and cooler, a mid-infrared excess, or associated reflection nebulosity. Fifty-seven objects with optical spectral types meet one or more of these criteria. We did not include any source solely on the basis of extinction criterion, however we have noted extinction criterion for objects too luminous to be main sequence objects at the distance to Serpens and with an estimate for A$_v$ too high to be foreground to the cloud (A$_v$ > 3.5 mag). A minimum A$_v$ of 3.5 was selected using the results of Straižys, Černis, & Bartašiūte (2003) who reported a maximum extinction in the direction of Serpens of A$_v$ = 3 mag at a distance <360 pc. Therefore, in general we

expect that sources with an $A_v > 3$ mags will be located behind foreground clouds from the Aquila Rift. Spectral types for an additional 7 YSOs were taken from the literature giving a total of 63 association members. These objects are listed in Table 4. Eighty percent of the YSOs in our sample have K or M spectral types, with the majority of these K stars due to the magnitude limit of our survey. A plot of the CaH index for the association members and giants with spectral types of K5 or cooler is shown in Figure 2. Most of the association members fall along the dwarf standard locus and justifies our use of dwarf standards for classification and dwarf colors for dereddening.

Sixteen sources which met the extinction criterion above and had either weak Hα emission (10 Å > EW(Hα) > 5 Å) or possible lithium absorption were identified as possible association members. These objects are listed in Table 5 as "weak criteria" sources and require further observations to confirm their status.

Fourteen sources were found to have strong Hα emission with EW(Hα) > 10 Å which is characteristic of classical T Tauri stars. An additional 7 objects showed weaker Hα emission (10 Å > EW(Hα) > 5 Å), all with either a K or M spectral type. Four of these 7 are association members and one is a weak criteria member. The remaining sources remain unclassified. The variable nature of Hα emission is apparent when comparing sources observed months or years apart.

3.3.   Spatial Distribution

The distribution of 63 confirmed and 16 possible association members is shown in Figure 3 relative to the Serpens molecular core as defined by contours of $C^{18}O$ integrated intensity (McMullin *et al.* 2000). Star symbols mark the locations of the two most massive association members in our survey: the B8 star HD 170634 and a B5 star [CDF88] 7. One has the impression that the B stars have helped shape the distribution of gas in the core. While our spectroscopic survey included sources

over the entire field, there is a tendency for association members to be concentrated toward the molecular core yet avoid the highest column density gas. The distribution of association members drops off sharply to the north but is continuous to the southern edge of our survey area. This is consistent with the distribution of cloud material which continues to the south where it overlaps with the Serpens South molecular core (Cambrésy 1997, Oliveira *et al.* 2009).

3.4. Hertzsprung-Russell Diagrams

Effective temperatures were derived from the spectral classifications with typical uncertainties of $\pm$250 K for K-M stars. We assumed dwarf, rather than subgiant, surface gravities leading to a possible *overestimate* of T_{eff} for stars with spectral types of G5-K5 by $<$250 K and an *underestimate* of T_{eff} for stars with spectral types of M2-M5.5 by $<$200 K (e.g., Drilling & Landolt 2000). Intrinsic colors and bolometric corrections for dwarf stars were taken from Drilling & Landolt (2000) for B4-B7 stars (converting the colors into the Kron-Cousins system), Schmidt-Kaler (1982) for B8-K5 stars and from Bessell (1991) for K5-M7 stars.

In order to derive luminosities, sources were dereddened using the $(V - R)$ color index assuming the reddening law derived by Cohen *et al.* (1981) in the Kron-Cousins system:

$A_v = 5$ E(V-R), Sp Ty $<$ A0 (early-type) (1)

$A_v = 5.5$ E(V-R), Sp Ty $\geq$ A0 (late-type) (2)

B, V, and R band data were taken from this study except where noted in Columns 9 and 11 of Table 2. For five sources, V and R band data were not available and sources were dereddened using J and H band data from the 2MASS survey (Cutri *et al.* 2003) and transformed into the CIT photometric system using the relationships derived by Carpenter (2001). These sources, were dereddened using the following reddening law

in the CIT photometric system

$$A_v = 9.09 \ E(J\text{-}H) \ (\text{Cohen } et \ al. \ 1981). \ (3)$$

For sources with an infrared excess and extinction values computed using equation 3, values for A_v and L_{bol} are quoted as upper limits in Table 4. A comparison between luminosities derived using (J-H) and (V-R) suggests that infrared colors systematically overestimate the extinction and thus the luminosity by 0.1 dex. For two sources, the errors in the photometry and/or spectral classifications yielded slightly negative values for the extinction and an extinction of 0.0 was assumed.

The absolute V magnitude, M(V), was computed given the extinction and assuming a distance of 429 pc. Then the bolometric magnitude and luminosity were derived given:

$$M_{bol} = M(V) + BC(V) \ (4),$$

and

$$\log(L_{bol}/L_\odot) = 1.89 - 0.4 \ M_{bol} \ , \ M_{bol}(\odot) = 4.74. \ (5)$$

In the situations where J and H were used to deredden, M(J) is recorded in Column 6 of Table 4 and was used along with BC(J) to derive M_{bol}. By adding quadratically errors in the V and R photometry, the median error in log(L) is estimated to be 0.12 dex. We assumed an uncertainty in the distance modulus of 0.05 mag corresponding to a depth of ± 10 pc, and an uncertainty of 0.03 mag in the intrinsic colors and bolometric corrections due to spectral type errors. In most cases, the dominant errors were the uncertainties in the distance modulus and the extinction, which were on average about the same.

H-R diagrams for association members and weak criteria members were made using tracks and isochrones from D'Antona & Mazzitelli (1997) and F. D'Antona & I. Mazzitelli (1998, private communication), Palla & Stahler (1999, PS99), and Siess *et*

al. (2000). The diagrams for the D'Antona & Mazzitelli models (hereafter DM) and PS99 are shown in Figure 4. The models give very similar results for our sample, even with the differences in treatments of the equations of state as a function of mass and of convection. Luminosities for several intermediate mass association members are only consistent with the current distance estimate of 429 pc; a distance to the cluster of 230-260 pc would place several association members below the main sequence. The masses and ages interpolated from the DM models are given in Tables 4 and 5. There is no clear separation of sources which have an infrared excess and/or Hα emission from sources with lithium absorption and/or X-ray emission. This implies that evolution occurs on different time scales for each source. Since most of the objects lie on convective tracks, uncertainties in the mass *relative to the DM models* were estimated from the errors in the spectral classifications and uncertainties in the age from errors in the luminosities. Uncertainties in the mass for objects in the range of 0.14-4.7 M$_\odot$ were typically 5%-23%. Uncertainties in the log(age) were 0.17-0.38 dex relative to DM models. It is important to note that theoretical mass tracks may underpredict absolute stellar mass by 30% - 50% and absolute age by up to a factor of two if optical colors are used (Hillenbrand 2009; Bell *et al.* 2012; 2013).

3.5.   Age Distribution

The values for log(age) derived from the models are consistent with a normal distribution with a median log(age) from the DM models of 6.2$\pm$0.6 (2 Myrs). This is in agreement with findings of Kaas *et al.* (2004) of 2 Myrs for class II sources based on modeling of luminosity functions. Median ages derived from the PS99 and Siess *et al.* models are systematically older by 1 Myrs and 2.5 Myrs, respectively, although all are consistent within the uncertainties. Simulations suggest an *intrinsic* age spread. Assuming Gaussian-distributed errors in log T and log L and using the DM models for 2 Myr, a Monte Carlo simulation derived values of log T and log L

for over 12,000 samples in the mass range of 0.12 - 1.0 $M_\odot$ weighted by the Chabrier (2003) system mass function. A Kolmogorov-Smirnov (K-S) test was run with the association members and simulation sources restricted to stars that overlapped with the DM models with masses between 0.14 $M_\odot$ (lowest association member mass) and 1.7 $M_\odot$ (the highest value in the simulation). The K-S test suggests that there is only a 0.05% chance that the two age distributions were drawn from the same parent population.

3.6.   Infrared Excesses and Transition Disk Objects

An initial assessment of the presence of a circumstellar disk can be determined by the slope of the mid-infrared energy distribution. Following the analysis of Lada *et al.* (2006), we performed a least squares fit to the IRAC flux densities observed with the Spitzer Space Telescope (SST). A spectral index $a{\geq}{-}1.80$ is indicative of an optically thick disk while $-1.80{\leq}a{\leq}{-}2.56$ is representative of an "anemic" and possibly a transition disk. The results of our fits are shown in Fig. 5 and suggests there are 22 association members with optically-thick disks and 3-4 sources with "anemic" disks.

We can refine these classifications given the spectral types, visual extinctions, and optical/infrared photometry available for each association member. Dereddened spectral energy distributions were constructed for each association member using optical data from this study, near-infrared data from the 2MASS catalog (Cutri *et al.* 2003), and mid-infrared data from 3.55 μm - 70 μm from the SST compiled in the C2D Fall '07 Full CLOUDS Catalog (Evans *et al.* 2003). The dereddened spectral energy distributions could then be compared to that expected from a stellar photosphere and from a face-on reprocessing disk scaled to the source flux at R or J. Disk models were taken from Hillenbrand et al. (1992) for A0, F0, G0, K0, K5, M0, or M3 stars.

The presence of an infrared excess from an optically-thick disk is indicated for 21 association members as noted in the last column of Table 4. Our results agree well

with previous classifications using data from the Infrared Space Observatory (Kaas *et al.* 2004) and the SST (Winston *et al.* 2009) with a few exceptions. Kaas *et al.* list BD+01 3687 as a possible transition object while our analysis indicates no excess out to 24 μm. We would include WMW 166 as having an optically-thick disk as opposed to the previous classification as a transition disk object (Winston *et al.* 2009). We identify six association members as possible transition objects and show their spectral energy distributions in Fig. 6. Three of the sources, WMW 124, WMW 128, and WMW 157 have been previously identifed as such by Winston et al. (2009). We add WMW 205 to this category (previously classified as class 3) and note two sources with evidence for inner disk holes: WMW 74 and WMW 79. None of our spectra for these six sources show Hα in emission, hence they do not show evidence of active accretion. However, as Hα maybe slightly filled in, it is possible that sources are weakly accreting. On average the ages for these sources are 1-6 Myrs, only WMW 74 is younger at 0.2 Myrs.

In summary, 21 association members show evidence for an optically-thick disk and 6 objects for an optically-thin or possible transition disk. At face value, this suggests a disk frequency of 42%(+10%,-8%) with the uncertainty estimated using Poisson statistics (Gehrels 1986). One obtains a nearly identical disk frequency of 37%, but with much greater uncertainties, if one considers only an extinction-limited sample of 19 association members with M$\geq$ 0.6 M$_\odot$ and A$_v$ $\leq$ 4.0 mag. This compares well with the disk frequency derived for optically-visible association members in the Rho Ophiuchi L 1688 cloud (Erickson *et al.* 2011).

3.7. Accretion and Rotation Rates

For association members with strong Hα emission, the Gaussian full width at 10% of maximum was used to estimate an accretion rate using the relation developed by Natta *et al.* (2004) when the velocity width at 10% maximum was greater than 270

km sec^{-1}. This relation assumes a negligible contribution from an outflow. Accretion rates were estimated for 10 sources, with a range of log $\dot{M}$ from -9.4 to -7.0. One source had a log $\dot{M}$ outside of this range, but with an Hα profile showing blue-shifted absorption that will result in an overestimate of the accretion rate. All ten sources had an infrared excess, with spectral indices determined from mid-infrared data between -0.24 and -1.30 (see Sec 3.5), however, there was no trend found between the spectral index and accretion rate.

The values we derived for $v \sin i$ are generally consistent with those found in main sequence and/or pre-main sequence stars of the same spectral type. Of the seven YSOs with $v \sin i$ values, all are on their radiative tracks (Fig. 4) and only WMW 124 shows evidence for a circumstellar disk, albiet with a large inner disk hole (Fig. 6). Both WMW 192 and WMW 124, with $v \sin i$ values around 30 km sec^{-1}, have projected rotational velocities slower than typical A stars which have median values around 100 km sec^{-1} (Glebocki & Gnacinski 2005; Wolff, Strom, & Hillenbrand 2004; Dahm, Slesnick, & White 2012). The presence of a circumstellar disk could explain the lower value for WMW 124 via a disk-braking mechanism (Koenigl 1991), although a low source inclination could equally well explain the values of both sources. Our echelle spectrum of the YSO J183037.4+0117581 has both the hydrogen lines and Ca II triplet partially filled in with emission. This is an X-ray source that has no infrared excess, leading us to believe this is a result of chromospheric activity. This interpretation is consistent with our estimate of $v \sin i = 39 \pm 3$ km sec^{-1} which is significantly higher than the median value of 5 km sec^{-1} for K0V stars (Glebocki & Gnacinski 2005) but consistent with pre-main sequence stars on radiative tracks in the Orion and Upper Sco OB associations (Wolff, Strom & Hillenbrand 2004; Dahm, Slesnick, & White 2012).

3.8. Radial Velocities and IMF

We attempted to derive radial velocities from the echelle spectra, using the cross-correlation IRAF routine *fxcor*, however we were unsuccessful. This was largely due to scarcity of usable lines in early type stars. We derived an Initial Mass Function using sources marked as association members. The slope of our IMF is consistent with the field star IMF for sources above 1 $M_\odot$ given our uncertainties.

4. Discussion

4.1. Is There an Age Spread?

A K-S test between the age distribution for our 63 association members and a simulated cluster suggests there is an apparent age spread in the Serpens Main cluster. To explore the origin of this spread, we followed the example of Reggianai *et al.* (2011) and increased the assumed error in log L in our Monte Carlo simulations to mimic an age spread of 0.5 Myr to 5 Myr in steps of 0.5 Myr. K-S tests between our sample and the simulations indicate that the age distribution of the association members is consistent with a median age of 2 Myr and an intrinsic age spread of 1-5 Myr assuming a constant star formation rate. Finding an age spread is not unexpected as other studies also report an age spread for this region (Casali, Eiroa, & Duncan 1993; Kaas *et al.* 2004; Harvey *et al.* 2007; Winston *et al.* 2009).

There are two potential explanations for this apparent age spread; the age spread is intrinsic to the cloud, or is a result of sampling YSOs over a wide range of distances. The latter could be due to contamination by YSOs formed in foreground clouds associated with the Aquila Rift. There is strong evidence for multiple cloud components toward the Serpens cloud core (McMullin *et al.* 2000; Duarte-Cabral *et al.* 2010; Levshakov *et al.* 2013). In order to investigate the latter possibility, a Monte Carlo simulation for an average age of 2 Myr was run using the procedure

described in Sec. 3.6 with error in distance of ± 170 pc designed to include YSOs at a distance of 260 pc where extinction from the Aquila Rift is first seen. A K-S test suggests that we cannot reject the null hypnosis that they are drawn from the same parent population with a probability of 11 %, i.e., the apparent age spread could be due to observing YSOs of the same age, distributed over a large distance. We then used our simulations to calculate the minimum spread in distance which results in an apparent age spread; we found this value to be approximately ± 100 pc. We would expect to underestimate the age of sources belonging to a foreground cloud. We would also expect sources having low extinction ($A_v < 3.5$ mag) and a young age (age < 1 Myrs) to be good candidates to belong to the foreground cloud. We found eight sources meet these criteria. When these eight sources were removed from our sample and a K-S test was run against a Monte Carlo simulation with no age spread, we could not reject the null hypothesis that they were drawn from the same population with a probability of 10%. While this is again not definitive, it does lend credence to the idea that the age spread may be the result of contamination from a foreground cloud.

4.2.   Comparisons with Other Regions

Optical spectroscopic studies have been done in several star-forming regions such as the Orion Nebula Cluster (ONC), Chamaeleon I, Lupus, and Rho Ophiuchi (Hillenbrand, Hoffer & Herczeg 2013; Luhman *et al.* 2003, 2007; Mortier, Oliveira, van Dishoeck 2011; Erickson *et al.* 2011). These studies are often biased towards a particular stage in stellar evolution, e.g., objects with infrared excesses or X-ray emission. Erickson *et al.* (2011) conducted an unbiased optical spectroscopic study of the Rho Ophiuchi molecular cloud using the same techniques as the moderate resolution portion of this study and identified 132 YSOs. This allows for direct comparisons with the Serpens Main region although this survey is biased toward slightly more massive

stars. The smaller number of observed YSOs (63-79) in this study is a result of the greater distance to Serpens and the larger number of candidate YSOs due to the location of the cloud near the galactic plane. Like other regions (i.e., Rho Ophiuchi, ONC), Serpens has a younger embedded population with class 0 and 1 spectral energy distributions in several dense molecular cores surrounded by a slightly older, more distributed population. This older population tends to avoid the highest density of gas in these regions. Like the optically-visible YSOs in Rho Oph, the distributed population may have been exposed by a large-scale event such as a supernova shock wave although we are not aware of candidates for this event. We report a disk frequency of 42%±10% for the optically-visible sources in Serpens. This is in agreement with disk frequencies found in other regions; 27% in Rho Ophiuchi (Erickson *et al.* 2011) and 30% in IC 348 (Lada *et al.* 2006). This is not surprising given the similar age estimates of the clusters of 3 Myrs for the surface population of Rho Ophiuchi (Erickson *et al.* 2011) and 2 Myrs for IC 348 (Luhman *et al.* 2003) and the trend of decreasing disk frequency with the age of the cluster (e.g., Briceño *et al.* 2007). It is difficult to compare the mass functions (IMF) of Serpens to other regions, as we were not able to probe the lower end of the mass function due to Serpen's greater distance. However at the high mass end (M>1 $M_\odot$), the IMF agrees with the field star IMF as is usually found in other regions (i.e., Rho Ophiuchi, ONC). In Serpens, we report an apparent age spread of 1-5 Myrs. While we cannot rule out that this age spread is an artifact of sources having a spread in distance between 260 pc and 429 pc, it may be intrinsic to the region. Other studies of young star-forming regions have reported both intrinsic age spreads such as in the ONC (Reggiani et al. 2011; Alves & Bouy 2012) and no age spreads such as in Rho Ophiuchi and Upper Sco (Erickson *et al.* 2011; Slesnick *et al.* 2008). The absence or presence of an age spreads may indicate differences in triggered vs. spontaneous formation mechanisms.

5.   Summary

We present the first deep B, V, and R band survey of a 30.7′ x 30.7′ area centered on the Serpens Main cluster. A V vs. (V-R) color magnitude diagram was used to select candidate YSOs for an unbiased optical spectroscopic survey. Over 700 moderate resolution optical spectra were obtained for 346 candidate YSOs.

Sixty-three objects with optical spectral types were identified as association members based on the presence of Hα in emission, lithium absorption, and when combined with published data, X-ray emission, a mid-infrared excess, and/or reflection nebulosity. Fifteen of these are newly identified pre-main sequence objects, 12 solely on the basis of Li absorption. This underscores the need for multi-wavelength surveys to obtain a complete census of YSOs in star-forming regions. An additional 16 possible association members have either a weak detection of Hα emission, possible lithium absorption, or association through extinction considerations; their pre-main sequence nature is in need of confirmation.

Masses and ages were derived for association and possible association members using multiple theoretical models. Our sample is complete for sources with M$\geq$0.6 M$_\odot$ and A$_v$ <4 mag. Luminosities for several association members are only consistent with the current distance estimate of 429 pc; a distance to the cluster of 230-260 pc would place several association members below the main sequence. Using the tracks and isochrones from DM models, we derive a median age of 2 Myr for this sample. When compared to simulations, we find an *intrinsic* age spread of 1-5 Myr. Contamination from foreground objects (particularly foreground YSOs located in the Aquila Rift) may be a contributing factor to this age spread. However, we cannot rule out the possibility that the age spread is inherent to the region.

Dereddened spectral energy distributions from optical through mid-infrared wavelengths were modeled for association members and compared to expected flux densi-

ties from a stellar photosphere and face-on reprocessing disk. We find a circumstellar disk frequency of 42% ±10% for our sample, which agrees fairly well with findings from other young star-forming regions of similar age for optically visible association members. Six sources are identified as candidate transition disk objects; three of these are newly identified. Accretion rates for sources with strong Hα emission range from log $\dot{M}$ of -9.4 to -7.0, however, no trend was found between the spectral index and accretion rate.

Surface gravities and rotation velocities were estimated from high resolution echelle spectra obtained for 12 association members. Estimates for log g are found to be consistent with dwarf or sub-giant stars. Twelve objects have been identified as background giants based on surface gravity indicators from moderate resolution spectra. From the CaH indices association members with spectral types K5 and cooler, have surface gravity values in agreement with dwarf standards. Values for $v \sin i$ are in agreement with values for pre-main sequence stars of the same spectral type with the exception of two A stars which have lower rotation rates. One of these is a candidate transition disk object, suggesting that disk braking could be playing a role in the slower rotation. Finally, the spectrum for J183037.4+0117581 shows hydrogen lines and Ca II triplet lines partially filled in with emission which is likely the result of chromospheric activity.

REFERENCES

Allen, L.E. & Strom, K.M. 1995, AJ, 109, 1379

Alves, J., & Bouy, H. 2012, A&A, 547, 97

Bastian, N., Covey, K. R., & Meyer, M. R. 2010, ARA&A, 48, 339

Bell, C. P. M., Naylor, T. ,Mayne, N. J. *et al.* 2012, MNRAS, 424, 3178

Bell, C. P. M., Naylor, T. ,Mayne, N. J. *et al.* 2013, MNRAS, 434, 806

Bessell, M.S. 1991, AJ, 101, 662

Briceño, C., Preibisch, T., Sherry, W.H., *et al.* 2007, Protostars and Planets V, 345

Cambrésy, L. 1997, 345, 956

Carpenter, J.M. 2001, AJ, 121, 2851

Casali, M. M., Eiroa, C., & Duncan, W. D. 1993, A&A, 275, 195

Chabrier, G. 2003, PASP, 115, 763

Chavarria-K., C., de lara, E., Finkenzeller, U., Mendoza, E. E., & Ocegueda, J. 1988,
    A&A, 197, 151

Cohen, J.G., Frogel, J.A., Persson, S.E., & Elias, J.H. 1981, ApJ, 249, 481

Cutri, R.M., et al. 2003, 2MASS All Sky Catalogue of Point Sources (The IRSA
    2MASS All-Sky Point Source Catalog, NASA/IPAC Infrared Science Archive,
    http://irsa.ipac.caltech.edu/applications/Gator/)

Dahm, S. E., Slesnick, C. L., & White, R. J. 2012, ApJ, 745, 56

D'Antona, F. & Mazzitelli, I. 1997, Mem. Soc. Astron. Ital., 68, 807

Davis, C.J., Matthews, H.E. & Ray, T.P., *et al.* 1999, MNRAS, 309, 141

Drilling, J. S. & Landolt, A.U. 2000, in Astrophysical Quantities, ed. A. Cox (4th
    ed.; New York: AIP Press),

Duarte-Cabral, A., Fuller, G.A., Peretto, N. *et al.* 2010, A&A, 519, A27

Dzib, S., Loinard, L., Mioduszewski, A. J. *et al.* 2010, ApJ, 718, 610

Dzib, S., Loinard, L., Mioduszewski, A. J. *et al.* 2011, RevMexAAC, 40, 231

Eiroa, C. & Casali, M. M. 1992, A&A, 262, 468

Eiroa, C., Djupvik, A, & Casali, M. 2008, in Handbook of Star Forming Regions Vol.II, Ed. B. Reipurth, (ASP: San Francisco), 693

Evans, N. J., II, Allen, L. E., Blake, G. A., *et al.* 2003, PASP, 115, 956

Erickson, K. L., Wilking, B. A., Meyer, M. R., Robinson, J. R., & Stephenson, L. N. 2011, AJ, 142, 140

Fabricant, D., Fata, R., Roll, J. *et al.* 2005, PASP, 117, 1411

Gehrels, N. 1986, ApJ, 303, 336

Giardino, G, Favata, F., Micela, G., Sciortino, S., & Winston, E. 2007, A&A, 463, 275

Ginestet, N., Carquillat, J. M., Jaschek, M., & Jaschek, C. 1994, A&A, 108, 359

Glebocki, R. & Gnacinski, P. 2005, Vizier On-line Data Catalog III/244

Gray, R. O., & Corbally, C. J. 2009, Stellar Spectral Classification (Princeton:Princeton University Press)

Gutermuth, R. A., Bourke, T. L., Allen L. E. *et al.* 2008, ApJ, 673, L151

Harvey, P. Merin, B., Huard, T. *et al.* 2007, ApJ, 663, 1149

Hernandez, J. , Calvet, N., Hartmann, L., *et al.* 2005, AJ, 129, 856

Hillenbrand, L. A., Strom, S. E., Vrba, F. J., & Keene, J. 1992, ApJ, 397, 613

Hillenbrand, L. A. 2009, in IAU Symp. 258, The Ages of Stars, ed. E. E. Mamajek, D. R. Soderblom, & R. Wyse (Cambridge: Cambridge Univ. Press), 81

Hillenbrand, L. A., Hoffer, A. S., & Herczeg G. J. 2013 AJ, 146, 85

Hogerheijde M.R., van Dishoeck, E.W., Salverda, J.M. *et al.* 1999 ApJ, 513, 350

Howell, S. B. 1989, PASP, 101, 616

Jacoby, G. H., Hunter, D. A., & Christian, C. A. 1984, ApJS, 56, 257

Kaas, A. A., Olofsson, G., Bontemps, S. *et al.* 2004, A&A, 421, 623

Koenigl, A.1991, ApJ, 37, L39

Knude, J. 2011, arXiv1103.0455K

Lada, C. J., Muench, A. A., Luhman, K. L., et al. 2006, AJ, 131, 1574

LeBorgne, J.-F., Bruzual, G., Pelló, R. *et al.* 2003, A&A, 402, 433

Levshakov, S.A., Henkel, C., Reimers, D. *et al.* 2013, A&A, 553, A58

Lopez-Santiago, J., Montes, D., Galvez-Ortiz, M. C. *et al.* 2010, A&A, 514, A97

Luhman, K. L., Stauffer, J. R., Muench, A. A., *et al.* 2003, ApJ, 593, 1093

McMullin, J. P., Mundy, L. G., Blake, G. A. *et al.* 2000, ApJ, 536, 845

Mink, D. J., Wyatt, W. F., Caldwell, N. *et al.* 2007, in Astronomical Data Analysis
    Software and Systems XVI ASP Conference Series, Vol. 376, ed. R. A. Shaw,
    F. Hill, & D. J. Bell (San Francisco, CA: ASP), 249

Mortier, A., Oliveira, I., & van Dishoeck, E. F., 2011, MNRAS418, 1194

Moultaka, J., Ilovaisky, S. A., Prugneil, P., & Soubiran, C. 2004, PASP, 116, 693

Natta, A., Testi, L., Muzzerolle, J., Randich, S., Comerón, F., & Persi, P. 2004, A&A,
    424, 603

Oliveira, I., Merin, B., Pontoppidan, K. M. *et al.* 2009, ApJ, 691, 672

Palacios, A., Gebran, M., Josselin, E., *et al.* 2010, A&A, 516, A13

Palla, F., & Stahler, S.W 1999, ApJ, 525, 772

Preibisch, T. 2003, A&A, 410, 951

Racine, R. 1968, AJ, 73, 233

Ridge, N. A., Di Francesco, J., Kirk, H., *et al.* 2006, AJ, 131, 2921

Schmidt-Kaler, Th. 1982, in Landolt-Bornstein New Series, Numerical Data and Functional Relationships in Science and Technology, Group 4, Vol. 2b, ed. K. Schaffers & H.H. Voigt (New York: Springer), 451

Schroeder, C., Reiners, A., Schmitt, J. H. M. M. 2009, A&A, 493, 1099

Siess, L., Dufour, E., & Forestini, M. 2000, A&A, 358, 593

Slesnick, C. L., Hillenbrand, L. A., & Carpenter, J. M. 2008, ApJ, 688, 377

Straižys,V., Černis, K., & Bartašiūte, S. 1996, Baltic Astron., 5, 125

Straižys,V., Černis, K., & Bartašiūte, S. 2003, A&A, 405, 585

Strom, S. E., Grasdalen, G. L., & Strom, K. M. 1974, ApJ, 191, 111

Strom, S. E., Vrba, F. J., & Strom, K. M. 1976, AJ, 81, 638

Testi, L., & Sargent, A. 1998, ApJ, 508, L91

Testi, L., Sargent, A., & Olmi,. L., *et al.* 2000, ApJ, 540, L53

Tonry, J. & Davis, M., 1979, AJ, 84, 1511

Torres-Dodgen, A. V. & Weaver, W. B. 1993, PASP, 105, 693

White, R. J., Gabor,J. M., Hillenbrand, L. A. 2007, AJ, 133, 2524

Wilking, B. A., Meyer, M. R., Robinson, J. G., & Greene, T. P., 2005, AJ, 130, 1733

Wilking, B., Dalba, P., Robinson, J., Meyer, M. *et al.* 2008, BAAS, Vol. 40. 199

Williams, G., Olszewski, E., Lesse, M., & Burge, J. 2004, in Proceedings of the SPIE, Vol. 5492, 787

Winston, E., Megeath, S. T., Wolk, S. J. 2007, ApJ, 669, 493

Winston, E., Megeath, S. T., Wolk, S. J. 2009, AJ, 137, 4777

Wolff, S. C., Strom, S. E., & Hillenbrand, L. A. 2004, ApJ, 601, 979
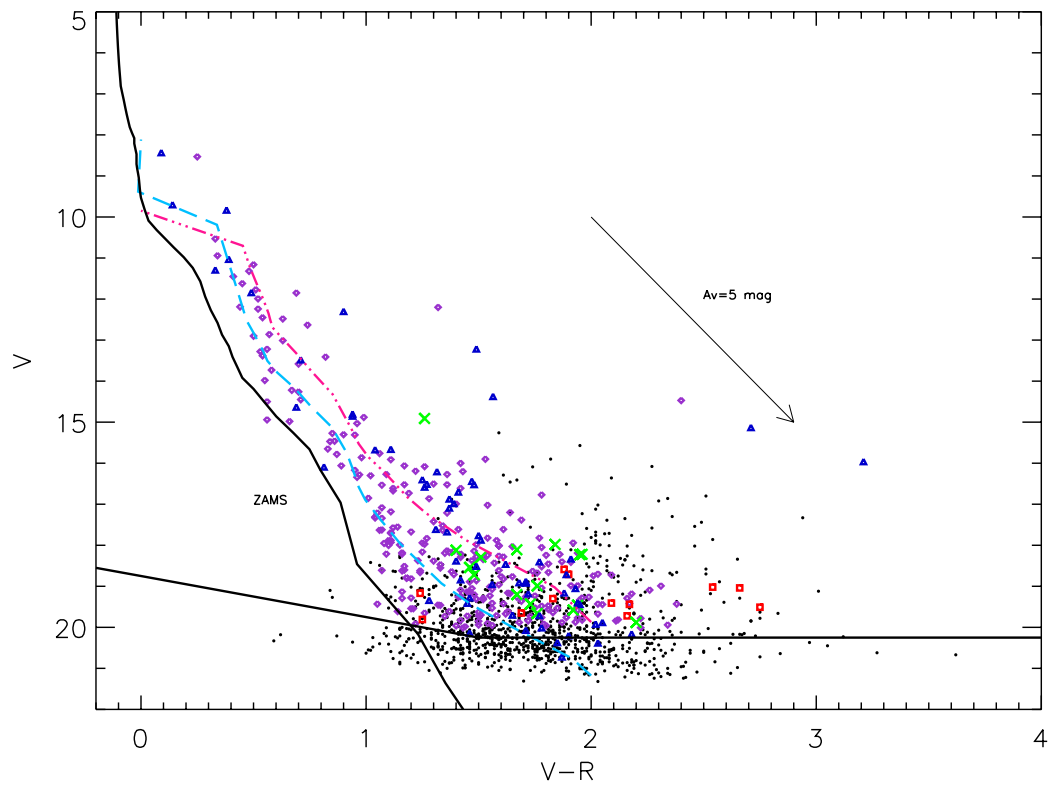
Fig. 1.— V vs. (V-R) color-magnitude diagram from our V- and R-band images. Isochrones for 1 Myr (dot-dashed, red) and 5 Myr (dashed, blue) derived from the DM models are shown as well as the ZAMS (solid black). Objects observed spectro-scopically are shown by triangles (association members), "x's" (possible association members), open squares (giants), or diamonds (unclassified). Black dots represent sources that were not observed spectroscopically.
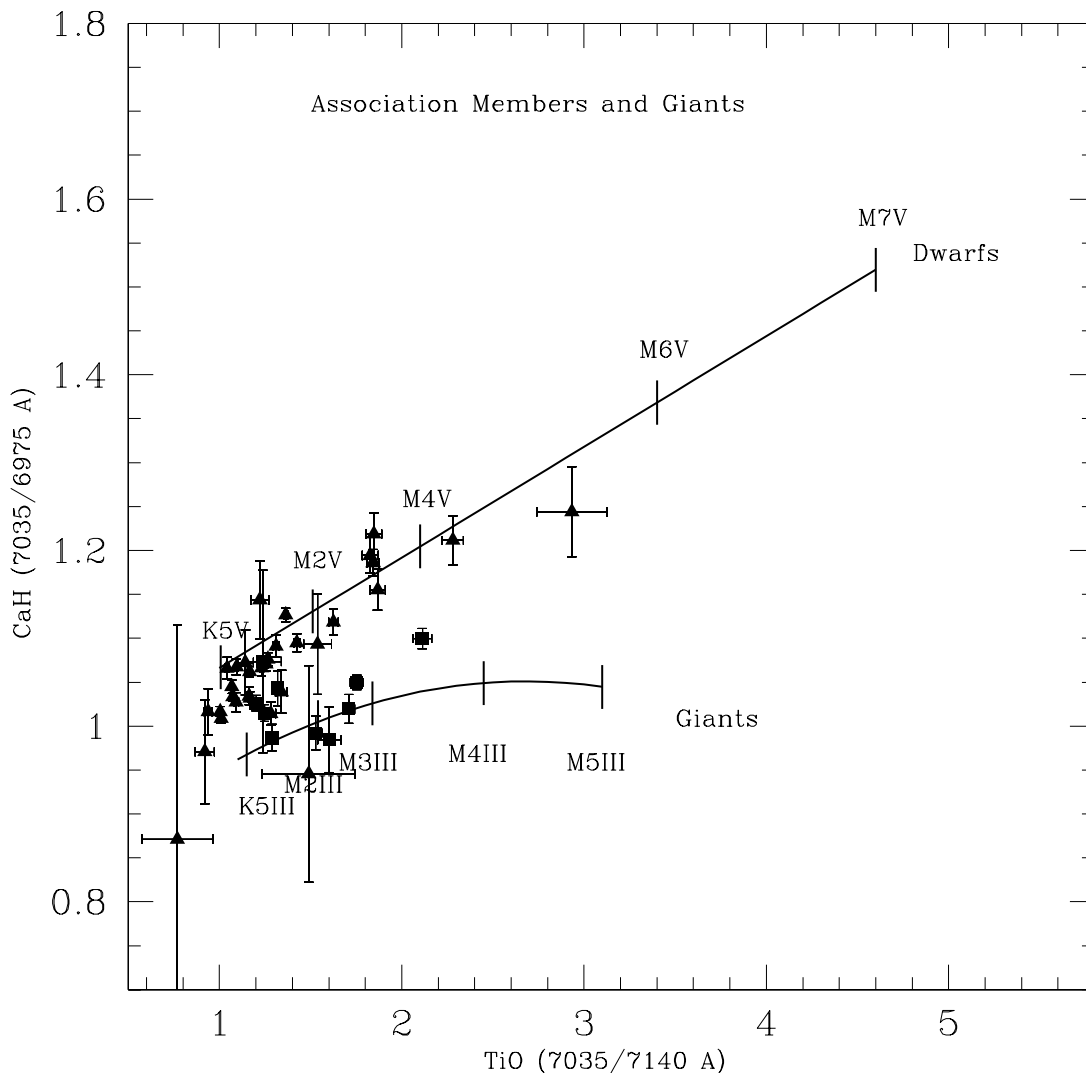
Fig. 2.— Plot of CaH vs. TiO indices as defined in the text for 32 association members (triangles) and 10 background giants (squares) with spectral types K5 and cooler. The solid lines were derived from fits to dwarf and giant spectral standards. Error bars are based on statistical errors in each band pass, and do not account for systematic errors in normalization. For the dwarf standards from K5-M7, the fit was $y = 0.126x + 0.940$ with a correlation coefficient of r=0.94. For the giant standards from K5-M5, the fit gave $y = -0.0357x^2 + 0.191x + 0.795$ with a correlation coefficient of r=0.82.

Serpens Main
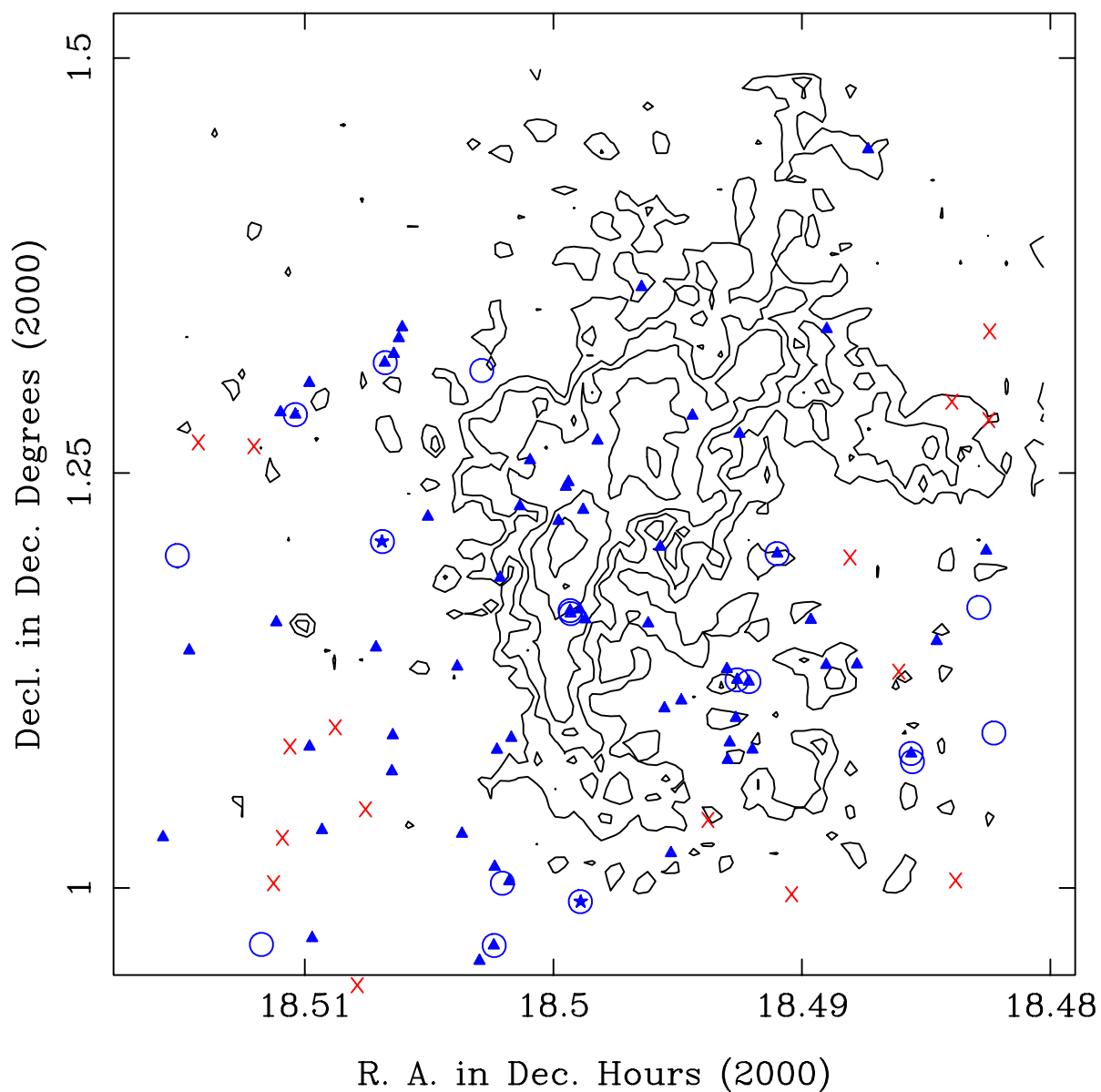
Fig. 3.— Distribution of association members is shown relative to contours of $C^{18}O$ integrated intensity (McMullin *et al.* 2000) that define the core of the Serpens molecular cloud. The map covers the $30.7'$ x $30.7'$ area of our imaging survey. Contours are in units of 1, 2, 3, 5, and 7.5 K km sec^{-1}. Association members are marked by triangles and possible association members by "x's". Circles locate sources for which echelle spectra were obtained. Star symbols mark the locations of the two most massive association members of the Serpens Main cluster: the B8 star HD 170634 (BD+01 3694) which illuminates S 68 and the B5 star [CDF88] 7.
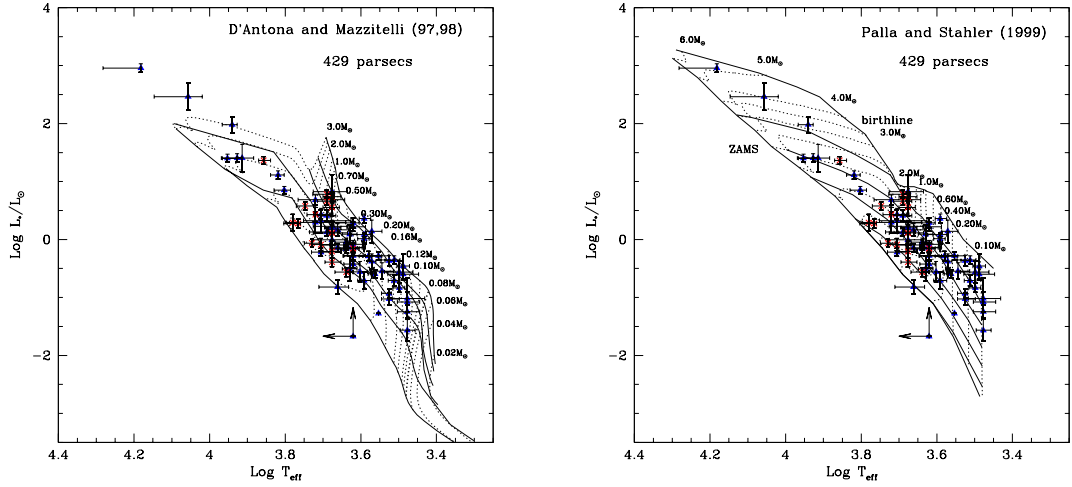
Fig. 4.— Hertzsprung-Russell diagrams for the Serpens Main association members with optically-determined spectral types assuming a distance of 429 pc. The solid triangles mark the positions of association members and "x's" of possible association members relative to the theoretical tracks and isochrones of D'Antona & Mazzitelli (1997,1998) in Figure 4a, or Palla & Stahler (1999) in Figure 4b. Error bars in Log T_{eff} were estimated from uncertainties in the spectral type and surface gravity. Error bars in Log L_{bol} were estimated from errors in the photometry and uncertainties in the distance modulus and bolometric correction. In Figure 4a, isochrones shown as solid lines are 10^5, 3×10^5, 10^6, 3×10^6, 10^7, and 10^8 years. Evolutionary tracks from 0.02 $M_\odot$ to 3.0 $M_\odot$ are shown by dashed lines. The bold dashed line marks the evolutionary track for a star at the hydrogen-burning limit. In Figure 4b, the birthline is shown as a solid line followed by isochrones for 10^6, 3×10^6, 10^7, and 10^8 years and the ZAMS. Evolutionary tracks from 0.1 $M_\odot$ to 6.0 $M_\odot$ are shown by dashed lines.
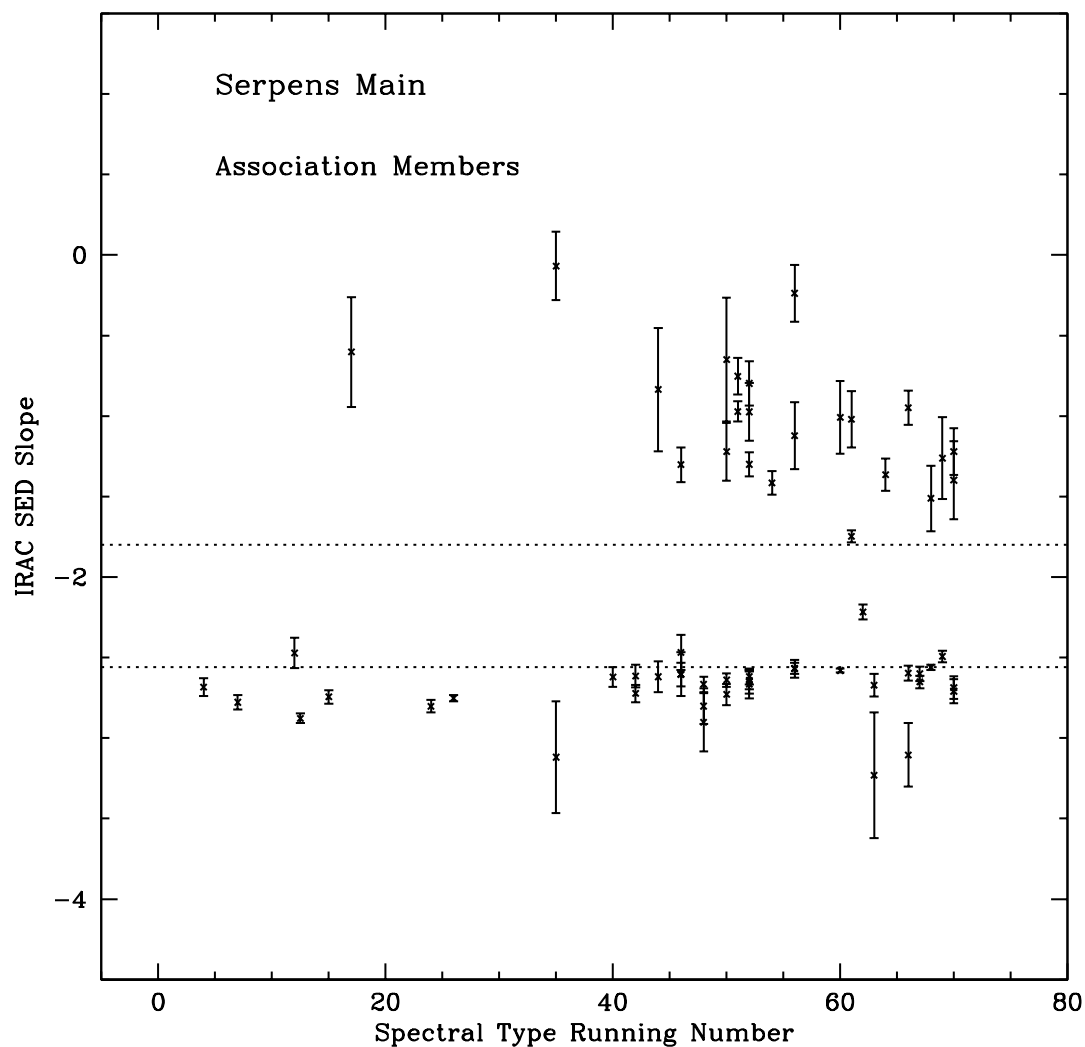
Fig. 5.— Spectral indices using the IRAC flux densities as a function of spectral type. Running numbers for spectral types B0, A0, F0, G0, K0, K5, M0, and M5 are 0,10, 20, 30, 40, 50, 60, and 70, respectively. Dotted lines are α = -1.80 and α = -2.56, sources above α = -1.80 have optically thick disks and sources below α = -2.56 have no disks, sources between these values are potential transition disk objects. The spectral index was computed using a linear least-squares fit to the 3.6-8.0 μm flux densities. Error bars were calculated from the fit given the statistical uncertainties in the flux densities.
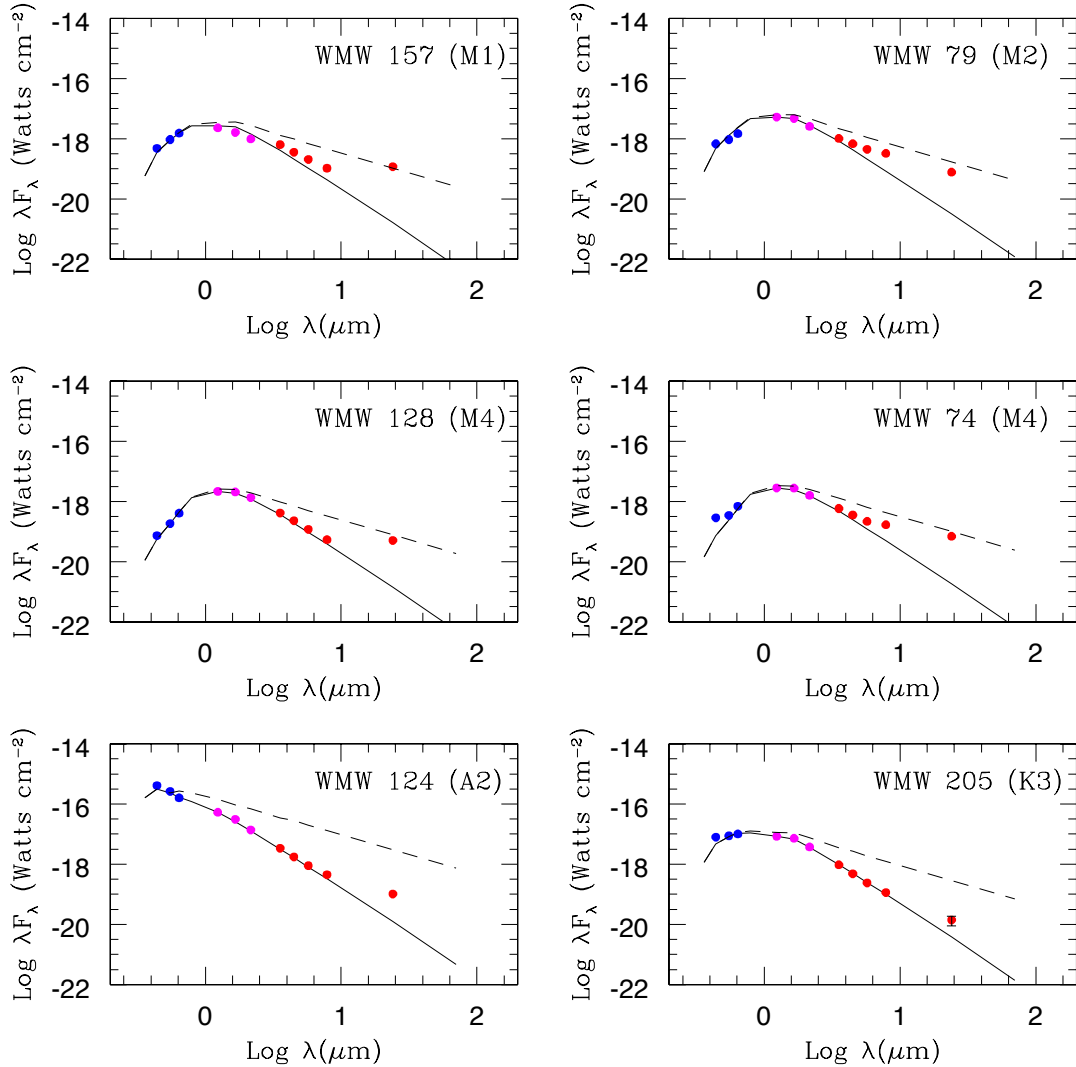
Fig. 6.— Dereddened spectral energy distributions are presented for six possible transition disk objects. B, V, and R band data points are from this study, J, H, and K band data from 2MASS, and 3.6-8 μm and 24 μm data from IRAC and MIPS on the Spitzer Space Telescope. The solid curve is the spectral energy distribution of a blackbody given the effective temperatures from our spectral classifications, normalized to the R or J band flux density. The dashed curve is the flux density expected from a face-on reprocessing disk.

Table 1. Spectroscopic Observation Details

Start Date (YYYYMMDD)	Telescope	Spectrograph	grating (gpmm)[a]	slit or fiber width (arcsec)	wavelength (Å)	dispersion (Å pixel^{-1})	resolution[b] (Å)	integration (minutes)
20060616	WIYN 3.5m	Hydra	1200	2.0	6249 - 7657	0.69	1.4	120
20080628	Bok 2.3m	B&C	1200	1.5	5954 - 7115	0.99	1.2	5 - 25
20080916	Bok 2.3m	B&C	400	1.5	3850 - 5566	1.43	2.3	5 - 15
20090627	WIYN 3.5m	Hydra	600	3.0	3966 - 5386	0.70	1.4	34 - 155
			1200	2.0	6300 - 7669	0.69	1.4	70 - 90
20100629	WIYN 3.5m	Hydra	600	3.0	3900 - 5315	0.70	1.4	30 - 110
			1200	2.0	6286 - 7662	0.69	1.4	39 - 245
20100703	MMT 6.5m	Hectospec	600	1.5	5462 - 8070	0.57	1.2	45
20110919	MMT 6.5m	Hectospec	270	1.5	3703 - 9146[c]	1.20	2.4	24
20090613	Magellen Clay 6.5m	MIKE	52.7	0.7 x 5.0	3360 - 4991	0.02	0.11	25 - 30
			52.6	0.7 x 5.0	4830 - 8928	0.05	0.24	25 - 30
20090810	Magellen Clay 6.5m	MIKE	52.7	0.7 x 5.0	3360 - 4991	0.02	0.11	10 - 24
			52.6	0.7 x 5.0	4830 - 8928	0.05	0.24	10 - 24
20100709	Magellen Clay 6.5m	MIKE	52.7	0.7 x 5.0	3360 - 4991	0.02	0.11	3 - 75
			52.6	0.7 x 5.0	4830 - 8928	0.05	0.24	3 - 75

[a] Groves per millimeter

[b] Spectral resolution at central wavelength

[c] For spectral classification, only the wavelengths from 5650-9100 Å were used.

Table 2. Optical Properties of Candidate Young Stellar Objects with Moderate Resolution Spectra

Name[a]	Yrs. obs.[b] & Tel.[c]	RA(J2000) (hhmmss.s)	DEC(J2000) (° ′ ″)	Sp. Ty. Range	Adopt Sp. Ty.	Li?[d]	EW(Hα) (Å)	V (mag)	(B-V) (mag)	(V-R) (mag)	No. obs.[e]
Photometric Standards											
SCB 41	08B,09W,10W	18:28:58.4	01:10:59.7	A9-F2	F1	no		11.16	0.81	0.50	3B, 3R
SCB 43	08B,09W,10W	18:29:08.0	01:05:25.4	F5-F9	F6	no		11.62	0.79	0.45	3B, 3R
BD+01 3686/SCB 47	08B,09W,10W	18:29:27.6	01:12:56.8	F2-F6	F4	no		11.03	0.68	0.39	3B, 3R
BD+1 3693/SCB 60	08B,09W,10W	18:30:10.4	01:19:33.7	A5-A8	A7	poss		10.53	0.53	0.33	3B, 3R
SCB 67	08B,09W,10W	18:30:35.0	01:20:21.9	A9-F2	F0	no		12.19	0.74	0.44	1B, 3R
SCB 70	08B,09W,10W	18:30:54.5	01:12:52.7	F3-F6	F4.5	no		11.99	0.86	0.52	2B, 4R
SCB 72	08B,09W,10W	18:30:56.2	01:14:15.8	F6-F8	F7	no		12.45	0.88	0.54	2B, 3R
Candidate YSOs											
SCB 40	09W,10W	18:28:55.5	01:12:18.4	K1-K3	K2	no		14.26	1.16	0.70	1B, 2R
	10W,11M	18:28:55.6	01:27:03.5	G5-K0	G7	no		17.93	1.79	1.11	2R
	11M	18:28:56.0	01:10:34.0	K0-K2	K1	no		19.26	2.43	1.99	1R
	11M	18:28:56.1	01:19:53.7	G5-K0	G9	no		19.61	1.68	1.37	1R
	08B,09W,10W	18:28:56.2	01:06:27.6	F7-G0	F9	yes		11.32	0.89	0.48	2B, 2R
	09W,10W,11M	18:28:56.3	01:20:41.3	A3-A6	A5	no		16.30	1.57	1.02	1B, 3R
	10W	18:28:56.5	01:23:55.5	M0-M1	M0	no		16.77	2.66	1.78	1B, 1R
	10W,11M	18:28:56.7	01:18:49.9	K6-K8	K8	no		17.71	1.70	1.11	1B, 2R
	10M,11M	18:28:56.8	01:21:03.2	K3-K4	K3	poss		18.54	2.06	1.46	2R
	11M	18:28:56.9	01:17:51.0	F7-G3	G0	poss		19.66	1.88	1.76	1R
	11M	18:28:57.0	01:26:20.7	K2-K3	K3	no		18.13	2.27	1.36	1R
	10W,10M,11M	18:28:57.3	01:12:15.8	A5-F1	F0	no		17.57	1.67	1.12	1B, 3R
	10M	18:28:57.3	01:13:03.0	K4-K6	K1	yes		19.92	...	2.02	1R
	10W,10M,11M	18:28:57.4	01:25:15.3	F4-G0	F7	no		16.85	1.70	1.01	1B, 3R
	10M	18:28:58.2	01:26:30.6	G5-K2	G9	no		18.62	2.17	1.24	1R
	09W,10W,10M	18:28:59.0	01:25:55.5	F4-F6	F5	no		15.46	1.57	0.86	1B, 3R
	10M	18:28:59.3	00:58:11.5	M0-M4	M2III	no		19.17	1.68	1.24	1R
	10M	18:28:59.3	01:22:03.4	K0-K4	K2	no		18.89	2.58	1.46	1R
	10M,11M	18:28:59.9	01:19:05.6	F0-F5	F3	yes		19.09	1.98	1.42	2R
	10W,11M	18:28:60.0	01:06:14.4	A9-F5	F4	no		17.52	1.96	1.34	1B, 2R

Table 2—Continued

Name[a]	Yrs. obs.[b] & Tel.[c]	RA(J2000) (hhmmss.s)	DEC(J2000) (° ′ ″)	Sp. Ty. Range	Adopt Sp. Ty.	Li?[d]	EW(Hα) (Å)	V (mag)	(B-V) (mag)	(V-R) (mag)	No. obs.[e]
	10W,11M	18:29:00.5	01:25:27.0	G9-K2	K0	no		17.21	2.24	1.36	2R
	09W,10W,11M	18:29:00.7	01:27:26.1	F4-G2	F7	no		16.17	1.63	0.95	1B, 3R
	10M	18:29:00.9	01:19:48.8	F5-G9	G3	no		19.33	2.54	1.95	1R
	10M,11M	18:29:01.2	01:10:28.0	G9-K3	K1	no		18.67	2.44	1.76	2R
	10M	18:29:01.3	01:02:25.0	G5-K5	K0	yes		18.99	2.67	2.31	1R
	10M	18:29:01.4	01:27:06.7	G5-G9	G7	no		19.29	1.96	1.16	1R
KOB 61	10W,10M,11M	18:29:01.7	01:01:12.2	K2-K4	K3	poss		18.22	2.62	1.96	3R
	10M	18:29:02.3	01:18:31.0	G9-K3	K0	poss		19.46	0.74	1.94	1R
	10M	18:29:02.3	01:11:53.8	G5-K2	K0	poss		19.53	2.35	1.85	1R
	10M	18:29:02.7	01:03:13.5	K0-K2	K1III	no		18.59	2.45	1.88	1R
	10M	18:29:02.9	01:10:00.7	G9-K3	K1	poss		18.55	2.02	1.33	1R
	10M	18:29:03.1	01:22:50.8	K0-K3	K1	no		16.20	2.23	1.43	1R
	10M	18:29:03.1	01:17:25.2	M3-M4	M3.5	poss	-3.9	19.83	1.66	1.42	1R
	09W,10W,11M	18:29:03.4	01:23:09.8	K2-K3	K2	no		16.00	2.39	1.42	1B, 3R
	10M	18:29:04.0	01:06:46.1	G5-K4	K1	no		18.98	2.88	1.91	1R
XMM	06W	18:29:04.5	01:09:47.0	<K6	<K6	poss		16.09[h]	⋯	0.813[h]	1R
	10M	18:29:05.2	01:05:28.6	G5-K0	G7	no		19.87	1.86	1.93	1R
	10W,11M	18:29:06.1	01:25:54.7	A7-F3	A8	no		15.91	1.85	1.11	1B, 2R
	09W,11M	18:29:06.1	01:21:46.0	G5-K0	G7	poss		15.65	1.39	0.83	2R
	10M	18:29:07.8	01:23:19.0	G4-K0	G5	no		19.45	1.75	1.32	1R
	10W,10M,11M	18:29:07.9	00:58:08.1	M2-M5	M3	no		18.00	1.63	1.10	3R
WMW 124	08B,09W	18:29:08.2	01:05:43.1	A1-A3	A2	no		13.48	1.15	0.71	1B, 2R
	10M	18:29:08.9	01:09:35.5	F4-G0	F7	poss		18.47	1.82	1.33	1R
	11M	18:29:09.6	01:22:47.7	G5-K0	G9	poss		18.71	2.00	1.39	1R
	11M	18:29:09.7	01:05:31.0	K3-K8	K6III	no		19.72	⋯	2.16	1R
	10M,11M	18:29:09.9	00:57:51.7	G9-K3	K2	no		19.94	⋯	2.34	2R
	10W,10M,11M	18:29:10.0	01:08:45.1	F6-G5	G3	poss		18.29	2.04	1.51	3R
	10W,10M,11M	18:29:10.2	01:17:25.1	K8-M5	M4	no		17.95	1.62	1.08	3R
	10M	18:29:10.6	01:06:40.2	G5-K2	K0	no		19.96	2.37	1.40	1R
	10M,11M	18:29:10.6	01:27:38.0	G5-K5	K1	no		19.48	2.42	1.78	2R

Table 2—Continued

Name[a]	Yrs. obs.[b] & Tel. [c]	RA(J2000) (hhmmss.s)	DEC(J2000) (° ′ ″)	Sp. Ty. Range	Adopt Sp. Ty.	Li?[d]	EW(Hα) (Å)	V (mag)	(B-V) (mag)	(V-R) (mag)	No. obs.[e]
	10W,11M	18:29:10.6	01:04:52.5	A9-F4	A9	no		17.42	1.88	1.30	1B, 2R
	10W	18:29:10.7	01:09:51.1	K3-K5	K4	no		18.16	1.73	1.25	1R
	10W	18:29:10.8	01:23:12.9	K0-K2	K2	no		14.22	1.28	0.67	2R
	10M,11M	18:29:10.8	01:11:10.2	K0-K4	K3.5	no		19.36	2.28	1.69	2R
KOB 84	11M	18:29:10.9	01:18:09.1	K3	K3	no		18.72	2.49	2.09	1R
	10W	18:29:10.9	01:23:46.7	K1-K4	K2	⋯		14.94	1.29	0.56	1B
	10M	18:29:11.6	01:20:32.9	G9-K3	K0	no		19.98	2.19	1.44	1R
	10M,11M	18:29:11.6	01:19:18.8	K0-K4	K2	no		19.20	2.17	1.48	2R
	10M	18:29:12.3	01:22:19.5	F5-G0	F7	no		18.17	1.95	1.37	1R
	11M	18:29:12.5	01:00:36.5	G5-K0	G9	no		18.52	2.38	1.78	1R
	10M	18:29:13.0	01:07:22.0	G5-K2	K0	no		19.91	2.18	1.22	1R
	10W,10M	18:29:13.0	01:20:54.0	F0-F5	F2	poss		16.52	1.67	1.17	1B, 2R
	10W	18:29:13.0	01:26:18.8	K4-K6	K5	no		18.24	2.34	1.54	1R
	10M,11M	18:29:13.5	01:09:26.4	K3	K3	no		18.38	1.79	1.30	2R
	09W,10W,11M	18:29:13.9	01:08:32.2	K4-M0	K5	poss		15.30	1.30	0.90	1B, 3R
	09W,10W,10M,11M	18:29:14.2	01:26:22.2	K4-K5	K5	no		14.98	1.38	0.66	1B, 4R
	10W,11M	18:29:14.3	00:58:52.7	G0-G4	G3	no		18.14	2.16	1.48	2R
	10M,11M	18:29:14.4	01:27:33.8	K3-K5	K4	yes		19.44	2.32	1.95	2R
	10W	18:29:14.8	01:21:04.2	K1-K2	K2	no		17.94	2.51	1.92	1R
	10M	18:29:16.0	01:08:56.2	K0-K5	K3	yes		19.40	2.61	1.94	1R
	10W,10M,11M	18:29:16.9	01:27:30.3	M2-M7	M5.5	poss	-0.48	18.21	1.69	1.09	3R
	10M,11M	18:29:17.1	01:12:52.8	K2-K3	K3	poss		19.88	⋯	2.20	2R
	10M	18:29:17.4	01:08:32.3	F6-G3	G0	no		19.12	1.91	1.46	1R
	10W,11M	18:29:20.4	01:14:54.4	K4-M2	K8	no		16.53	1.55	1.07	1B, 2R
	09W	18:29:20.4	01:21:47.9	G2-G4	G4	no		14.50	1.14	0.56	1R
WMW 104		18:29:20.4	01:21:03.8	K9-M2[g]	M0.5[g]	⋯		20.16	1.90	2.18	⋯
XMM	06W,10W,11M	18:29:20.5	01:08:55.1	K4-K5	K5	yes		16.40	1.61	1.25	1B, 3R
WMW 232	09W,10W,11M	18:29:21.2	01:04:18.7	K3-K4	K4	no		16.06	1.38	0.89	2B, 4R
	10M	18:29:22.6	01:07:03.8	K7-M2	M1III	no	-1.5	19.30	2.31	1.83	1R
WMW 221/XMM	06W,10W,11M	18:29:22.7	01:10:33.0	K5-K8	K6	yes	-3.0 to -3.3	16.87	1.82	1.37	3R

Table 2—Continued

Name[a]	Yrs. obs.[b] & Tel.[c]	RA(J2000) (hhmmss.s)	DEC(J2000) (° ′ ″)	Sp. Ty. Range	Adopt Sp. Ty.	Li?[d]	EW(Hα) (Å)	V (mag)	(B-V) (mag)	(V-R) (mag)	No. obs.[e]
	11M	18:29:23.4	01:12:58.0	M2-M7	M5	no	-5.7	19.90	2.03	1.54	1R
	10M	18:29:25.5	01:00:42.4	K0-K5	K3	poss		19.58	··	1.92	1R
	08B,09W,10W	18:29:25.9	01:24:43.6	F9-G6	G3	poss		12.90	1.07	0.50	2B, 3R
	10W,11M	18:29:27.2	01:07:03.0	K7-M3	M1	poss		17.69	1.70	1.11	1B, 2R
	11M	18:29:27.4	01:09:41.6	K6-M0	K8	no		16.67	1.49	1.12	1R
	10W,11M	18:29:28.6	01:11:39.1	F7-G5	G4	no		17.67	1.59	1.20	1B, 2R
	09W,10W,11M	18:29:28.6	00:58:14.3	F9-G9	G7	no		16.27	1.62	1.09	1B, 3R
	10M	18:29:28.9	01:00:12.0	G1-G5	G3	no		18.43	2.05	1.57	1R
	09W	18:29:29.2	01:05:45.4	F9-G9	F9	no		13.98	0.97	0.55	1B, 1R
	10M	18:29:30.7	01:13:39.9	G5-K2	K0	poss		19.73	2.03	1.35	1R
KOB 153	10M	18:29:31.1	01:15:21.7	G9-K2	K1	no		19.81	··	2.12	1R
XMM	06W	18:29:31.2	01:05:51.6	M3	M3	yes		18.88	1.97	1.71	1R
BD+01 3687	08B,09W,10W	18:29:31.7	01:08:19.1	F3-F9	F6	poss	-7.8	11.29	0.67	0.33	1B, 2R
	11M	18:29:32.0	01:16:17.1	F7-G4	G1	no		18.34	1.80	1.52	1R
KOB 166	11M	18:29:32.6	01:09:50.3	K2-K3	K3	no		19.09	2.95	2.26	1R
WMW 225/XMM	06W,10W,11M	18:29:33.1	01:17:16.5	G5-K5	K0	yes		16.52	1.68	1.48	1B, 3R
WMW 82/KOB 173	08B,09W,10W	18:29:33.4	01:08:22.8	A5-A8	A7	poss		11.84	0.81	0.49	2B, 2R
XMM	06W,10W,10M,11M	18:29:33.6	01:07:00.0	M2-M4	M3.5	poss	-1.4 to -4.7	17.76	1.94	1.50	4R
XMM	06W	18:29:34.5	01:06:06.9	U	U	no	-1.7	18.51	1.90	1.49	1R
XMM	06W,10W,11M	18:29:34.7	01:05:28.9	K7-K8	K8	poss	-0.6 to -2.6	16.70	1.96	1.41	1B, 3R
	09W,10W	18:29:34.9	01:08:46.2	K5-K8	K6	yes	-0.5	14.85	1.51	0.94	2B, 1R
	06W	18:29:35.9	01:23:24.5	F5-K5	G5	no		··	··	··	1R
	11M	18:29:37.6	01:03:23.6	K5-K6	K6	poss	-1.4	18.99	2.22	1.76	1R
	11M	18:29:38.3	00:57:50.3	G9-K2	K1	no		19.84	··	2.11	1R
WMW 94/XMM	06W	18:29:39.9	01:17:56.0	M0-M1	M0.5	yes	-124.0	14.37[h]	··	1.56[h]	1R
	09W,10W,11M	18:29:40.1	00:59:58.9	K6-M0	K8	no		15.03	1.44	0.96	1B, 3R
	10M,11M	18:29:40.6	01:25:26.5	F7-G4	G0	no		19.84	1.78	1.72	2R
KOB 209	11M	18:29:41.0	01:20:58.5	M3.5-M4.5	M4III	no		19.02	2.63	2.54	1R
	10W,11M	18:29:41.3	01:23:46.4	M2-M4	M3	no		17.63	1.50	1.06	1B, 2R
WMW 103/XMM	06W,11M	18:29:41.5	01:07:37.9	K4-K6	K5	yes	-21.6 to -52.0	16.98	1.74	1.39	2R

Table 2—Continued

Name[a]	Yrs. obs.[b] & Tel.[c]	RA(J2000) (hhmmss.s)	DEC(J2000) (° ′ ″)	Sp. Ty. Range	Adopt Sp. Ty.	Li?[d]	EW(Hα) (Å)	V (mag)	(B-V) (mag)	(V-R) (mag)	No. obs.[e]
WMW 65/KOB 219	10M	18:29:43.0	01:02:06.8	K7-M0	M0	yes	-1.0	18.92	2.07	1.71	1R
WMW 100/XMM		18:29:43.9	01:07:21.0	K5.5-K8.5[g]	K7[g]	...		20.01	1.87	1.78	...
		18:29:44.5	01:13:11.6	M3-M6[g]	M4.5[g]	...		19.18	1.98	1.72	...
WMW 79	10M	18:29:45.9	01:24:13.6	K1-K3	K2	no		19.76	2.47	1.89	1R
		18:29:46.3	01:10:25.3	M0.5-M3.5[g]	M2[g]	...		19.71	2.02	1.77	...
	11M	18:29:46.7	00:57:45.9	M3.5-M5.5	M4.5	no		19.28	1.81	1.20	1R
WMW 199/XMM	06W,11M	18:29:47.2	01:22:34.7	K8-M0	K8	yes	-2.6 to -3.4	18.33	2.40	1.91	2R
	10W,11M	18:29:49.5	01:11:30.9	M0-M4.5	M3.5	no		16.61	1.50	1.12	1B, 2R
	10W,11M	18:29:50.0	01:09:40.6	A4-F6	F3	no		18.28	2.12	1.61	2R
	11M	18:29:51.6	01:11:19.6	K8-M1	M0	no		17.55	1.58	1.14	1R
	10M	18:29:51.6	01:24:24.0	F9-G9	G5	no		19.88	1.63	1.68	1R
	10W,11M	18:29:52.9	00:57:29.1	M2-M4	M3	no		17.31	1.53	1.04	1B, 2R
WMW 81/XMM	06W,11M	18:29:53.6	01:17:01.7	K5-K8	K6	yes	-11.2 to -32.1	18.91	1.99	1.68	2R
	09W,10W	18:29:54.1	01:11:50.1	F6-F9	F7	no		13.73	0.96	0.58	3B, 1R
	10M	18:29:54.4	01:18:17.6	M2-M4	M3	poss		19.43	1.60	1.05	1R
WMW 201/XMM	06W	18:29:55.4	01:10:34.0	M5	M5	poss		20.14	1.57	1.46	1R
WMW 38/XMM	06W	18:29:55.7	01:14:31.5	<K6	<K6	poss	-11.4	15.13[h]	...	2.708[h]	1R
[CDF88] 7/XMM	06W,08B,09W,10W	18:29:56.1	01:00:21.7	B3-B5	B4	no		12.30	1.27	0.90	2B, 3R
WMW 205/XMM	10W,11M	18:29:56.2	01:10:55.8	K0-K5	K3	yes	-0.6 to -1.6	16.58	1.54	1.26	1B, 2R
	10M	18:29:56.2	01:10:20.4	M2-M4	M3	no		18.60	1.66	1.17	1R
WMW 193	08B,09W	18:29:57.5	01:10:46.4	A1-A8	A5	no		9.70	0.31	0.14	2B, 1R
WMW 192	06W,08B,09W,10W	18:29:57.6	01:10:52.9	A1-A3	A2.5	no		8.43	0.21	0.09	2B, 2R
WMW 83/KOB 319	06W	18:29:57.8	01:15:31.9	K0-K5	K3	no		15.96[h]	...	3.21[h]	1R
WMW 27/XMM	06W	18:29:58.2	01:15:21.7	K5-K6	K5.5	poss	-30.3	20.37	...	1.85	1R
	10W,11M	18:29:58.7	01:19:08.0	K4-K6	K5	no		17.34	1.59	1.07	1B, 2R
WMW 59/XMM	06W,10M	18:29:59.3	01:14:07.7	K6-K8	K6	poss	-17.3 to -21.8	18.71	2.20	1.89	2R
	11M	18:30:00.3	01:06:10.6	K5-M0	K8	no		18.37	1.80	1.23	1R
	10W,10M,11M	18:30:00.5	01:21:57.8	K7-M2	M1	no		17.33	1.52	1.04	1B, 3R
KOB 339	11M	18:30:00.6	01:19:40.1	K3-K9	K6III	no		19.04	3.04	2.66	1R
	09W,10W,11M	18:30:02.5	00:57:15.9	K4-K6	K4	no		15.78	1.39	0.87	1B, 3R

Table 2—Continued

Name[a]	Yrs. obs.[b] & Tel.[c]	RA(J2000) (hhmmss.s)	DEC(J2000) (° ′ ″)	Sp. Ty. Range	Adopt Sp. Ty.	Li?[d]	EW(Hα) (Å)	V (mag)	(B-V) (mag)	(V-R) (mag)	No. obs.[e]
EC 131	10M,11M	18:30:02.8	01:13:21.8	M1-M4	M3	no	-1.0	19.61	1.60	1.14	2R
WMW 78/XMM	06W,10W,10M,11M	18:30:03.4	01:16:19.1	K3-K6	K5	yes	-5.4 to -7.6	17.87	1.98	1.51	1B, 3R
	10W,10M,11M	18:30:04.1	01:17:18.8	K8-M3	M1	no		17.88	1.67	1.11	3R
	11M	18:30:04.3	01:21:40.2	G5-K0	G9	no		19.01	2.13	1.55	1R
	10M,11M	18:30:04.8	00:59:57.6	G0-G9	G4	poss		19.05	1.97	1.47	2R
WMW 98/GFM 71		18:30:04.9	01:14:39.5	M3.5-M6.5g	M5g	...		20.72	1.36	1.87	...
WMW 84/XMM	06W,10M,11M	18:30:06.1	01:06:17.0	K8-M2	M0	yes	-9.8 to -13.9	18.46	2.08	1.62	3R
	10M,11M	18:30:06.4	01:22:48.5	F5	F5	no		19.29	1.83	1.52	2R
KOB 359	06W,10W,11M	18:30:06.4	01:01:05.8	K5-K6	K6	yes	-2.3 to -18.8	17.67	1.65	1.36	1B, 3R
	10M,11M	18:30:07.2	00:58:48.6	G3-G5	G4	no		18.96	2.05	1.59	2R
	09W,10W	18:30:07.3	01:01:14.9	K5-K8	K6	no		14.88	1.42	0.99	1B, 2R
	08B,09W,10W	18:30:07.4	01:01:01.5	G6-K2	G9	no		11.77	0.93	0.51	2B, 3R
WMW 73/XMM	06W,10M,11M	18:30:07.7	01:12:04.3	K5-K6	K5.5	yes	-9.1 to -34.4	19.88	2.34	2.05	3R
	10M	18:30:07.8	01:20:36.0	M3-M4	M3.5III	no	-0.6	19.81	1.70	1.25	1R
XMM	06W	18:30:08.2	01:05:51.0	M4-M5	M4.5	yes	-14.3	20.38	1.48	2.03	1R
KOB 367	10M	18:30:08.5	01:01:37.4	K7-M0	K8	no	-58.9	19.70	2.03	1.65	1R
	10M,11M	18:30:08.6	01:25:52.9	A7-F3	F1	no		19.26	2.50	1.67	2R
KOB 370	09W,10W,11M	18:30:08.7	00:58:46.5	G9-K4	K2	yes	-2.4 to -9.5	15.66f	1.63	1.11	1B, 3R
	11M	18:30:10.4	01:22:47.0	F7-G3	G0	no		19.82	1.84	1.96	1R
	08B,09W,10W	18:30:10.6	01:10:52.7	G2-G9	G8	poss		13.28	0.91	0.53	2B, 3R
	10W,10M,11M	18:30:10.7	00:58:13.3	K5-M3	M1.5	yes	-1.0 to -4.8	17.09	1.84	1.37	1B, 3R
	11M	18:30:11.3	01:21:51.5	F7-G1	G0	yes		19.76	2.15	1.78	1R
SVS Ser 12	10M	18:30:11.4	01:08:33.7	K1-K3	K2	no		19.43	...	2.38	1R
	11M	18:30:11.4	01:04:33.8	F5-F7	F6	no		18.76	2.22	1.65	1R
	10M	18:30:12.1	01:04:21.8	G9-K2	K1III	no		19.44	2.44	2.17	1R
	10W,10M,11M	18:30:12.3	01:06:46.9	A9-F4	F1	no		18.01	2.12	1.59	3R
	10W,11M	18:30:12.4	01:24:47.1	K6-M1	K8	no		18.21	1.68	1.16	2R
	10W,10M	18:30:13.0	00:58:34.7	F7-G4	G0	no		18.01	2.17	1.59	2R
	10M,11M	18:30:13.1	01:15:52.7	M1-M4	M3	poss		18.61	1.64	1.07	2R
	11M	18:30:13.2	01:04:06.0	G1-G5	G3	yes		19.25	1.94	1.71	1R

Table 2—Continued

Name[a]	Yrs. obs.[b] & Tel.[c]	RA(J2000) (hhmmss.s)	DEC(J2000) (° ′ ″)	Sp. Ty. Range	Adopt Sp. Ty.	Li?[d]	EW(Hα) (Å)	V (mag)	(B-V) (mag)	(V-R) (mag)	No. obs.[e]
WMW 74		18:30:13.3	01:02:48.9	M2.5-M5.5[g]	M4[g]	⋯		20.20	1.67	1.90	⋯
	10M	18:30:13.5	01:24:49.0	M3-M4	M3.5	poss		19.13	1.56	1.16	1R
	10W	18:30:13.9	01:00:42.1	K6-M3	K9	no		17.62	1.54	1.07	1B, 1R
WMW 166/KOB 407		18:30:14.0	01:08:51.5	M4-M6[g]	M5[g]	⋯		20.07	1.99	1.71	⋯
	10M	18:30:14.0	01:19:04.8	G0-K0	G5	no		19.95	2.30	1.56	1R
	10W,11M	18:30:14.2	00:58:28.0	F7-G4	G0	no		16.50	1.85	1.30	1B, 2R
	10M	18:30:14.5	00:57:38.8	K2-K4	K3	no		19.31	2.37	1.49	1R
	11M	18:30:14.8	01:21:49.0	F1-F5	F2	no		19.71	2.11	1.58	1R
	10M	18:30:15.2	01:24:44.0	G0-G9	G5	poss		19.85	1.86	1.50	1R
	10W,10M,11M	18:30:17.1	01:25:09.4	A1-A5	A3	no		17.98	2.03	1.49	3R
	10M,11M	18:30:17.2	00:59:49.2	F7-G3	G3	no		19.42	2.14	1.61	2R
	10M,11M	18:30:18.1	01:27:18.2	M3-M6	M5.5III	no		19.51	⋯	2.75	2R
WMW 40/XMM	06W	18:30:18.2	01:14:16.8	K6-M0	K8	poss	-78.3	13.22[h]	⋯	1.49[h]	1R
	10M,11M	18:30:19.0	01:02:52.0	K3	K3	no		19.18	2.61	2.18	2R
	10W,11M	18:30:19.5	01:13:08.0	K4-K5	K5	no		18.98	2.72	1.94	1B, 2R
	10M	18:30:19.5	01:18:57.0	K2-K4	K3	no		16.28	1.44	0.97	1R
	11M	18:30:19.7	01:00:54.1	F7-G4	G0	yes		19.52	⋯	1.75	1R
	09W,10W,11M	18:30:20.5	01:17:22.2	K3-K5	K4	poss		15.86	1.35	0.98	1B, 3R
	10M	18:30:20.7	01:02:31.7	G9-K0	G9	no		19.72	2.33	1.45	1R
	10M	18:30:21.5	01:05:44.5	M2-M4	M3	no		19.54	1.56	1.21	1R
	11M	18:30:21.7	01:21:55.3	K2-K3	K3	no		19.88	1.97	1.87	1R
XMM	06W,10M	18:30:21.9	01:21:07.7	M2-M4	M3	no	-2.1 to -2.8	19.28	1.75	1.46	2R
WMW 157/XMM	06W,10W,11M	18:30:22.4	01:20:44.0	M0-M1	M1	yes	-3.9 to -9.4	17.61	1.72	1.31	1B, 3R
	10M,11M	18:30:22.5	01:16:01.0	K7-M1	M0	no		18.80	1.69	1.18	2R
WMW 128/GFM 85	11M	18:30:23.1	01:20:09.7	M3.5-M4.5	M4	poss		18.38	1.67	1.40	1R
	10W,11M	18:30:23.2	01:06:19.3	M3-M4	M3.5	no		17.61	1.83	1.41	1B, 2R
	10M	18:30:23.3	01:06:22.6	M3-M4	M3.5	yes	-2.4	18.95	2.36	1.56	1R
WMW 33/XMM	06W	18:30:23.4	01:05:04.6	M2-M3	M3	yes	-18.8	18.84	1.40	1.42	1R
	10W,11M	18:30:23.6	01:04:09.7	K5-K6	K6	poss		17.63	1.70	1.34	1B, 2R
	10W	18:30:23.7	01:04:11.5	A9-G4	F6	no		17.82	1.97	1.54	1R

Table 2—Continued

Name[a]	Yrs. obs.[b] & Tel.[c]	RA(J2000) (hhmmss.s)	DEC(J2000) (° ′ ″)	Sp. Ty. Range	Adopt Sp. Ty.	Li?[d]	EW(Hα) (Å)	V (mag)	(B-V) (mag)	(V-R) (mag)	No. obs.[e]
	10M	18:30:23.8	01:19:19.5	G5-G9	G7	no		20.01	2.28	2.22	1R
	09W,10W,11M	18:30:23.9	01:12:38.3	K3-K5	K4	no		15.27	1.26	0.85	1B, 3R
WMW 220	09W,10W	18:30:24.5	01:19:50.7	K0-K2	K1	poss		14.63	1.08	0.69	1B, 2R
HD 170634	08B,09W,10W	18:30:24.9	01:13:23.0	B6-B8	B7	no		9.83	0.59	0.38	2B, 2R
	10W,11M	18:30:25.2	01:26:51.8	M3.5-M4.5	M4	no		16.34	1.47	0.96	1B, 2R
	10M	18:30:25.3	01:15:02.8	G9-K0	G9	no		19.58	2.44	1.94	1R
XMM	06W,10M	18:30:25.7	01:09:32.9	M4-M6	M5	no	-4.0	19.34	1.63	1.28	2R
	11M	18:30:25.8	00:57:36.6	G1-G5	G3	no		19.67	2.10	1.62	1R
	11M	18:30:26.3	01:00:05.8	K6-M1	K8	no		18.51	1.77	1.17	1R
	10M	18:30:26.8	01:27:23.4	G2-G9	G5	no		19.16	2.20	1.63	1R
	09W,10W	18:30:27.2	01:25:21.5	A7-F0	A9	no		13.58	1.06	0.70	2B, 2R
	09W,10W	18:30:27.2	01:03:46.8	A9-F2	F0	poss		14.91	1.77	1.26	1B, 2R
	10W,11M	18:30:28.4	00:57:25.1	G5-G9	G7	poss		18.11	2.27	1.67	2R
	10M,11M	18:30:29.2	01:27:21.3	M3-M6	M4.5	no		18.79	1.68	1.18	2R
	10M	18:30:29.5	01:01:21.9	G1-G5	G3	no		18.86	2.13	1.49	1R
	10M	18:30:29.7	00:58:27.8	G2-K0	G6	poss		19.96	· · ·	1.80	1R
	10M	18:30:29.8	01:22:54.2	G2-G9	G5	poss		19.61	2.19	1.63	1R
	10M	18:30:30.0	01:02:49.0	F5-G5	G0	no		19.70	1.97	1.51	1R
	11M	18:30:30.1	01:25:41.6	K6-M1	K8	no		18.81	1.75	1.20	1R
	10M	18:30:30.5	01:16:25.9	G9-K2	K0	no		19.44	2.38	2.05	1R
	10M	18:30:30.6	01:15:32.9	K3-K5	K4	no		19.78	2.29	2.22	1R
	10W,11M	18:30:31.6	01:06:44.5	K1-K3	K2	poss		17.98	2.55	1.84	2R
	10W,10M	18:30:31.9	01:18:38.7	K1-K3	K2	no		18.19	2.58	1.94	2R
	09W,10W,11M	18:30:32.3	00:59:07.6	A9-F5	F3	no		16.19	1.70	1.22	1B, 3R
	08B,09W,10W	18:30:32.3	01:04:40.9	F9-G6	G3	no		12.20	2.02	1.32	2B, 3R
	10W,11M	18:30:32.6	01:11:34.7	F5-F7	F7	no		17.88	2.20	1.58	2R
	10W,10M,11M	18:30:32.7	01:17:36.2	M1-M2	M2	no		17.21	1.48	1.05	1B, 3R
	10M	18:30:33.2	01:26:42.3	G4-G9	G5	no		19.63	1.92	1.50	1R
	11M	18:30:33.5	01:02:56.8	K1-K5	K4	yes		19.41	1.93	1.45	1R
	10W,11M	18:30:34.8	01:23:17.6	A7-F0	A9	poss		17.94	1.87	1.25	2R

Table 2—Continued

Name[a]	Yrs. obs.[b] & Tel.[c]	RA(J2000) (hhmmss.s)	DEC(J2000) (° ′ ″)	Sp. Ty. Range	Adopt Sp. Ty.	Li?[d]	EW(Hα) (Å)	V (mag)	(B-V) (mag)	(V-R) (mag)	No. obs.[e]
	10M,11M	18:30:35.0	00:59:02.7	K3-K4	K3	yes		19.16	2.44	1.88	2R
	11M	18:30:35.1	01:27:12.1	K3	K3	no		19.28	2.59	1.96	1R
	10M	18:30:35.1	01:07:31.9	F7-K0	G2	poss		19.53	1.98	1.56	1R
XMM	06W,10W,11M	18:30:35.3	01:05:57.8	K6-K7	K6	yes	-0.6 to -2.3	16.51	1.62	1.27	1B, 3R
	10M	18:30:35.4	01:19:07.0	K1-K2	K1	yes		18.40	2.46	1.77	1R
	10M,11M	18:30:35.9	01:13:36.3	G0-G4	G2	no		19.17	2.20	1.64	2R
	10M	18:30:36.0	01:24:28.2	G0-G4	G2	no		18.37	2.13	1.47	1R
	10W,11M	18:30:36.4	00:59:54.8	F5-G4	F9	no		16.61	1.99	1.42	1B, 2R
	10W,11M	18:30:36.5	01:12:49.1	M2-M4.5	M3	no		17.99	1.54	1.15	2R
	08B,09W,10W	18:30:37.1	01:01:36.2	K4-M2	K7	no		14.47	2.97	2.40	1B, 3R
XMM	06W,08B	18:30:37.4	01:17:58.3		K5	yes		14.80	1.37	0.94	2R
	10M	18:30:38.1	01:00:19.0	G4-K0	G7	no		19.23	2.51	1.75	1R
	10M,11M	18:30:38.1	01:23:39.1	K0-K4	K2.5	no		18.05	2.52	1.78	2R
	10W	18:30:38.2	01:06:02.9	G9-K0	G9	poss		18.12	1.88	1.40	1R
	10W,11M	18:30:38.5	01:25:17.2	A1-A8	A5	no		16.86	1.72	1.28	1B, 2R
	11M	18:30:38.6	01:20:08.2	K2-K3	K3	no		17.38	⋯	1.69	1R
	10M	18:30:38.6	00:57:07.0	G9-K2	K0	no		19.64	2.42	1.83	1R
	11M	18:30:38.6	01:11:40.8	K3-K5	K3	no		18.40	2.45	1.87	1R
	11M	18:30:39.1	01:20:58.8	G9-K1	K0	no		19.07	2.33	1.56	1R
	10M	18:30:39.2	01:11:54.6	M3-M4	M3.5	no		18.62	1.55	1.16	1R
	10M	18:30:39.3	01:02:44.9	K2-K4	K3	poss		19.43	1.91	1.73	1R
	10M	18:30:39.3	01:07:43.6	G0-K0	G5	poss		18.76	2.07	1.60	1R
XMM	06W,09W,10W,11M	18:30:39.6	01:18:03.1	K4-K5	K4	yes	-0.1 to -0.2	15.67	1.48	1.04	4R
	10M,11M	18:30:39.9	01:05:04.0	K1-K2	K2	no		17.08	1.54	1.07	2R
XMM	06W	18:30:40.2	01:10:27.6	M1-M2	M1.5	poss		16.21[h]	⋯	1.32[h]	1R
	10M,11M	18:30:40.5	01:01:06.1	K0-K2	K1	poss		19.20	1.96	1.67	2R
	10W,10M	18:30:40.7	01:08:48.8	G9-K2	G9	no		18.24	2.48	1.80	2R
	08B,09W,10W	18:30:41.9	01:06:15.2	F6-F9	F8	yes		13.01	0.98	0.63	2B, 3R
	10W,11M	18:30:42.2	01:22:42.5	F0-F9	F5	no		16.73	1.78	1.19	1B, 2R
	10W,11M	18:30:42.2	01:20:03.1	F7-G4	G1	no		16.52	1.75	1.36	1B, 2R

Table 2—Continued

Name[a]	Yrs. obs.[b] & Tel.[c]	RA(J2000) (hhmmss.s)	DEC(J2000) (° ′ ″)	Sp. Ty. Range	Adopt Sp. Ty.	Li?[d]	EW(Hα) (Å)	V (mag)	(B-V) (mag)	(V-R) (mag)	No. obs.[e]
	08B,09W,10W	18:30:42.3	00:58:48.9	F9-G0	G0	no		13.41	1.23	0.82	2B, 3R
	10M	18:30:42.7	01:07:30.2	K2-K4	K3	no		18.45	2.50	1.81	1R
	09W,10W,11M	18:30:42.8	01:04:47.9	A9-F3	F0	no		19.26	2.10	1.41	1B, 3R
	11M	18:30:42.8	01:27:12.4	G5-K0	G9	yes		16.08	1.79	1.26	1R
	10M	18:30:42.9	01:20:38.0	K7-M0	K8III	no		19.41	2.69	2.09	1R
	10W,11M	18:30:43.3	01:06:06.7	K3-K5	K3	no		17.82	2.51	1.77	2R
	10W	18:30:43.4	01:16:54.0	K0-K2	K2	poss		18.23	2.45	1.95	1R
	10M	18:30:43.6	01:18:03.3	K2-K4	K3	no		17.20	2.20	1.64	1R
	10M,11M	18:30:43.8	01:14:47.0	K2-K4	K3	no		19.43	2.50	2.03	2R
	10M,11M	18:30:44.4	01:13:56.5	G5-K0	G9	no		19.23	2.29	1.55	2R
	08B,09W,10W	18:30:44.9	01:20:44.8	F6-F7	F6	no		18.66	2.59	1.81	2B, 3R
	11M	18:30:44.9	01:13:16.3	K0-K3	K1	no		13.38	0.86	0.54	1R
	10M	18:30:45.1	01:00:31.2	G0-G5	G3	poss		19.72	2.26	1.50	1R
	10M,11M	18:30:45.2	01:24:55.8	K3-K4	K4	no		18.41	2.68	1.91	2R
	10W,10W,11M	18:30:45.2	01:08:53.5	K1-K4	K3	no		18.22	2.62	1.86	3R
	11M	18:30:45.3	01:17:10.0	K3-K4	K4	no		18.70	2.67	2.03	1R
	09W,10W	18:30:46.0	01:11:03.8	K0-K3	K1.5	no		20.01	1.57	1.43	1B, 2R
	10M	18:30:46.0	01:26:50.7	K0-K4	K2	no		14.45	1.11	0.71	1R
	10W,11M	18:30:46.2	01:16:43.0	K3	K3	no		17.61	⋯	1.61	1B, 2R
	10M	18:30:46.5	01:26:21.0	K3-K5	K4	no		19.47	2.41	1.81	1R
	09W,10W	18:30:47.2	01:09:11.8	A2-A5	A3	no		16.06	1.59	1.17	1B, 2R
	10W,10M,11M	18:30:47.4	00:58:46.4	G5-G9	G7	no		17.02	2.18	1.54	1B, 3R
	10M	18:30:47.5	01:12:36.9	G9-K2	K0	no		19.77	2.50	1.94	1R
	10M	18:30:48.1	01:03:44.4	M2-M3	M2III	no		19.65	1.82	1.69	1R
	10M	18:30:48.2	01:24:51.3	G5-G9	G5	poss		18.66	1.83	1.24	1R
	10M	18:30:48.7	01:11:27.5	G5-K0	G7	poss		19.94	2.11	1.50	1R
	08B,09W	18:30:49.1	01:04:48.9	F0-F2	F1	poss		12.24	0.90	0.52	1B, 2R
	09W,10W,10M	18:30:49.6	01:20:18.8	A1-A3	A3	poss		15.76	1.54	1.06	2B, 4R
	10M,11M	18:30:50.1	01:08:17.5	F0-F4	F4	no		19.32	2.14	1.52	2R
	10M	18:30:50.5	01:16:16.3	G9-K2	K1	no		19.56	2.23	1.81	1R

Table 2—Continued

Name[a]	Yrs. obs.[b] & Tel.[c]	RA(J2000) (hhmmss.s)	DEC(J2000) (° ′ ″)	Sp. Ty. Range	Adopt Sp. Ty.	Li?[d]	EW(Hα) (Å)	V (mag)	(B-V) (mag)	(V-R) (mag)	No. obs.[e]
	11M	18:30:50.7	01:07:24.8	F3-F9	F4	no		18.29	1.99	1.42	1R
	10W,11M	18:30:51.1	01:16:08.7	A1-A5	A3	no		17.18	1.59	1.11	1B, 2R
	10W,11M	18:30:51.1	00:59:21.8	G3-K2	G5	no		18.14	1.98	1.39	2R
	10M	18:30:51.5	01:17:02.5	K4-K5	K5	no	-6.4	18.72	1.88	1.48	1R
	11M	18:30:52.0	01:08:51.5	K3-K4	K3	no		19.73	2.27	1.73	1R
	10M	18:30:52.1	00:58:59.2	K4-K5	K5	no		19.42	..	2.17	1R
	10W,11M	18:30:52.1	01:15:38.8	M2-M4	M3	poss		17.88	1.55	1.10	2R
	11M	18:30:52.3	01:10:35.2	G0-G9	G5	yes		19.13	2.05	1.45	1R
	10M,11M	18:30:52.8	01:09:26.6	K1-K3	K2	yes		19.05	2.64	1.93	2R
	10M	18:30:52.9	01:05:14.9	K7-M0	K8	no		19.41	1.81	1.56	1R
	09W,10W,10M,11M	18:30:53.0	01:21:32.2	G5-K2	K0	no		15.90	2.19	1.53	1B, 4R
	10W,10M,11M	18:30:53.2	01:14:37.6	M1-M3	M2	no		18.18	1.57	1.16	3R
	10W	18:30:53.4	01:22:30.1	F2-F5	F3	no		18.19	1.97	1.35	1R
	10M	18:30:53.6	01:18:39.5	F6-G9	G5	no		19.24	1.89	1.42	1R
	10M	18:30:53.6	01:27:26.1	G0-G9	G5	poss		19.65	1.75	1.26	1R
	10M	18:30:53.7	01:08:08.7	G5-K3	K0	no		19.04	2.43	1.78	1R
	10M	18:30:54.1	01:22:55.8	G9-K1	K0	no		19.92	2.15	1.79	1R
	11M	18:30:54.1	01:26:44.4	M3-M5.5	M3.5	no		19.54	1.80	1.20	1R
	11M	18:30:54.4	01:13:29.6	F3-F9	F5	yes		18.64	1.98	1.38	1R
	10M	18:30:54.6	01:02:14.5	K4-K6	K5	no		19.29	2.39	2.16	1R
	11M	18:30:54.8	01:19:47.8	F3-F5	F5	no		17.97	1.85	1.26	1R
	10W	18:30:55.0	01:21:20.2	G9-K0	K0	no		18.26	2.24	1.59	1R
	11M	18:30:55.0	01:22:11.3	K8-M1	M0	no		18.74	2.63	2.01	1R
	10W,10M,11M	18:30:55.1	01:18:15.6	F7-G1	G0	poss		18.21	1.96	1.42	3R
	09W,10W,10M	18:30:55.2	01:15:57.8	K3-K5	K4	no		15.47	1.40	0.84	1B, 3R
	10M	18:30:55.5	01:25:51.4	G5-K4	K0	no		19.46	1.78	1.33	1R
	10W,10M,11M	18:30:55.5	01:08:40.9	F4-G1	F6	no		18.28	1.89	1.49	3R
	09W,10W,11M	18:30:55.9	01:24:09.2	G9-K1	K0	no		16.27	1.87	1.36	2B, 4R
	10W	18:30:55.9	01:06:07.5	F3-F9	F5	no		18.82	2.12	1.61	1R
	10W,11M	18:30:56.3	01:30:17.2	K6-M3	M1	no		17.83	1.68	1.27	2R

Table 2—Continued

Name[a]	Yrs. obs.[b] & Tel.[c]	RA(J2000) (hhmmss.s)	DEC(J2000) (° ′ ″)	Sp. Ty. Range	Adopt Sp. Ty.	Li?[d]	EW(Hα) (Å)	V (mag)	(B-V) (mag)	(V-R) (mag)	No. obs.[e]
	08B,09W,10W	18:30:56.5	01:23:06.6	G2-G7	G5	yes		13.22	0.92	0.56	2B, 3R
	09W,10W	18:30:56.5	01:10:49.1	F6-F8	F7	poss		12.63	0.95	0.74	2B, 2R
	10W,11M	18:30:56.6	01:02:41.4	K3-K6	K6	yes	-3.0	16.44	1.68	1.47	1B, 2R
	10M	18:30:56.7	00:58:19.9	G5-K0	G7	no		19.67	2.56	2.03	1R
	09W,11M	18:30:57.1	01:25:40.3	G0-G5	G2	no		15.31	1.42	0.95	2R
	10M,11M	18:30:57.6	01:21:11.6	K7-M2	M0	poss	-2.5 to -2.8	16.99	⋯	1.40	2R
	10M,11M	18:30:57.6	01:13:37.2	M3-M5.5	M4.5	no	-4.6 to -6.3	18.61	2.00	1.59	2R
	10W,10M	18:30:57.7	01:19:46.4	K2-K4	K3	no		18.03	2.40	1.65	2R
	11M	18:30:58.3	01:26:53.5	K3	K3	no		18.63	2.33	1.74	1R
	10M	18:30:58.3	01:24:32.0	M2-M4	M3III	no		18.71	2.63	1.90	1R
SCB 75	09W	18:30:59.6	01:27:34.8	G9-K2	K0	no		12.86	1.09	0.57	1B, 1R
SCB 76	09W	18:31:00.1	01:30:28.1	G4-G5	G4	yes		12.48	1.13	0.63	1B, 1R
SCB 86	09W	18:31:40.5	01:17:22.3	F6-F7	F7	poss		11.85	1.11	0.69	1B, 1R
SCB 87	09W	18:31:52.5	01:12:01.5	F4-F7	F5	⋯		11.45	0.66	0.41	1B
SCB 78	09W	18:31:08.0	01:09:05.9	A5-A8	A7	⋯		10.94	0.67	0.34	1B
HD 170784	09W	18:31:09.0	01:26:58.6	B3	B3	⋯		8.53	0.47	0.25	1B

[a]Sources names from xray, optical or infrared studies by: (SCB) Straižys, Černis, & Bartašiūte (1996); (XMM) XMM-Newton survey by Preibisch (2003); (WMW) Spitzer survey by Winston et al. (2007); (CDF88) reflection nebulae study by Chavarria-K. et al. (1988); (GFM) Chandra survey by Giardino et al. (2007); (EC) Eiroa, & Casali (1992); (SVS) Strom, Vrba, & Strom(1976); (KOB) ISO survey by Kaas et al. (2004); (2MASS) 2Micron All-Sky Survey.

[b]Years that sources were observed: 2006, 2008, 2009, 2010 and 2011

[c]Telescopes used for observation: M for the MMT, W for the WIYN telescope, and B for the Bok telescope.

[d]"poss" stands for possibly

[e]Spectral region observed and number of observations in each wavelength range: B stands for blue and R for red (see text for exact wavelength range for each telescope/set of observations).

[f]Source has a known companion, not resolved in our photometry

[g]Spectral types from Winston et al. (2009) and Oliveira et al. (2009)

[h]Photometry from 2MASS: J replaces V and (J-H) replaces (V-R)

Table 3. Optical Properties of Candidate Young Stellar Objects with Echelle Spectra

Object[a]	RA(2000) (hh mm ss.s)	DEC(2000) (°′″)	Date (YYMMDD)	Sp. Ty. Range	Sp. Ty.[b]	Surface Gravity	$v \sin i$[d] (km sec^{-1})	YSO?[d]
SCB 40	18:28:56.2	01:06:27.6	20090811	F7-G0	G0	V-IV	13±2 - 25±3	
SCB 41	18:28:58.4	01:10:59.7	20090811	A9-F2	F4	...	30±5	
SCB 43	18:29:08.0	01:05:25.4	20090811	F6-F9	F7	V-III	...	
WMW 124	18:29:08.2	01:05:43.1	20090609 20100710	A1-A3	A1	V-III	33±5	IRX, TD
BD+01 3686	18:29:27.6	01:12:56.8	20090811	F2-F6	F6	V-III	25±2	X
BD+01 3687	18:29:31.7	01:08:19.1	20090609 20100710	F3-F9	F6	V-IV	12±3	ref. neb.
WMW 82/KOB 173	18:29:33.4	01:08:22.8	20090609	A3-A4	A3.5	V	...	IRX, ref. neb.
[CDF88] 7/XMM	18:29:56.1	01:00:21.7	20100710	B3-B6	B6	III	...	X, ref
WMW 193/BD+01 3689B	18:29:57.5	01:10:46.4	20100710	A1-A8	A5	V-III	135±9	X
WMW 192/HD 170545	18:29:57.6	01:10:52.9	20100710	A1-A3	A2.5	V	31±5	X
	18:30:07.4	01:01:01.5	20090811	G6-K2	G9	IV	...	
KOB 370	18:30:08.7	00:58:46.5	20100711	G9-K4	K1	IV	...	Li,Hα,IRX[e]
BD+1 3693	18:30:10.4	01:19:33.7	20090811	A5-A8	A7	III	...	
WMW 220	18:30:24.5	01:19:50.7	20090811	K0-K2	K1	...	12±2	X
HD 170634	18:30:24.9	01:13:23.0	20100710	B6-B9	B9	III	...	ref. neb.
XMM	18:30:37.4	01:17:58.3	20100711	F8-K5	K0	V-IV	39±3	X
	18:30:42.3	00:58:48.9	20100711	F4-F6	F5	III	34±4	
SCB 70	18:30:54.5	01:12:52.7	20090811	F4-F7	F7	V-IV	22±2	X

[a] Source names from xray, optical or infrared studies by: (SCB) Straižys, Černis, & Bartašiūte (1996); (WMW) Spitzer survey by Winston et al. (2007); (XMM) XMM-Newton survey by Preibisch (2003); (CDF88) reflection nebulae survey by Chavarria-K. et al. (1988) ; (KOB) ISO survey by Kaas et al. (2004).

[b] Spectral types derived from Magellan spectra only; See Table 4 for adopted spectral type.

[c] In most cases, the value of $v \sin i$ was not sensitive to surface gravity and is represented by a single value. A range is given only for SCB 40. When the surface gravity was indeterminate, a dwarf surface gravity was assumed.

[d] YSO criteria include an infrared excess (IRX) including transition disk objects (TD), X-ray emission (X), association with reflection nebulosity (ref. neb.), Hα emission with EW>10 Å (Hα), or lithium absorption (Li).

[e] Hα emission is variable and not detected in the echelle spectrum.

Table 4. Association Members

Name[a]	RA(J2000) (hhmmss.s)	DEC(J2000) (° ′ ″)	Sp. Ty. Adopt	A_v (mag)	M_V (mag)	$\log (L/L_\odot)$	$\log T$ (K)	Mass[b] ($M_\odot$)	log age (yrs)	Criteria[c]
	18:28:57.3	01:13:03.0	K1	7.4	4.32	0.33	3.71	1.5	6.55	Li/ext
XMM	18:29:04.5	01:09:47.0	<K6	>1.6[e]	<8.9[e]	>-1.7	>3.62	...	...	X
WMW 124	18:29:08.2	01:05:43.1	A2	3.8	1.49	1.40	3.95	2.3	6.75	TD
	18:29:14.4	01:27:33.8	K4	6.4	4.85	0.17	3.66	0.77	5.98	Li/ext
	18:29:16.0	01:08:56.2	K3	6.6	4.66	0.23	3.68	1.1	6.23	Li/ext
WMW 104	18:29:20.4	01:21:03.8	M0.5[d]	6.3	5.67	0.14	3.57	0.28	4.85	IRX/ext
XMM	18:29:20.5	01:08:55.1	K5	2.6	5.62	-0.09	3.64	0.71	6.21	Li/X
WMW 221/XMM	18:29:22.7	01:10:33.0	K6	3.0	5.71	-0.09	3.62	0.56	5.99	Li/X
BD+01 3686	18:29:27.6	01:12:56.8	F4	0.83	2.04	1.11	3.82	2.0	6.75	X
XMM	18:29:31.2	01:05:51.6	M3	3.0	7.67	-0.37	3.53	0.22	5.63	Li/X
BD+01 3687	18:29:31.7	01:08:19.1	F6	0.39	2.73	0.85	3.80	1.7	6.89	ref. neb.
WMW 225/XMM	18:29:33.1	01:17:16.5	K0	5.0	3.38	0.69	3.72	2.0	6.25	Li/X/ext
WMW 82/KOB 173	18:29:33.4	01:08:22.8	A3	2.3	1.41	1.41	3.93	2.3	6.71	IRX/ref. neb.
XMM	18:29:33.6	01:07:00.0	M3.5	1.7	7.90	-0.35	3.51	0.17	4.96	X
XMM	18:29:34.5	01:06:06.9	U	...	...	...	...	...	...	X
XMM	18:29:34.7	01:05:28.9	K8	2.8	5.79	0.01	3.59	0.38	5.62	X
XMM	18:29:34.9	01:08:46.2	K6	0.85	5.84	-0.14	3.62	0.59	6.09	Li
WMW 94/XMM	18:29:39.9	01:17:56.0	M0.5	<8.2[e]	>4.04[e]	<-0.38	3.57	0.40	6.04	Li/Hα/X/IRX/ext
WMW 103/XMM	18:29:41.5	01:07:37.9	K5	3.3	5.50	-0.05	3.64	0.69	6.14	Li/Hα/X/IRX
	18:29:43.0	01:02:06.8	M0	4.1	6.66	-0.29	3.58	0.42	5.97	Li/ext
WMW 65/KOB 219	18:29:43.9	01:07:21.0	K7[d]	4.8	7.10	-0.56	3.60	0.69	6.74	ext/IRX
WMW 100/XMM	18:29:44.5	01:13:11.6	M4.5[d]	1.8	9.17	-0.60	3.49	0.14	5.23	X/IRX
WMW 79	18:29:46.3	01:10:25.3	M2[d]	3.9	7.70	-0.55	3.54	0.27	6.03	TD/ext
WMW 199/XMM	18:29:47.2	01:22:34.7	K8	5.2	4.92	0.36	3.59	0.32	4.66	Li/X/ext
WMW 81/XMM	18:29:53.6	01:17:01.7	K6	4.6	6.20	-0.28	3.62	0.66	6.36	Li/Hα/X/IRX/ext
WMW 201/XMM	18:29:55.4	01:10:34.0	M5	0.0	11.98	-1.57	3.48	0.14	6.83	Hα/X
WMW 38/XMM	18:29:55.7	01:14:31.5	<K6	...	...	...	>3.62	...	...	X/IRX
[CDF88] 7/XMM	18:29:56.1	01:00:21.7	B5	5.3	-1.21	2.96	4.18	5.1	7.81	X/ref. neb.
WMW 205/XMM	18:29:56.2	01:10:55.8	K3	3.2	5.24	-0.01	3.68	1.1	6.59	Li/X/TD
WMW 193/BD+01 3689B	18:29:57.5	01:10:46.4	A5	0.16	1.37	1.41	3.91	2.3	6.68	X

Table 4—Continued

Name[a]	RA(J2000) (hhmmss.s)	DEC(J2000) (° ′ ″)	Sp. Ty. Adopt	A_v (mag)	M_V (mag)	log ($L/L_\odot$)	log T (K)	Mass[b] ($M_\odot$)	log age (yrs)	Criteria[c]
WMW 192/HD 170545	18:29:57.6	01:10:52.9	A2.5	0.25	0.02	1.98	3.94	3.0	6.36	X
WMW 83/KOB 319	18:29:57.8	01:15:31.9	K3	<24[e]	>1.35[e]	<0.83	3.68	1.2	5.52	X/IRX
WMW 27/XMM	18:29:58.2	01:15:21.7	K5.5	5.5	6.70	-0.51	3.63	0.85	6.97	Hα/X/IRX/ext
WMW 59/XMM	18:29:59.3	01:14:07.7	K6	5.6	4.95	0.22	3.62	0.48	5.56	Hα/X/IRX/ext
WMW 78/XMM	18:30:03.4	01:16:19.1	K5	3.9	5.79	-0.16	3.64	0.75	6.35	Li/X/IRX/ext
WMW 98/GFM 71	18:30:04.9	01:14:39.5	M5[d]	1.9	10.61	-1.02	3.48	0.14	6.18	X/IRX
WMW 84/XMM	18:30:06.1	01:06:17.0	M0	3.7	6.65	-0.29	3.58	0.42	5.97	Li/Hα/X/IRX/ext
KOB 359	18:30:06.4	01:01:05.8	K6	3.0	6.56	-0.43	3.62	0.75	6.68	Li/Hα/X/IRX
WMW 73/XMM	18:30:07.7	01:12:04.3	K5.5	6.5	5.21	0.09	3.63	0.57	5.80	Li/Hα/X/IRX/ext
XMM	18:30:08.2	01:05:51.0	M4.5	3.4	8.82	-0.46	3.49	0.14	4.93	Li/Hα/X
KOB 367	18:30:08.5	01:01:37.4	K8	3.9	7.59	-0.71	3.59	0.70	6.97	Hα/IRX/ext
KOB 370	18:30:08.7	00:58:46.5	K2	2.6	4.85	0.13	3.69	1.3	6.55	Li/IRX
	18:30:10.7	00:58:13.3	M1.5	2.0	6.93	-0.28	3.55	0.29	5.77	Li
WMW 74	18:30:13.3	01:02:48.9	M4[d]	3.3	8.69	-0.56	3.50	0.16	5.28	TD
WMW 166/KOB 407	18:30:14.0	01:08:51.5	M5[d]	1.2	10.76	-1.08	3.48	0.14	6.25	IRX
WMW 40/XMM	18:30:18.2	01:14:16.8	K8	<7.5[e]	>3.07[e]	<0.08	3.59	0.36	5.54	Hα/X/IRX/ext
XMM	18:30:21.9	01:21:07.7	M3	1.8	9.32	-1.03	3.53	0.26	6.59	X
WMW 157/XMM	18:30:22.4	01:20:44.0	M1	1.8	7.60	-0.59	3.56	0.41	6.31	Li/X/TD
WMW 128/GFM 85	18:30:23.1	01:20:09.7	M4	0.85	9.37	-0.83	3.50	0.17	6.09	X/TD
	18:30:23.3	01:06:22.6	M3.5	2.0	8.79	-0.71	3.51	0.18	6.03	Li
WMW 33/XMM	18:30:23.4	01:05:04.6	M3	1.6	9.08	-0.93	3.53	0.25	6.43	Li/Hα/X/IRX
WMW 220	18:30:24.5	01:19:50.7	K1	0.79	5.68	-0.22	3.71	0.99	7.28	X
HD 170634	18:30:24.9	01:13:23.0	B8	2.3	-0.63	2.46	4.06	4.5	6.02	ref. neb.
XMM	18:30:25.7	01:09:32.9	M5	0.0	11.18	-1.25	3.48	0.15	6.44	X
	18:30:33.5	01:02:56.8	K4	3.9	7.32	-0.82	3.66	0.72	8.00	Li
	18:30:35.0	00:59:02.7	K3	6.3	4.72	0.20	3.68	1.1	6.27	Li/ext
XMM	18:30:35.3	01:05:57.8	K6	2.5	5.85	-0.14	3.62	0.59	6.09	Li/X
	18:30:35.4	01:19:07.0	K1	6.2	4.05	0.43	3.71	1.6	6.42	Li/ext
XMM	18:30:37.4	01:17:58.3	K0	2.3	4.36	0.29	3.72	1.5	6.72	Li/X
XMM	18:30:39.6	01:18:03.1	K4	1.9	5.63	-0.14	3.66	0.91	6.55	Li/X

Table 4—Continued

Name[a]	RA(J2000) (hhmmss.s)	DEC(J2000) (° ′ ″)	Sp. Ty. Adopt	A_v (mag)	M_V (mag)	log (L/L$_\odot$)	log T (K)	Mass[b] (M$_\odot$)	log age (yrs)	Criteria[c]
XMM	18:30:40.2	01:10:27.6	M1.5	6.0[e]	6.46[e]	-1.27	3.55	0.39	7.31	X
	18:30:52.8	01:09:26.6	K2	6.7	4.14	0.41	3.69	1.3	6.16	Li/ext
	18:30:56.6	01:02:41.4	K6	3.5	4.78	0.29	3.62	0.46	5.48	Li/ext

[a]Source names from xray, optical or infrared studies by: (XMM) XMM-Newton survey by Preibisch (2003); (WMW) Spitzer survey by Winston *et al.* (2007); (GFM) Chandra survey by Giardino *et al.* (2007); (CDF88) reflection nebulae survey by Chavarria-K. *et al.* (1988); (KOB) ISO survey by Kaas *et al.* (2004).

[b]Masses and ages estimated from the tracks and isochrones of D'Antona & Mazzitelli 1997 and F. D'Antona & I. Mazzitelli 1998, private communication except for the two B stars for which the Siess *et al.* (2000) models were used.

[c]Association membership established through location above the main sequence and $A_v > 3.5$ mag (ext), the presence of Hα emission EW(Hα) >10 Å(Hα), an infrared excess (IRX), identification as a possible transition disk object (TD), lithium absorption (Li), reflection nebulosity (ref. neb.), or X-ray emission (X). See text for details.

[d]Spectral types from Winston *et al.* (2009) and Oliveira *et al.* (2009)

[e](J-H) photometry from 2MASS used to compute A_v and M(J)

Table 5. Weak Criteria Sources

Name[a]	RA(J2000) (hhmmss.s)	DEC(J2000) (° ' ")	Sp. Ty. Adopt	Av (mag)	M(V) (mag)	log (L/L⊙)	log T (K)	Mass[b] (M⊙)	log age (yrs)	Criteria[c]
	18:28:56.8	01:21:03.2	K3	4.2	6.20	-0.39	3.68	0.9	7.22	ext/poss Li
	18:28:56.9	01:17:51.0	G0	7.3	4.20	0.29	3.78	1.2	7.30	ext/poss Li
	18:29:01.7	01:01:12.2	K3	6.7	3.38	0.74	3.68	1.2	5.61	ext/poss Li
KOB 61	18:29:02.3	01:18:31.0	K0	7.3	4.02	0.43	3.72	1.7	6.56	ext/poss Li
	18:29:10.0	01:08:45.1	G3	5.9	4.27	0.28	3.77	1.2	7.26	ext/poss Li
	18:29:17.1	01:12:52.8	K3	7.9	3.84	0.55	3.68	1.1	5.82	ext/poss Li
	18:29:25.5	01:00:42.4	K3	6.5	4.94	0.11	3.68	1.1	6.40	ext/poss Li
	18:29:37.6	01:03:23.6	K6	5.0	5.88	-0.15	3.62	0.6	6.11	ext/poss Li
	18:30:27.2	01:03:46.8	F0	5.4	1.37	1.36	3.86	2.3	6.64	ext/poss Li
	18:30:28.4	00:57:25.1	G7	6.4	3.57	0.58	3.75	1.6	6.81	ext/poss Li
	18:30:31.6	01:06:44.5	K2	6.3	3.52	0.66	3.69	1.4	5.84	ext/poss Li
	18:30:38.2	01:06:02.9	G9	4.7	5.22	-0.06	3.73	1.1	7.28	ext/poss Li
	18:30:39.3	01:02:44.9	K3	5.5	5.74	-0.21	3.68	1.0	6.92	ext/poss Li
	18:30:40.5	01:01:06.1	K1	5.7	5.35	-0.09	3.71	1.1	7.09	ext/poss Li
	18:30:43.4	01:16:54.0	K2	6.8	3.22	0.78	3.69	1.4	5.71	ext/poss Li
	18:30:51.5	01:17:02.5	K5	3.8	6.79	-0.56	3.64	0.8	7.18	ext/weak Hα

[a]Sources name from infrared ISO survey by Kaas et al. (2004)).

[b]Masses and ages estimated from the tracks and isochrones of DAntona & Mazzitelli 1997 and F. DAntona & I. Mazzitelli 1998, private communication.

[c]Weak Criteria Sources have an Av > 3.5 mag (ext) and possible lithium absorption (poss Li) or the presence of Hα emission EW(Hα) > 5 Å(Hα)

SECTION

4   DISCUSSION

4.1   INTRODUCTION

An unbiased, optical spectroscopic survey of two low mass star-forming regions, the Rho Ophiuchi and Serpens Main clusters, has been conducted. In both regions, photometry was used to place sources in a color-magnitude diagram. Candidate YSOs were then selected for spectroscopic observation based on their position in the color-magnitude diagram. These spectra have been used to confirm youth, determine effective temperatures, visual extinctions, and bolometric luminosities. Comparisons with theoretical tracks and isochrones for pre-main sequence stars led to estimates for the ages and masses of association members. Data from the Spitzer Space Telescope was also used to determine infrared excesses and disk frequencies for the regions. Distributions of ages and masses place limits on star formation timescales and mechanisms, while studies of disk frequencies limit timescales for planet formation.

4.2   CONTRIBUTIONS AND LIMITATIONS OF WORK

Both the Rho Ophiuchi and Serpens molecular clouds are well-studied regions of low mass star formation. The young clusters associated these clouds have been observed by numerous surveys ranging from X-ray to submillimeter wavelengths (See sections 1.1.3, I.1, and II.1 for details). However, previous studies have been biased towards particular phases in the formation process and few have yielded spectral types. The surveys of Rho Ophiuchi and Serpens described here have filled in the gaps of these previous studies; 35 (Rho Ophiuchi) and 15 (Serpens) new PMS objects have been identified. These are mainly YSOs which have dissipated their circumstellar

disks and can be identified though Li absorption or variable Hα or X-ray emission. This study, combined with previous surveys, provides a more complete sample of YSOs with class 2 or class 3 spectral energy distributions. As star formation takes place in stages which are best observed at different wavelengths, it is necessary to probe all stages in order to form a complete picture of star formation within a region. However, optical studies are only complete for pre-main sequence objects; protostars in the earliest stages of star formation are not included (class 0 and 1 sources; see section 1.3). It is of interest to note that median ages for class 2 and class 3 objects in this study are not distinct; this would suggest that the timescales for these stages are source dependent.

In Rho Ophiuchi, the first IMF for the region based on an unbiased extinction-limited spectroscopic survey has been presented. While this is not the first IMF derived for the region (see section I.1.2), an unbiased extinction-limited spectroscopic study provides a more direct measurement of the mass distribution and therefore the IMF. The mass function is found to peak and turn over with a characteristic mass of 0.13 M$_\odot$. There is marginal evidence for a deficit of brown dwarfs, however, the lowest mass bin suffers from incompleteness and hence any firm determinations about the extent of the lowest mass population of Rho Ophiuchi cannot be made. The situation in Serpens is much less clear. While the high end of the IMF is in agreement with the field star IMF, one cannot make any statement at all about sources below 1 M$_\odot$. See figure 4.1.

The average age in most star-forming regions is found to be less than 5 Myrs (Lada & Lada 2003; Hillenbrand 2009). This supports the idea of star formation being a relatively fast process. Median ages of 3 Myrs and 2 Myrs are found for the optically visible members of the Rho Ophiuchi and Serpens Main clusters, respectively. However, these ages are based on theoretical tracks which are highly uncertain and may under-predict low mass stellar ages by 30-100% and over predict high mass stellar
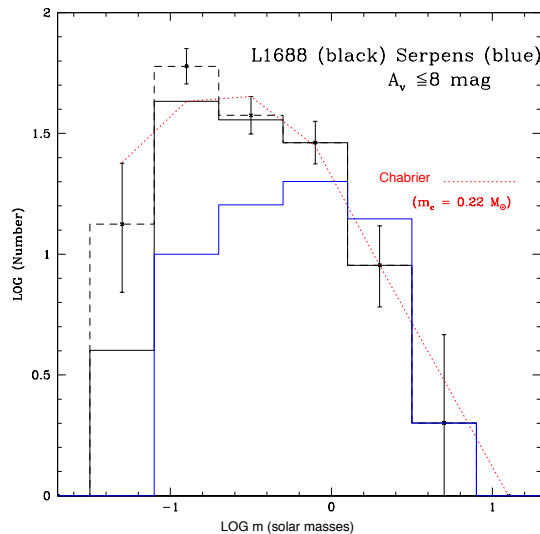
Figure 4.1 The initial mass function for the Serpens (Blue) and Ophiuchi (Black) clusters. Dashed lines show the members added from the completeness corrections. The red dotted line is the Chabrier (2003) system mass function which is lognormal for M<1.0 $M_\odot$ and a power law for M>1.0 $M_\odot$.

ages by 20-100% (Hillenbrand *et al.* 2007). Hence, while these age determinations are useful for relative comparisons, they are not absolute ages.

A disk frequency of approximately 30% is found in both regions and 9 (Rho Ophiuchi) and 6 (Serpens) potential transition disk objects have been identified. Sample sizes in both regions are not large enough to investigate variations in disk frequency with spectral type or with age. The limited sample size also means that the errors on the disk frequency are large. In Serpens the sample was so small that one could not meaningfully analyze the extinction-limited subsample of sources, a reflection of the bias towards brighter sources. Transition disk object studies (e.g., Muzerolle *et al.* 2009) have suffered from small sample size; the 15 sources identified in this study as potential transition disk objects will add to the sample size of future studies.

In Serpens, assuming a distance of 260 pc places YSOs below the main sequence while assuming a distance of 429 pc fixes this problem. This study therefore

supports the idea that the distance to Serpens should be revised to 429 pc (Dzib *et al.* 2010, 2011).

4.3 FUTURE WORK

With the new, larger distance to Serpens, an unbiased extinction-limited survey that probes down to lower mass would be needed to derive a complete IMF for the region. This would hopefully also provide a larger sample for disk studies, allowing for an unbiased disk frequency to be derived. This could be done with use of GMOS (Gemini multi-object spectrograph) at optical/ near infrared wavelengths. With the 8.1 m Gemini optical/ infrared telescopes, lower luminosities, hence lower masses could be probed. Similarly the use of FLAMES (Fibre Large Array Multi-Element Spectrograph) at optical wavelengths on the 8.2m VLT would not only allow probing to lower masses but would provide high-resolution optical spectra. This could also be done with further observation using Hectospec on the MMT at moderate resolution.

In Rho Ophiuchi, the low mass regime of the IMF could be inferred via observation of lower luminosity sources, determining if the possible deficit of brown dwarfs is real or not. This could easily be accomplished using Hectospec on the MMT. In Serpens the sub-stellar IMF could be inferred using NIRSpec at medium resolution on the James Webb Space Telescope

Studies of other star forming regions (i.e., NGC 1333 and/or Chamaeleon I), using the same techniques as used in this study to survey an unbiased extinction-limited sample of candidate YSOs would allow for direct comparison of several regions. Hectospec on the MMT would be best to observe sources in NGC 1333, with its distance of 240 pc (Hirota *et al.* 2008). Sources in Chamaeleon I could be observed using Hydra-CTIO, given the cluster's distance of 165 pc (Whittet *et al.* 1997; Wichmann *et al.* 1998; Bertout *et al.* 1999). Both of these regions could also be studied using FLAMES on the VLT, so that even lower mass objects could be observed.

High-resolution spectroscopic studies of both regions would be useful to derive radial velocities, vsini, and surface gravities. These would further confirm association membership. Meaningful radial velocities for the more massive Serpens members could not be derived by this study due to the lack of usable lines. For lower mass members high resolution spectra could be obtained using NIRSPEC on Keck II with infrared echelle spectra or with further observation using MIKE on the Magellan telescopes. This would provide a larger sample of sources in both regions and allow one to probe to the low mass regime. With these data, kinematic studies of star formation regions could be used to derive velocity dispersions and to set limits to timescales for stellar encounters. These studies also could be used to determine sub-structures within star forming regions providing further insight into the star formation process. These same high-resolution spectra could also be used for follow-up observations of possible transition disk objects in order to measure accretion rates. In Serpens, echelle spectra were obtained for only one potential transition disk object and no echelle spectra were taken for sources in Rho Ophiuchi. With low-resolution spectra, weakly accreting sources can be misidentified as non-accreting sources. As outlined above, there is still a lot of work to be completed in both regions in order to form a complete picture of star formation.

REFERENCES

Bertout, C., Robichon, N., & Arenou, F. 1999, A&A, 352, 574

Chabrier, G. 2003, PASP, 115, 763

Dzib, S., Loinard, L., Mioduszewski, A. J. *et al.* 2010, ApJ, 718, 610

Dzib, S., Loinard, L., Mioduszewski, A. J. *et al.* 2011, RevMexAAC, 40, 231

Hillenbrand, L. A. 2009, in IAU Symp. 258, The Ages of Stars, ed. E. E. Mamajek, D. R. Soderblom, & R. Wyse (Cambridge: Cambridge Univ. Press), 81

Hillenbrand, L.A., Bauermeister, A., & White, R. 2007 in Cool Stars, Stellar Systems, and the Sun XIV: ASP Conference Series, Vol. XX

Hirota, T., Bushimata, T., Choi, Y.K., *et al.* 2008, PASJ, 60, 37

Lada, C., & Lada, E. 2003, ARA&A, 41, 57

Muzerolle, J., Flaherty, K., Balog, Z., *et al.* 2009, ApJ, 704, L15

Whittet, D. C. B., Prusti, T., Franco, G.A.P, *et al.* 1997, A&A, 327, 1194

Wichmann, R., Bastian, U., Krautter, J., Jankovics, I., & Ruciński, S. M. 1998, MNRAS, 301, L39

5 CONCLUSIONS

Rho Ophiuchi and Serpens appear to be fairly typical low mass star-forming regions and bear many similarities. The highest mass stars in both regions are B type stars. The total mass of molecular gas in both regions, adjusted for the distance used in this study, is approximately 1000 $M_\odot$ (Loren 1989b; Omli and Testi 2002). Hence the size of these two clouds is comparable. Several new PMS objects have been identified in both regions, demonstrating the need for unbiased spectroscopic samples in star-forming regions. From these spectra, temperatures and luminosities have been obtained and used to derive ages and masses for association members.

Median ages of 3 Myrs (Rho Ophiuchi) and 2 Myrs (Serpens) have been found. Both of these ages support the theory that star formation is a relatively fast process (Hartmann 2001). Both regions have a younger embedded population with class 0 and 1 spectral energy distributions in several dense molecular cores surrounded by a slightly older, more distributed population. This older population tends to avoid the highest density of gas in both regions. Taken together, the young age of both the distributed and embedded populations indicate that either the star formation rate has increased in the last few Myrs (Palla & Stahler 2000), or molecular clouds are younger than previously assumed.

No age spread is found in Rho Ophiuchi. In Serpens, an age spread of 1-5 Myrs is inferred. It is difficult to interpret these results. Age spreads of greater than 10 Myrs would indicate long lifetimes for molecular clouds and that magnetic flux is important in regulating star formation (Hartmann 2001). However it is not clear what a small age spread (less than 10 Myrs) indicates in comparison to regions with no age spread. Perhaps this is a result of different formation mechanisms (i.e., triggered vs. spontaneous star formation or a combination of the two).

At the high mass end, both regions agree with the field star IMF, indicating that the IMF may be universal for M>1 $M_\odot$. However this study did not probe to low enough masses in Serpens to detect a turnover (and hence a characteristic mass) and see variations from the field star IMF at the lower masses. In Rho Ophiuchi, even with completeness corrections, the expected number of sources in the lowest mass bin was not observed which may suggest a deficit of brown dwarfs. Although the error bars are such that this is a marginal result, if the deficit is real it would indicate that at the lowest mass end the IMF may depend on environmental factors.

Both clouds also show similar disk frequencies: $27\% \pm 5\%$ in Rho Ophiuchi and $42\% \pm 10\%$ in Serpens. This is not surprising given the similar relative ages of the two clusters (3 Myrs for Rho Ophiuchi; 2 Myrs for Serpens from the DM models) and the trend of decreasing disk frequency with the age of the cluster (Lada *et al.* 2006; Sicilia-Aguilar *et al.* 2006; Hernandez *et al.* 2007). Ultimately, these studies of Rho Ophiuchi and Serpens have added sources to the list of known association members toward a complete sample, and support the picture that star formation takes place on relatively fast time scales.

REFERENCES

Hartmann, L. 2001, AJ, 121, 1030

Hernandez, J., Calvet, N., Briceño, C. *et al.* 2007, ApJ, 671, 1784

Lada, C. J., Muench, A. A., Luhman, K. L., *et al.* 2006, AJ, 131, 1574

Loren, R. B. 1989, ApJ, 338, 925

Olmi, L., & Testi, L., 2002, A&A 392, 1053

Sicilia-Aguilar, A., Bohac, C., Bouwman, J., *et al.* 2006, ApJ, 638, 897

Palla, F., & Stahler, S. W., 2000, ApJ, 540, 255

APPENDIX

PERMISSIONS FOR FIGURES

Permission from Dr. Philippe André for Figures 1.2 and 1.4

Dear Kristen,

Thank you for your message. Sorry to reply only today but I was attending a very dense conference on Herschel results last week.

You have my permission to you use both figures in your dissertation provided that you clearly state where the figures are coming from.

With best wishes,

Philippe ANDRÉ

Permission from Dr. Isabelle Grenier for Figure 1.3

Dear Kristen, I will be honoured that you include the figure. If you plan to post your PhD somewhere, please let me know. I would be interested to read about your results. Good luck with the defence. Isabelle Grenier

Prof. Isabelle Grenier Laboratoire AIM, Universit Paris Diderot CEA Saclay Irfu DSM/Irfu/SAp, CEA Saclay, 91191 Gif/Yvette, France tel: +33 1 69 08 44 00 fax: +33 1 69 08 65 77 isabelle.grenier@cea.fr

Permission from Dr. Gilles Chabrier for Figure 1.1

No problem, please feel free to use the figure. And please keep me posted if you publish a paper on your results. Best regards Gilles Chabrier

Permission from Dr. Melissa Enoch for Figure 1.5

Hi Kristen, Yes, you may certainly use the figure. I assume that you can get it from the article, but if you need a copy please let me know.

Best of luck with your dissertation!

Melissa

Permission from AAS for chapter 2

Dear Kristen Erickson

Thank you very much for your permissions enquiry relating to your material published previously in the journals of the American Astronomical Society.

On behalf of AAS, we are pleased to grant the necessary permission for your use of this material in your thesis and we ask that the Society is acknowledged through the wording: "Reproduced by permission of the AAS".

Please could you ensure that the proper bibliographic citation details are given for your paper in your thesis.

Thank you again for your interest in the AAS journals.

Yours sincerely

Jill Membrey Managing Editor, Copyright and Permissions

VITA

Kristen Erickson was born in Okinawa Japan in 1980. She completed her B.S. in Physics and Astronomy in 2003 from the University of Arizona. She received her M.S. in Physics from the University of Missouri St. Louis in 2008. She has completed her Ph.D. in Physics from the University of Missouri St. Louis in December of 2013.